The Role of Epiregulin in Idiopathic Pulmonary Fibrosis

Inaugural Dissertation
in partial fulfillment of the requirements
for the degree Doctor of Medicine (Dr. med.)
submitted to the
Faculty of Medicine
of the Justus-Liebig-University Gießen

by
Schramm, Fabian
from Essen, Germany

Gießen 2025

From the Faculty of Medicine of the Justus-Liebig-University Gießen

Department of Internal Medicine:

Center for Infection and Genomics of the Lung (CIGL)

Supervisor and Reviewer: Prof. Dr. Malgorzata Wygrecka

Reviewer: Prof. Dr. Andreas Hecker

Date of Doctoral Defense: 12.08.2026

Table of Contents

1 Introduction 6

1.1 Diffuse Parenchymal Lung Diseases 6

1.2 Idiopathic Interstitial Lung Diseases 6

1.3 Idiopathic Pulmonary Fibrosis 7

1.3.1 Definition and Epidemiology 7

1.3.2 Risk Factors 7

1.3.3 Pathogenesis 8

1.3.4 Clinical Presentation, Comorbidities and Prognosis 11

1.3.5 Diagnosis 12

1.3.6 Treatment 13

1.4 ErbB Signaling System 14

1.4.1 Biology of ErbB Receptors and Ligands 14

1.4.2 ErbB Signaling System in Physiology 15

1.4.3 ErbB Signaling System in Pathology 16

1.4.4 ErbB Signaling System in the Lung 17

1.4.5 ErbB Signaling System in Idiopathic Pulmonary Fibrosis 17

1.5 Epiregulin 20

1.5.1 Structure and Cellular Activities 20

1.5.2 Functions in Physiology 20

1.5.3 Role of Epiregulin in Pathology 21

1.6 Cellular Senescence 23

1.6.1 Biology of Senescence 23

1.6.2 Cellular Senescence in Idiopathic Pulmonary Fibrosis 24

1.6.2.1 Findings for ErbB Signaling System and Senescence. 25

1.7 Aim of the Study 27

2 Material and Methods 28

2.1 Material 28

2.1.1 Apparatuses and Equipment 28

2.1.2 Software 30

2.1.3 Chemicals, Reagents and Solutions 31

2.1.4 Expandable Materials 35

2.1.5 Kits 36

2.1.6 Antibodies 37

2.1.6.1 Primary Antibodies 37

2.1.6.2 Secondary Antibodies 38

2.1.6.3 Fluorescence-Activated Cell Sorting Antibodies 39

2.1.7 Buffer 41

2.1.8 Human and Murine Samples 41

2.1.8.1 Human Lung Sections / Cells for Air Liquid Interface 41

2.1.8.2 Murine Lung Sections, Bronchoalveolar Lavage Fluid 41

2.1.8.3 Cell Lines 42

2.2 Methods 42

2.2.1 Cell Culture 42

2.2.2 Senescence / β-Galactosidase Assay in Cell Culture 43

2.2.3 Comet Assay in Cell Culture 43

2.2.4 Air Liquid Interface Cell Culture 44

2.2.5 Animal Experiments 45

2.2.5.1 Mice Strains 46

2.2.5.2 Bleomycin Instillation 46

2.2.5.3 Lung Function Measurement and Collection of Bronchoalveolar Lavage Fluid 46

2.2.5.4 Processing of Lung Tissue for Further Analysis 47

2.2.5.5 Preparation for Histology 47

2.2.5.6 Preparation for Fluorescence-Activated Cell Sorting 48

2.2.6 Fluorescence-Activated Cell Sorting Analysis 49

2.2.6.1 Epiregulin Instillation 51

2.2.7 ELISA of Bronchoalveolar Lavage Fluid 51

2.2.8 Histology and Cytology 53

2.2.8.1 Preparation of Lung Sections 53

2.2.8.2 Preparation of Air Liquid Interface Filter Sections 53

2.2.8.3 Hematoxylin and Eosin Staining 54

2.2.8.4 Immunohistochemistry 54

2.2.8.5 Immunocytochemistry / Immunofluorence 55

2.2.8.6 Light Microscopy Imaging 58

2.2.8.7 Immunofluorescence Microscopy Imaging 58

2.2.8.8 Electron Microscopy 59

2.2.9 Data Analysis and Statistical Analysis 60

3 Results 61

3.1 Effects of Epiregulin on Airway Epithelial Cells 61

3.1.1 Epiregulin Stimulation Alters Epithelial Morphology and Cell Differentiation of Airway Epithelial Cells 61

3.1.2 Epiregulin Treatment Induces DNA Damage and Senescence in Airway Epithelial Cells 63

3.1.3 Epiregulin Stimulation Enhances DNA Damage and Cellular Senescence in Basal Cells and Proliferation in Non-Basal Cells in the Respiratory Epithelium 64

3.2 In vivo effects of Epiregulin Experimental Pulmonary Fibrosis in Mice 68

3.2.1 Histological Fibrosis and Lung Function Is Unaltered in Bleomycin Exposed Mice Treated with Epiregulin 68

3.2.2 Senescence-Associated Secretory Phenotype Mediator Levels in Bronchoalveolar Lavage Fluid Are Altered after Bleomycin Treatment in Mice but Are Unaltered after Additional Epiregulin Application 69

3.2.3 Administration of Epiregulin Promotes Proliferation and Senescence in Bleomycin Exposed Mice 70

4 Discussion 76

4.1 Epiregulin-Induced Morphological Changes in Airway Epithelial Cells 76

4.2 DNA Damage and Cellular Senescence Are Driven by Epiregulin in Airway Epithelial Cells 79

4.3 Limited Role of Epiregulin in Pulmonary Fibrosis Progression and Senescence Induction in Mice after Bleomycin Instillation and Novel Insights into the Pathogenesis of Fibrosis 80

4.4 Limitations of the Study and Future Outlook 84

5 Summary 86

6 Zusammenfassung 87

7 List of Abbreviations 89

8 List of Figures and Tables 94

9 References 95

10 Publication List.....118

11 Declaration.....119

12 Acknowledgements 120

1 Introduction

1.1 Diffuse Parenchymal Lung Diseases

Diffuse parenchymal lung diseases (DPLD), also known as interstitial lung diseases (ILD), are a heterogenous group of diseases affecting the lung parenchyma. According to the consensus statement by the American Thoracic Society and the European Respiratory Society, there are four subgroups of DPLD (1):

I. DPLDs of known causes (e.g. drugs, exogen noxae, etc.)
II. Idiopathic interstitial pneumonias (IIPs)
III. Granulomatous DPLDs caused by connective tissue disorders or vasculitis
IV. Other rare heterogenous forms of DPLD

In general, the feature of all these diseases is a non-neoplastic damage to the lung parenchyma by inflammatory and fibrotic processes. Ultimately, these alterations affect the alveolo-capillary gas exchange, leading to clinical symptoms of compromised respiratory function. Overall, the histological changes do not only affect the parenchyma but also the peripheral airways and the vascular compartment (2). Differentiation between the different groups of DPLD helps to provide the appropriate diagnostic path and therapeutic options in clinical medicine.

1.2 Idiopathic Interstitial Lung Diseases

Idiopathic interstitial lung diseases, also known as IIPs, are a heterogenous group of diseases that belong to the superordinate group of DPLD. Idiopathic describes the unknown etiology of these diseases, even though certain risk factors for their development have been identified (see 1.3.2). IIPs are divided into two main groups: Idiopathic pulmonary fibrosis (IPF), the most common form of IIP and a heterogenous group of other IIPs, classified by clinical, radiological and pathological features. The six classified diseases are non-specific interstitial pneumonia (NSIP), cryptogenic organizing pneumonia (COP), acute interstitial pneumonia (AIP), respiratory bronchiolitis-associated interstitial lung disease (RB-ILD), lymphoid interstitial pneumonia (LIP) and desquamative interstitial pneumonia (DIP) (1).

1.3 Idiopathic Pulmonary Fibrosis

1.3.1 Definition and Epidemiology

IPF stands as the most common type of DPLD, marked by excessive deposition of extracellular matrix (ECM) proteins within the lung tissue (3). Over the last decades, the incidence of IPF has risen worldwide, with a generally higher incidence in men. In Europe and North America, the incidence ranged from three to 18 cases per 100 000, while several studies reported lower rates in East Asia and South America (4–6).

1.3.2 Risk Factors

IPF, as the name suggests, is a condition of unknown cause. However, several risk factors and theories regarding its pathogenesis have been identified. Widely recognized risk factors for IPF include male gender, advanced age and a history of smoking (7–10). Various studies have also linked IPF to occupational exposure to dust particles including those encountered by farmers, metal production workers and hairdressers (9). Treatment with certain drugs has also been statistically associated with IPF, particularly tricyclic antidepressants such as imipramine and dothiepin (11). However, drugs with established profibrotic potential, such as amiodarone, nitrofurantoin and certain cytotoxic agents like bleomycin, are infrequently used and rarely serve as risk factors for the development of IPF (11). Other suspected drugs including beta-blockers, anticonvulsants, non-steroidal anti-inflammatory drugs (NSAIDs) and certain antibiotics, have not been linked to IPF in statistical studies (11).

Genetic variants and mutations play a role in both sporadic and familial cases of IPF (12). The most common genetic risk factor associated with IPF development is the gain-of-function mucin-5B (MUC5B) promotor variant rs35705950 (13), which leads to a higher concentration of MUC5B in IIP lung tissue (14), particularly in the distal lung epithelium (15). Overexpression of MUC5B is thought to contribute to the pathogenesis of IIPs through impaired mucociliary clearance, resulting in reduced host defense and dysregulated repair mechanisms (15, 6).

In addition to MUC5B variants, genetic variants of surfactant proteins have also been linked to susceptibility to IIPs and IPF. The surfactant protein C (SFTPC) variant c.460+1 G→A (16) and surfactant protein A2 (SFTPA2) variants G231V and F198S (17) are believed to induce endoplasmatic reticulum (ER) stress in alveolar type II (ATII) cells,

potentially leading to ILDs. Subsequent studies have shown that these variants are primarily found in familial forms of IPF or IIP (18, 19).

Additionally, genetic variants in the genes encoding desmoplakin (DSP), a protein crucial for cell-cell adhesion and dipeptidyl peptidase 9 (DPP9), an important protein for fibroblast activation, have also been associated with IIPs. These variants may impair the barrier function of the respiratory epithelium, contributing to the pathogenesis of IIPs (14). Another risk factor involves mutations in telomere-related genes named telomerase reverse transcriptase (TERT), telomerase RNA component (TERC) (20–23) and oligonucleotide/oligosaccharide-binding fold-containing protein 1 (OBFC1) (14), which lead to telomere shortening in alveolar epithelial cells. Telomere shortening may contribute to early cell senescence, a process that plays a role in the pathogenesis of IPF (14) (see Section 1.6.2).

1.3.3 Pathogenesis

The pathogenesis of IPF is believed to be triggered by recurrent microinjuries in a genetically predisposed distal respiratory epithelium (see 1.3.2), leading to excessive and uncontrolled activation of (myo)fibroblasts. This activation is thought to be mainly induced by injured and aberrantly activated alveolar epithelial cells, which produce several mediators including platelet-derived growth factor (PDGF) (24), tumor necrosis factor alpha (TNF-α) (25), endothelin 1 (ET-1) (26) and transforming growth factor-β (TGF-β) (27). Upon secretion and binding to their respective receptors, these mediators trigger abnormal mesenchymal cell behavior rather than restoring epithelial integrity and inducing repair processes (26). Myofibroblasts are fully differentiated and specialized mesenchymal cells that exhibit characteristics of both fibroblasts and smooth muscle cells (28, 29). Under physiological conditions, they play an important role in wound healing by producing ECM proteins that are crucial for tissue repair (30, 31). In tissue affected by pulmonary fibrosis, activated myofibroblasts proliferate in nests (fibroblast foci) and produce excessive amounts of collagen, which accumulates in the lung tissue and contributes to the clinical manifestation of IPF (3). The fibroblast foci are covered by an epithelium of either alveolar or bronchial origin (32, 33). In early stages of IPF, hyperplastic ATII cells respond to lung injury by producing the above-mentioned mediators to restore epithelial integrity. However, this initially adaptive response transitions to a maladaptive remodeling, leading to the formation of honeycomb cysts. These cysts are lined by a mucociliary bronchiolized epithelium that replaces the alveolar epithelium, a process called

bronchiolization (34, 13). This bronchiolized epithelium consists of ciliated cells, abnormal basal cells and mucus-producing cells that express, among other proteins, high amounts of MUC5B (13, 15, 34).

While in cancer, tumor cells usually have a monoclonal origin, myofibroblasts in fibroblast foci in IPF show a polyclonal origin in clonality analyses (35). This indicates that myofibroblasts may arise from different types of cells. There are three concepts that have been discussed in the literature regarding how cells may differentiate into myofibroblasts and ultimately, all three may contribute to the population of activated myofibroblasts:

1. The first possibility is that resident lung fibroblasts differentiate into myofibroblasts (36, 37).
2. Another possibility is that fibrocytes, which are fibroblast precursors derived from the stem cell pool, differentiate into myofibroblasts upon reaching the injured lung tissue and being stimulated by cytokines that sense tissue damage (38).
3. The last and most widely discussed possibility is that distal respiratory epithelial cells transform into myofibroblasts, a process called epithelial-mesenchymal transition (EMT) (39–42).

EMT is a process in which epithelial injury leads to a change in phenotype from already differentiated epithelial cells to mesenchymal cells. While EMT plays an important role in embryonal development (43), it is also very important in cancer metastasis (44, 45). In fibrogenesis, EMT is mediated by several cytokines including TGF-β, which is the most potent profibrotic and EMT-inducing cytokine (46–48). In IPF, TGF-β has also been found to be highly expressed in fibrotic tissue (49, 50). Other EMT-inducing cytokines are epidermal growth factor (EGF) (51), insulin-like growth factor 2 (IGF-II) (52), or fibroblast growth factor 2 (FGF-2) (53). The phenotypic change in epithelial cells during EMT is typically recognized by a decrease in the expression of epithelial markers E-cadherin and surfactant protein-C (SPC) and an increase in the expression of mesenchymal markers α-actin-2/α-smooth muscle actin 2 (ACTA-2/α-SMA), collagen I and F-actin, which are also markers of myofibroblasts (47, 54). EMT has been observed in epithelial cells lining fibroblast foci in IPF patients, where colocalization of both epithelial and mesenchymal markers has been detected (55). In in vitro studies, TGF-β was capable of inducing α-SMA expression only in fibroblasts (39) but also in alveolar epithelial cells, transforming them into myofibroblasts (40). Additionally, in experimental lung fibrosis in mice, TGF-β overexpression or bleomycin application triggered EMT in affected lungs

(41, 42). Another feature of TGF-β and another profibrotic mediator, endothelin-1, is that they promote resistance to apoptosis via the phosphoinositide 3-kinase/protein kinase B (PI3K/AKT) pathway in IPF fibroblasts (56), which may further potentiate the dysregulated activation of fibroblasts. A different process associated with IPF fibroblasts and epithelial cells is cellular senescence (57, 58). Cellular senescence is a state in which cell cycle arrest is triggered by DNA damage, oxidative stress or telomer shortening. Cells permanently arrest their cell cycle, leading to an arrest of proliferation and growth, but simultaneously release inflammatory mediators instead of going into apoptosis (59). Although senescence is typically associated with aging, IPF lung tissue shows expression of senescence markers in fibroblasts and hyperplastic epithelial cells (57, 58). Additionally, profibrotic mediators are produced in senescent fibroblasts (60). A deeper discussion of the association between senescence and IPF is provided in section 1.6.2.

While the latent form of TGF-β is usually stored in the ECM, mechanical stress and contraction of myofibroblasts can release active TGF-β from the ECM stores, activating other myofibroblasts (61). The ECM produced by activated myofibroblasts may, in turn, trigger further cell contraction and release of additional TGF-β, creating a potent self-amplifying loop (61). The effects of TGF-β are also potentiated by other cytokines including interleukin-1-β (IL-1β), interleukin-6 (IL-6) and TNF-α (62, 63). These cytokines are overexpressed during the wound healing process and maladaptive remodeling after tissue injury. One of the most prominent cytokines associated with these processes is IL-6, which is overexpressed in IPF-fibroblasts and has been shown to potentiate the TGF-β signaling pathway (64, 65). These complex mechanisms depict a powerful amplification system of profibrotic effects driven by multiple mediators including TGF-β, which is one of the most profibrotic cytokines (66). However, numerous mediators contribute to fibrogenesis through a dense network of interactions, leading to uncontrolled activation of myofibroblasts, culminating in the pathological and clinical manifestations of IPF.

Besides the pivotal role of TGF-β in fibrogenesis, several other mechanisms contribute to the maladaptive remodeling of lung tissue observed in IPF. Dysregulation of angiogenic and angiostatic signaling plays an important role in IPF pathogenesis (26). Mediators like angiostatic pigment epithelium-derived factor (PEDF) and vascular endothelial growth factor (VEGF) are secreted from epithelial and mesenchymal cells (26). Interestingly, PEDF has been shown to be expressed in TGF-β stimulated fibroblasts and is thought to be responsible for the avascular and downregulated vascularization observed

in fibroblast foci, as PEDF expression was present in avascular fibroblast foci, while VEGF levels were decreased in these areas (67).

Another system associated with IPF is the hemostatic system. Elevated levels of tissue factor, plasminogen activator inhibitor 1 (PAI-1) and plasminogen activator inhibitor 2 (PAI-2) have been detected in the bronchoalveolar lavage fluid (BALF) of IPF patients and their levels correlate with disease severity (68). Histological analysis of IPF lung tissue has also revealed high expression of tissue factor in epithelial cells, whereas PAI-1 is expressed in both epithelial cells and alveolar macrophages. It has been speculated that dysregulation of fibrinolysis and tissue factor expression leads to the persistent deposition of fibrin in the lung parenchyma, contributing to the abnormal remodeling of the alveolar spaces (26).

Another component of the coagulation cascade, suggested to have potential profibrotic effects in IPF, is coagulation factor XII (FXII), which was found to be overexpressed in histological analysis of IPF lungs compared to donor lungs. Interestingly, IL-6 was also expressed in most $FXII^+$ cells. Subsequent in vitro studies demonstrated that FXIIa-stimulated fibroblasts produce IL-6 in a protease-activated receptor 1 (PAR-1) and nuclear factor kappa-light-chain-enhancer of activated B (NF-κB)-dependent manner. As previously discussed, IL-6 is known to be overexpressed in IPF fibroblasts and can activate the profibrotic TGF-β pathway (64, 65), linking Factor XII to IPF pathogenesis.

The erythroblastic leukemia viral oncogene homolog (ErbB signaling) system has also been associated with IPF. All IPF-relevant findings will be discussed in section 1.4.5.

1.3.4 Clinical Presentation, Comorbidities and Prognosis

Patients with IPF often present with non-specific respiratory symptoms including breathlessness and cough, along with reduced exercise capacity (6, 69). Initially, patients are diagnosed in later stages of the disease. Diagnosis is based on exclusion criteria as described in 1.3.5. Patients usually present because of acute exacerbation, an acute worsening of the disease, due to their underlying impaired respiratory function. In clinical examination, patients primarily show crackles in lung auscultation, digital clubbing and cyanosis (69). Pulmonary symptoms are mainly caused by decreased lung function due to restrictive lung disease (70). Furthermore, patients may develop signs of secondary right heart failure due to IPF-associated pulmonary hypertension (69). Most common comorbidities are gastrointestinal disorders with mainly gastro-esophageal reflux disease and disorders in metabolism such as hypercholesterolemia and diabetes mellitus (12).

Diseases associated to a smoking history like cardiovascular diseases, chronic obstructive pulmonary disease (COPD), lung emphysema or bronchial carcinoma (71) are also very common in patients with IPF (12). At the time of diagnosis, average length of survival varied from 1 to approximately 7 years in several studies. The main cause of death was respiratory failure, followed by heart failure according to these studies (69).

1.3.5 Diagnosis

The diagnostic workup of suspected IPF requires a multidisciplinary approach. It is crucial that IPF is differentiated from other fibrotic diseases of the lung (72). First assumptions can be made after taking the patients history. Classical risk factors like older age over 60 years, male gender or smoking history (see section 1.3.2) may include IPF as a potential diagnosis. Medication and environmental exposure to profibrotic agents or a history of familial pulmonary fibrosis may strengthen the suspicion (see section 1.3.2). Clinical examination is very unspecific and respiratory symptoms can be absent or mild depending on disease progression and adaption (6, 69). Causes like connective tissue diseases can be ruled out by serological testing (73). The most important tool in IPF diagnosis is the high-resolution computed tomography (HRCT) of the lung. The pattern of usual interstitial pneumonia defines IPF and consists of honeycombing, traction bronchiolectasis and bronchiectasis, fine reticulation and ground glass opacities. Honeycombing is typically seen in subpleural regions of the lung and appears as clusters of cystic air spaces, usually with 3-10 mm in diameter, with thickened walls. It is often accompanied by a network of fine lines (reticulation) and small dilated airways (traction bronchiolectasis). These cysts can appear in clusters or as a single layer of cysts. Traction bronchiectasis and bronchiolectasis are a typical pattern of pulmonary fibrosis. They usually can be found subpleurally in the peripheral lung spaces. In both conditions, the terminal airways (bronchial or the bronchiolar spaces) are widened abnormally (73, 74). Ground-glass opalization is another typical sign of pulmonary fibrosis. It is characterized by a denser opacity of the surrounding lung tissue with preservation of the bronchial and vascular pattern in the background. If the bronchial and vascular pattern are not present, then it is likely to be an opacity that is not pure, which is not classical for pulmonary fibrosis (73, 74). On HRCT, the patterns can be assigned to four diagnostic categories: Usual interstitial pneumonia (UIP) pattern, probable UIP pattern, indeterminate for UIP pattern and alternative diagnosis. These categories determine how likely it is that the radiological pattern correlates with the UIP pattern in histopathology (73). While the UIP pattern and

probable UIP pattern do not require further histological confirmation according to the newest recommendations from the 2022 consensus statement by the American Thoracic Society and European Respiratory Society, histological confirmation is needed for indeterminate for UIP and alternative diagnosis patterns (75).

When diagnostic findings are not distinct, histological diagnosis of UIP can be achieved through transbronchial or surgical lung biopsy to specify the underlying pathology. Since alterations of the parenchyma first occur in the basal and subpleural regions, biopsy from these areas is most likely to be diagnostic. Features of UIP diagnosis should contain the following histological features: patchy dense fibrosis with architectural distortion such as honeycombing or scar tissue, predilection for subpleural and paraseptal lung parenchyma, accumulation of (myo)fibroblasts (fibroblast foci) and no features of alternative diagnoses (75). As for radiological classification, there is also a recommended classification for pathohistology, which follows the same scheme as the radiological concept (73).

1.3.6 Treatment

Since IPF and other IIP's pathogenesis is still not completely understood, there are very few therapeutic options available and the prognosis still remains very poor (29). Therapeutic approaches that were used in the past, like corticosteroid or immunosuppressive drugs, are only recommended in acute exacerbation (75). With pirfenidone and nintedanib, there are two therapy concepts available that can delay the disease's progression. Nintendanib acts as a tyrosine kinase inhibitor for different receptors: PDGF-, VEGF- and FGF-receptors, which all have profibrotic potential after activation (76). The second available drug, pirfenidone, modulates TGF-β signaling and sonic-hedgehog-pathways, but the mechanism behind this is still unknown (77, 78). Besides pirfenidone and nintedanib, therapeutic approaches focus on symptomatic oxygen supplementation and rehabilitation programs. If comorbidities like pulmonary hypertension, gastroesophageal reflux or obstructive sleep apnea exist, treatment of the underlying diseases or their symptoms is also recommended (75). The only available therapeutic option that significantly improves patient survival rate is a total lung transplantation (29, 70). Since current therapies are rather ineffective, new treatment strategies are needed to improve the fatal outcome of the disease.

1.4 ErbB Signaling System

1.4.1 Biology of ErbB Receptors and Ligands

The ErbB receptors, also known as epidermal growth factor receptors (EGFR) or human epidermal growth factor receptors (HER), are a family of transmembrane proteins that act as tyrosine kinase receptors (79, 80). Besides EGFR (also known as ErbB1 or HER1), there are three more receptors that belong to the family of ErbB receptors: ErbB2/HER2 (81), ErbB3/HER 3 (82) and ErbB4/HER 4 (83). ErbB receptors are activated upon binding of specific ligands. The most common ligand is EGF (84, 85). Over the years, several molecules have been identified that share the so called EGF-domain and are able to bind ErbB receptors (86, 87). So far, besides EGF, known ligands are transforming growth factor-α (TGF-α) (88), amphiregulin (AREG) (89), heparin-binding EGF-like growth factor (HB-EGF) (90), betacellulin (BC) (91), epiregulin (EREG), (92), epigen (EPG) (93) and a group of several ligands known as neuregulins (NRGs) (94). The family of NRGs can be divided into four smaller heterogenous groups: NRG1, NRG2 or neural- and thymus-derived activator for ErbB kinases (NTAK) (95, 90), NRG3 (96) and NRG4 (97). For NRG1, different isoforms exist that form a heterogenous group of its own: Type I NRG1, which includes the heregulins (HRG, consisting of hereregulin- α und -β) (98), the neu differentiation factor (NDF) (99, 100) and the acetylcholine receptor-inducing activity (ARIA) (101). Type II NRG1 includes the glial growth factors (GGFs) (99) and type III NRG1, which consists of the sensory and motor derived factor (SMDF) (102).
Upon binding of EGF ligands, ErbB receptors form homodimers with receptors from the same class or heterodimers with other receptors from the ErbB-family. This leads to autophosphorylation of the tyrosine residues by receptor intrinsic tyrosine kinase activity (103). Phosphorylated ErbB receptors then activate multiple downstream signaling pathways. The most common downstream signaling pathways are the mitogen-activated protein kinase/extracellular signal-regulated kinase (MAPK/ERK) pathway (104), the PI3K/AKT pathway (105), the phospholipase Cγ (PLCγ) pathway (106) and the Janus kinase signal transducer and activator of transcription (JAK/STAT) pathway (85). These pathways translate the signal into the nucleus and activate a number of transcription factors including Myc, Fos, Jun (94), finally leading to gene transcription and regulation of cell survival, growth, proliferation, migration and collagen deposition (107).

Not all ligands are capable of binding to all ErbB receptors. There are ligands such as EGF, TGF-α, AREG and EPG that can only bind ErbB1. Also, NRG3 and NRG4 from

the family of NRGs are only capable of binding to ErbB4 (94). Other ligands can bind different ErbB receptors. For example, EREG, BC, HB-EGF can bind ErbB1 and ErbB4. Also, NRG1 and NRG2 from the family of NRGs can bind ErbB3 and ErbB4 (94). No ligands for ErbB2 have been identified so far. Nevertheless, ErbB2 forms heterodimers with other ErbB receptors and plays a crucial role in the activation of all ErbB receptors (108, 109). For example, ErbB3 lacks an intrinsic catalytic activity but is phosphorylated by ErbB2 to activate downstream signaling (110). All ErbB ligands have precursor proteins that are bound to cell membranes as membrane-anchored proteins. They are shed and activated by matrix metalloproteases (MMPs) and a disintegrin and metalloproteinases (ADAMs) and released into the extracellular space (111–113). The most important proteinases for cleavage and activation of ErbB ligands are ADAM-10 and ADAM-17. ADAM-10 mainly cleaves EGF and BC, while ADAM-17 cleaves TGF-α, AREG, HB-EGF and EREG (112–114).

1.4.2 ErbB Signaling System in Physiology

ErbB receptors and their ligands play a crucial role in various physiological processes including cell growth, proliferation, differentiation, tissue regeneration and repair (115). Expression of ErbB receptors has been found in various tissues but mostly in basal cells of the skin epithelium and epithelial layered organs including the lungs, gastrointestinal tract, urogenital tract and many more. Besides the epithelial layer of the surface, the expression of ErbB receptors was also high in duct cells from secretory glands of the skin, lung, gastrointestinal and urogenital tract (116). Proliferating fibroblasts beneath the epithelial layers and in the connective tissue were also shown to have high expression of ErbB receptors (116). On the other hand, ErbB ligands have been found to be expressed in more differentiated tissues like acini of glandular tissue (116).

In development, the ErbB signaling system is crucial for early embryonic processes such as implantation, trophoblast invasion and blastocyst formation (117, 118). It is also essential for organogenesis, influencing heart formation (119, 120), nervous system development (121), lung branching and maturation (122) as well as mammary gland development (123, 124). Additionally, it plays a critical role in the development of epithelialized organs (125), regulating differentiation and tissue renewal in the skin, lungs and gastrointestinal epithelium (126–128).

Transcriptional changes in mRNA of EGFR and TGF-α have been found in wound healing processes in rats (129) and were also colocalized with proliferation markers like

proliferating cell nuclear antigen (PCNA) during regeneration (130). Topical administered EGF and TGF-α are able to accelerate epidermal regeneration of the skin (131) and the epithelial layer of the gastrointestinal tract (132). While ErbB receptors are usually located at the basolateral side of polarized cells, ligands are often located on the apical side and overlying fluids in different tissues (133, 134). Discontinuity of epithelial layers may bring receptors and ligands together, leading to the instant activation of the ErbB signaling system to restore integrity of the epithelial layer (133). The importance of ErbB1 in the maintenance of the epithelium integrity is best pointed out when looking at patients receiving tyrosine kinase inhibitors (TKIs) against ErbB1. Here, one percent of patients with non-small cell lung cancer (NSCLC) who were treated with the TKI gefitinib or erlotinib against ErbB1, developed acute lung injury and ILD (135).

1.4.3 ErbB Signaling System in Pathology

With ErbB signaling being such an important regulatory system for cell growth, proliferation, differentiation and survival, it is not surprising that it plays a crucial role in many forms of cancer. Many malignancies are linked to mutations of ErbB family receptors or their overexpression. Often, such mutations are associated with decreased survival. Associations of the ErbB signaling system have been predominantly found in lung malignancies (NSCLC) (136), breast and ovarian cancer (137, 138), gastric carcinoma (139, 140), pancreatic carcinoma (141), colorectal carcinoma, glioblastoma (142) and head and neck cancer (143).

Therefore, drugs targeting ErbB receptors are widely used in cancer therapy and may improve survival dramatically. Gefitinib, a quinazoline derivative, was the first reversible ErbB1 inhibitor that was introduced into therapy of NSCLC (144). Erlotinib, another quinazoline derivative and reversible ErbB1 inhibitor, targeting a different mutation in ErbB1, followed (145). Afatinib, an irreversible inhibitor of ErbB1 is the newest drug targeting ErbB1 in NSCLC patients (146). In pancreatic adenocarcinoma, ErbB1 is also expressed and is associated with a poor prognosis (141). Erlotinib has been used for treatment of such mutations and showed increased survival in combination with gemcitabine therapy (147). Despite a positive initial response to treatment, resistance to TKIs often develops over time due to second-site mutations in the EGFR tyrosine kinase domain (148).

One of the most notable uses of ErbB inhibitors is targeting ErbB2 mutations in breast cancer. Trastuzumab, a monoclonal antibody against HER2, was introduced in 1998 as

the first agent for targeted therapy in breast cancer. It significantly improved the survival rate of patients with the aggressive HER2-positive subtype (149, 150).

The frequent occurrence of ErbB mutations has led to the development of a wide range of substances targeting ErbB receptors for cancer therapy. However, other diseases involving the ErbB signaling system could potentially benefit from these advances, paving the way for future therapeutic applications in various fields.

Some other disorders that are associated with the ErbB signaling system are colitis (151), rheumatoid arthritis (152) and dermatitis (153) (see section 1.5.3). Fibrotic diseases, such as pancreatic fibrosis (154), liver fibrosis (155, 156) and lung fibrosis, have also been linked to the ErbB signaling pathway. The next sections will explore the associations of ErbB and lung fibrosis in more detail.

1.4.4 ErbB Signaling System in the Lung

ErbB receptors and their ligands are expressed in the epithelial layer of the lungs and glands of the submucosal tissue under physiological conditions (157, 158). More precisely, ErbB1, ErbB2, ErbB3 and ErbB4 are expressed in cells of the bronchial epithelium and in the alveolar epithelium in ATII cells. ErbB ligands on the other hand are expressed in the glands of the respiratory tract and bronchial epithelial cells (157, 158). Interestingly, expression of ErbB ligands TGF-α, HB-EGF, HRG and AREG was also found in subepithelial lung fibroblasts (159). The connection between ErbB ligands that are released from fibroblasts and ErbB receptors in airway epithelial cells is best described in patients with breast cancer who had HER2 mutations and received TKI trastuzumab targeting ErbB2 (159). Here, trastuzumab treatment and the following inactivation of ErbB2 showed dedifferentiation and height reduction of the respiratory epithelial layer as well as development of clinical symptoms of impaired mucociliary clearance (159). Vermeer et al. demonstrated in vitro that the ErbB ligand HRG-α may stimulate the differentiation of airway epithelial cells in a similar way to fibroblasts co-cultured with airway epithelial cells (159).

1.4.5 ErbB Signaling System in Idiopathic Pulmonary Fibrosis

Among the molecular mechanisms that are believed to participate in the pathogenesis of IPF, ErbB signaling system has drawn attention since it may regulate cell proliferation, differentiation, migration and survival, all processes that are important in our understanding of the pathogenesis of IPF (115). Most evidence for the association of ErbB receptors

with IPF pathobiology exists for ErbB1 followed by ErbB2 and ErbB3, while TGF-α, AREG and NRG1-α are the ligands with the most reported relevance in IPF. Overexpression of ErbB receptors and ligands as well as their role as para- and autocrine mediators in IPF pathogenesis have been well described. Several experimental approaches of targeting ErbB receptors and ligands have been documented and have shown a pivotal role of the ErbB signaling system in IPF (160).

Fibroblasts were also found to overexpress ErbB1. Especially fibroblasts in fibroblast foci from IPF patients showed an increased ErbB1 expression (161). In cell culture, supernatants from IPF fibroblasts stimulated donor fibroblasts enhancing their proliferation rate, viability and overall ErbB1 expression. Additionally, the downstream signaling pathways of the ErbB system, such as AKT and ERK1/2 signaling pathways, were found to be more activated in donor fibroblasts after stimulation with supernatant form IPF fibroblasts (161). Furthermore, the ErbB ligand AREG was able to activate fibroblasts in vitro, leading to the upregulation of key profibrotic genes including PDGF, TGF-β and collagen type I (162). This molecular mode of action of AREG resembles that of TGF-β in fibroblasts (163). Besides inducing profibrotic signaling, TGF-β also upregulates the expression of AREG and two other ErbB ligands, HB-EGF and EREG, in fibroblasts (164, 165). Notably, the expression of all three ErbB ligands was found to depend on PDGF receptor expression (165), which is another key mediator of acute lung epithelial injury and mesenchymal cell activation (24).

Among ErbB ligands associated with IPF, TGF-α has the highest profibrotic potential. TGF-α is elevated in IPF BALF (166) and shows increased expression in ATII cells, endothelial cells and fibroblasts in IPF lungs (167, 168). In animal models, fibrotic lungs from bleomycin-treated rats exhibited elevated ErbB1 and TGF-α expression in epithelial cells, alveolar septal cells and macrophages, while TGF-α-deficient mice showed reduced fibrosis (169). Mouse models with TGF-α overexpression, controlled by a doxycycline-regulated Clara cell secretory protein (dox-CCSP), showed that TGF-α strongly promotes fibrosis, leading to collagen accumulation, tissue remodeling and increased cell proliferation (170). mRNA analysis revealed upregulation of ECM genes and downregulation of vasculogenesis genes upon TGF-α overexpression, which normalized upon halting the overexpression (171). Additionally, inducible TGF-α overexpression in club cells (tetracycline-inducible Clara cell secretory protein (rtTA-CCSP) promotor) induced pulmonary fibrosis and hypertension (172). Conflicting results were reported in a

polytetrafluoroethylene fume model, where TGF-α overexpression under a rtTA-CCSP promotor protected mice against fibrosis by reducing inflammation including IL-6 levels (173).

The ErbB signaling system also plays a critical role in the jamming transition, a shift from a mobile (unjammed) to a rigid (jammed) cellular state, closely linked to EMT and IPF pathogenesis (162). While the jammed state includes stationary epithelial cells, unjammed cells are more like mesenchymal cells and mobile. In IPF, airway epithelial cells undergoing EMT may unjam and migrate to the interstitial spaces of the distal respiratory tract and contribute to tissue remodeling, ECM production and fibrosis progression. This process may also replace the functional alveolar epithelium with an altered honeycomb cyst lining (162). Stancil et al. demonstrated that distal airway epithelial cells from IPF patients remain longer in the unjammed state, dependent on ErbB and Yes-associated Protein (YAP) signaling pathways. (162). YAP signaling regulates epithelial proliferation, differentiation (174) and TGF-β-induced EMT (175). Notably, RNA levels of AREG, ErbB2 and YAP were elevated in IPF epithelial cells, especially in the unjammed state. AREG, expressed in distal epithelial cells, promotes the unjammed state in vitro, activates fibroblasts and induces profibrotic gene expression, further emphasizing its role in IPF pathogenesis. Additionally, genetic factors like the MUC5B promoter variant (rs3570950) extended the unjammed state in AREG-treated cells (162).

Furthermore, ErbB3 deficiency (SP-C-ErbB3 model) reduced fibrosis and improved survival in bleomycin-treated mice (176). NRG1-α, a ligand for ErbB3 and ErbB4, was elevated in BALF and epithelial cells from IPF honeycomb areas and submucosal glands (34). Similarly, NRG1-β regulates airway epithelium differentiation and induces MUC5B expression, a hallmark of bronchiolized epithelium in honeycomb cysts (177).

Targeting the ErbB signaling system has emerged as a promising strategy in experimental pulmonary fibrosis models. Inhibition of ErbB1 with TKIs like AG1478 reduced fibroblast proliferation and collagen levels in vanadium pentoxide-induced fibrosis in rats (178) and protected mice against bleomycin-induced fibrosis (163). The ErbB1 TKI gefitinib, used in NSCLC treatment (179), reduced fibrosis and improved lung mechanics in bleomycin-treated (180, 181) and TGF-α-overexpressing mice (172). However, conflicting data suggest that gefitinib may impair ATII cell regeneration, worsening fibrosis in certain contexts (182). Inhibiting ErbB2 has also been effective. Dual TKI lapatinib, targeting ErbB1 and ErbB2, combined with a PDGFR inhibitor imatinib, stabilized lung function and prevented myofibroblast activation (165), while an ErbB2-antibody 2C4

blocked fibrosis progression in bleomycin-treated mice (183). Direct targeting of AREG using siRNA protected mice from fibrosis in a dox-CCSP-TGF-β1 overexpression model (163). Further downstream, inhibition of the PI3K/AKT pathway with PX-866 (184) and inhibition of the MEK/ERK pathway with ARRY-142886 successfully reduced fibrosis and preserved lung function in a TGF-α overexpression model in mice (185). While these results are promising, caution is needed due to ErbB's role in tissue integrity and regeneration. Reports of TKI-induced ILD (135) and conflicting findings (173, 182) highlight the need to consider patient history, genetic susceptibility and treatment timing (186). Future research is essential to determine the safety of targeting the ErbB system and the efficacy of such treatment strategies in IPF.

1.5 Epiregulin

1.5.1 Structure and Cellular Activities

EREG is a member of the ErbB family, acting as a ligand for ErbB1 and ErbB4 receptors. Like all ligands of the ErbB family, EREG is a peptide hormone that regulates cell growth, differentiation, proliferation and cell survival (32, 111, 187, 188). On a molecular level, EREG is a 46 amino acid-long protein that shares the structural EGF domain (86, 87). EREG is proteolytically cleaved by MMPs and ADAMs from its transmembrane-precursor-protein and is released into the extracellular space (112, 113). Upon binding to the ErbB receptors ErbB1 and ErbB4, EREG triggers their homo- or heterodimerization (92, 95). Phosphorylation of the ErbB receptors by their intrinsic tyrosine kinase activity (103) leads to the initiation of multiple downstream signaling pathways including the MAPK/ERK pathway (104), the PI3K/AKT pathway (105), the PLCγ pathway (106) and the JAK/STAT pathway (85), finally triggering transcriptional changes that are critical for processes such as cell growth, proliferation, migration, survival and collagen gene expression (107).

1.5.2 Functions in Physiology

Cell differentiation is a key function of the ErbB signaling system, with EREG playing a central regulatory role. In vitro studies show that EREG, along with other ErbB ligands, stimulates lung epithelial cell growth and differentiation, leading to thicker, more differentiated epithelial layers (159). EREG also supports epithelial proliferation in tissues like the intestine, where it contributes to the maintenance of mucosal integrity via induction of ErbB ligand expression (189). Additionally, EREG promotes skin keratinocyte

proliferation in vitro (190) and induces the expression of angiogenic genes during cutaneous (191) and corneal wound healing (192, 193).

Most evidence of EREG's role in angiogenesis and vascular remodeling comes from research on cancer progression, metastasis and atherosclerosis research, as discussed in section 1.5.3. However, EREG also plays a crucial role in these processes under normal conditions. In vascular smooth muscle cells (VSMCs), EREG is involved in regulating remodeling through vasoactive agents such as angiotensin II, endothelin-1 and α-thrombin (194). These agents stimulate VSMCs to overexpress the EREG gene and release EREG. EREG, through autocrine stimulation, promotes mitogenesis and DNA synthesis in VSMCs, similar to PDGF, suggesting its role in vascular remodeling (194). Additionally, EREG is secreted by VSMCs in response to coagulation factor Xa, promoting cell proliferation and mitogenesis independently of PDGF (195).

The role of EREG in inflammation is complex and not fully understood, with overlapping effects in wound healing and tumorigenesis. EREG is expressed in tissue-resident antigen-presenting cells (APCs), such as macrophages and dendritic cells (188), but not in lymphatic tissues such as bone marrow, thymus, lymph nodes or the spleen (153). In EREG-deficient mice, dendritic cells and macrophages stimulated with toll-like receptor (TLR) agonists (lipopolysaccharide (LPS) and peptidoglycan (PGN)) showed reduced IL-6 and TNF-α levels, suggesting that EREG regulates proinflammatory cytokine production (153, 196). IL-1β and TNF-α can induce EREG expression and thereby proliferation of colonic subepithelial myofibroblasts (197), while TLR4 activation upregulates EREG and AREG during intestinal wound healing (198). Since inflammation in homeostasis and pathological processes overlap considerably, the pathological findings related to inflammation are addressed in the following section 1.5.3.

1.5.3 Role of Epiregulin in Pathology

The role of EREG in various pathologies is primarily linked to its function as a growth-regulating peptide hormone, influencing cell proliferation, differentiation and survival (188). Like the entire ErbB signaling system, EREG is predominantly associated with cancer biology. Here, EREG mainly affects tumor growth, metastasis and angiogenesis (188). In addition to its association with cancer, EREG is also important for several inflammatory processes due to its role in regulating immunomodulatory mechanisms (188). In the lung, EREG transcription is upregulated in response to various carcinogens found in cigarette smoke, a well-known risk factor for lung cancer and IPF (8, 199). These

carcinogens include substances such as benzo[a]pyrene (200), vinyl carbamate (201), urethane (202) and 3-nitrobenzanthrone (203) that promote malignant transformation of airway epithelial cells. Upregulated expression of EREG in cancer tissue is often correlated with poor prognosis and resistance to tumor therapy (204). EREG expression has been observed and correlated with poor prognosis in various types of cancer including breast (205), cervical (206), lung (207, 208), oral squamous cell (OSCC) (209), gastric, bladder, esophageal, pancreatic and head and neck squamous cell carcinoma (210). Besides carcinomas, EREG is also associated with other tumor entities like glioblastoma (211).

Association of EREG expression with lung cancer is widely studied. While EREG expression is not detected in small cell lung cancer (SCLC), in NSCLC it acts as a strong oncogene (212). The most common targetable oncogenic mutations in NSCLC are Kirsten rat sarcoma viral oncogene homolog (KRAS) (213), EGFR (214) and B-Raf proto-oncogene **(**BRAF) mutations (215). Such mutations have been identified to induce overexpression of EREG in cancer cells (216). Interestingly, KRAS mutations in NSCLC cells activate the MEK/ERK pathway, which induces transcriptional upregulation of ADAM17 (217). Since ADAM17 cleaves ErbB ligands, including EREG, from its precursors, it was suspected to be a major producer of mature ErbB ligands and of ErbB activation in NSCLC. Consequently, tissue from NSCLC patients showed increased expression of ADAM17 (218) and in ErbB1 mutated NSCLC cells, ADAM17 inhibition led to impaired cell growth (219). Other sources of EREG in the tumor microenvironment are mainly cancer-associated fibroblasts (CAF), where upregulated EREG expression has been found in several tumors including colitis-associated tumors (114) and OSCC (220). These EREG expressing CAFs are associated with invasion, metastasis or recurrence of these tumors and correlate with a poor prognosis (114, 220, 221). Also in in vitro and in vivo studies, EREG directly and EREG from EREG-expressing fibroblasts were able to stimulate proliferation, invasion and migration of cancer cells (114, 220). Interestingly, EREG overexpression in donor fibroblasts promotes the expression of CAF markers, implying that EREG plays a crucial role in auto- and paracrine activation of CAFs (220).

Another oncogenic feature in which EREG is involved is EMT. In cancer, EMT is crucial for tumor invasion and metastasis (222). TGF-β, a potent inducer of EMT (see 1.3.3), activates intracellular pathways that regulate cell proliferation and angiogenesis in oral squamous carcinoma cells. Additionally, TGF-β also upregulates the expression of EREG and HB-EGF in these cells (223). As reported earlier, supernatant from CAFs induced EMT in OSCC cells via EREG- and JAK2/STAT3-dependent pathways (220)

In addition to its role in cancer, EREG also affects the immune system and inflammatory processes (188). EREG is able to induce cyclooxygenase-2 (COX-2), an enzyme that promotes the synthesis of prostaglandin E2 (PGE2) (224). Prostaglandins like PGE2 are usually released in response to pro-inflammatory signals (225). In rheumatoid arthritis, EREG and AREG have been reported to stimulate COX-2 expression and thereby increase the levels of PGE2 in fibroblast-like synoviocytes, which are key players in the disease's progression (152, 226). In macrophages, Toll-like receptor activation by LPS and PGN induces the synthesis of several cytokines including IL-6 and TNF-α, which were found to be dependent on the presence of EREG (153). Additionally, EREG released from macrophages regulates interleukin-1-α (IL-1α)-mediated interleukin-18 (IL-18) downregulation, which modulates the inflammatory response. This mechanism contributes to chronic dermatitis in mice (153). Additionally, EREG is produced by dendritic cells in response to type I interferon, a key cytokine in the regulation of inflammatory processes. In type I interferon-stimulated dendritic cells, released EREG activates EGFR on fibroblasts, promoting ECM protein production and fibrogenesis in the skin and lung during inflammatory processes (227). Also, in the lung, various infectious diseases like rhinovirus or mycoplasma pneumoniae infections can lead to upregulation of EREG in respiratory epithelial cells, which, in turn, leads to interleukin-8 (IL-8) production, contributing to proinflammatory processes and tissue remodeling in such diseases (228, 229). Overall, EREG seems to play an important role in tumorigenesis as well as inflammatory processes and diseases. Given EREG's involvement in oncogenic processes like EMT and TGF-β driven profibrotic mechanisms, it may similarly contribute to fibrotic mechanisms underlying the development of IPF.

1.6 Cellular Senescence

1.6.1 Biology of Senescence

One of the recently discussed mechanisms contributing to the pathogenesis and progression of IPF is cellular senescence. Cellular senescence, in contrast to apoptosis or necrosis, is a state in which cells stop dividing but remain metabolically active through altered gene expression, without going into apoptosis and cell death (59). Cellular senescence can be triggered by DNA damage, oxidative stress, telomere shortening or oncogene activation in cancer (230–232). In detail, these triggers activate the DNA damage response (DDR) pathway leading to the p53-induced $p21^{Waf1/Cip1}$ (p21) activation, which inhibits

cyclin dependent kinase (CDK) 2 (CDK2) (233). Alternatively, the $p16^{Ink4a}$ pathway inhibits CDK4 and CDK6 independently of the DDR (59). CDK inhibition by p21 or p16 unblocks the retinoblastoma protein (Rb), which is normally blocked by CDKs. Rb then halts the S phase of the cell cycle by repressing E2F genes (233). Another CDK-independent pathway is the activation of BRAF, which creates mitochondrial redox stress to induce senescence (234).

If the activation of the $p16^{Ink4a}$ and p53-p21 axes is persistent (235), the cells undergo permanent senescence, characterized by genetic and epigenetic remodeling (236, 237), finally leading to the secretion of a number of mediators referred to as the senescence-associated secretory phenotype (SASP). SASP is characterized by the release of several pro-inflammatory cytokines (e.g. IL-6, IL-1β, IL-8), growth factors (e.g. TGF-β, VEGF), proteases (MMPs, serine proteases like urokinase plasminogen activator (uPA) and tissue plasminogen activator (tPA) (238)), as well as several other mediators, including ECM components like fibronectin and collagens (59). Senescent cells affect various biological processes in physiology and pathology by their SASP, including inflammation (239), angiogenesis (240), EMT (241) and repairing as well as healing processes (242). Here, senescent cells and SASP can either promote tissue repair, cell clearance and tumor suppressor functions (59) or enhance chronic inflammation, maladaptive remodeling and tissue damage (60).

1.6.2 Cellular Senescence in Idiopathic Pulmonary Fibrosis

In IPF, markers of cellular senescence like p16, p21 and β-galactosidase activity have been identified by several studies in fibroblasts from fibroblast foci and hyperplastic airway epithelial cells lining honeycomb cysts (57, 58, 60). While DNA damage is associated with activation of cellular senescence, the amount of DNA damage marked by phosphorylated histone H2Ax (γH2Ax) levels and senescence biomarker telomere-associated foci (TAF) were also elevated in IPF patients (60). Additionally, p16 levels correlated with disease progression and severity in IPF patients, while their lung secretome, showed an increased expression of matrix-remodeling proteins and collagen type I and vascular cell adhesion molecule I (VCAM) (60)

Also in animal models, mice receiving bleomycin showed increased DNA damage due to activation of the p53-p21 axis and an altered secretome represented by a number of SASP proinflammatory and profibrotic mediators, such as IL-6, TNF-α, MMP-2 and MMP-9 in the lung tissue (243). In a separate study on bleomycin-induced lung fibrosis,

fluorescence-activated cell sorting (FACS) analysis of lung tissue showed that bleomycin-treated mice exhibited upregulation of p16 and several components of the SASP in fibroblasts and epithelial cells. The SASP components included monocyte chemotactic protein 1 (MCP-1), PAI-1, TNF-α, MMP-10, MMP-12, collagen type I and TGF-β (60).

In in vitro studies, ATII cells showed increased β-galactosidase activity and p21 levels after treatment with bleomycin (244), while fibroblasts, in which senescence was experimentally induced by irradiation, showed upregulated expression of TGF-β and IL-6 (60). Interestingly, the media from senescent fibroblasts not only stimulated donor fibroblasts to express α-SMA, similarly to the effects of the TGF-β, but also induced collagen type I and II, fibronectin and ACTA-2 (60).

Targeting senescent cells as an approach to reverse aging effects has been featured by several studies. For instance, targeting 16^{Ink4a}-positive senescent cells using a transgene-inducible elimination model (INK-ATTAC) was able to reverse age-related pathologies and delay their onset (245). Additionally, age-related decreases in lung function were restored in mice by targeting $p19^{ARF}$-positive senescent cells using a toxin receptor-mediated cell knockout (246). Senescent fibroblasts were also successfully targeted in vitro by treatment with senolytic drugs, and in mice treated with bleomycin, eradication of senescent cells using the same drugs attenuated the expression of SASP-associated factors, halted the progression of pulmonary fibrosis, improved lung function, but did not affect lung histology (60). Both findings offer a promising therapeutic approach and potential tool for the treatment of lung fibrosis.

1.6.2.1 Findings for ErbB Signaling System and Senescence.

Contradictory results have been published regarding the role of the ErbB system in the regulation of senescence (247, 248). For instance, EGF treatment of donor fibroblasts and endothelial cells induced cellular senescence by activating the Ras-BRAF-Erk1/2 pathway. Moreover, EGF triggered the release of SASP-associated factors such as IL-8 and MMP3 in vitro. Additionally, activation of senescence by the cytokine stromal cell-derived factor 1-α (SDF-1α) led to increased ErbB1 phosphorylation and treatment with an ErbB1 TKI markedly attenuated the activity of senescence-inducing cytokines (249).

An analysis of the secretome from HER2-overexpressing breast cancer cells of various origins revealed that cytokines including IL-6, were almost exclusively secreted by senescent cells. Notably, the proportion of senescent cells was directly related to the level

of HER2 expression. Additionally, inhibition of IL-6 reduced the proliferation of HER2-positive patient-derived xenografts. HER2 expression-associated senescence appears to be essential for the progression of HER2-positive breast cancer in vivo, as the secretome including IL-6, is required to promote the growth of non-senescent cells through a paracrine mechanism (250).

In conclusion, the role of the ErbB signaling system in senescence is not yet fully understood. So far, promoting effects have been observed, but more research is required to determine its role in senescence and its implications for diseases such as cancer and age-related conditions like fibrosis.

1.7 Aim of the Study

The ErbB signaling system is known to affect the cellular differentiation, proliferation and survival in the lung (see 1.4.4). Additionally, it is well integrated into the complex network of paracrine and autocrine cell interactions in lung fibrosis. Especially the ErbB1 receptor is known to be overexpressed in IPF lungs and IPF fibroblasts (161, 251). It has also been identified as a key regulator of fibroblast activation as well as EMT and has already been targeted by TKIs in many experimental approaches (163, 172, 178, 180, 181, 252). While the role of ErbB ligand TGF-α (169, 170) and AREG (162) in fibrogenesis is well established, the role of other ErbB ligands including EREG is elusive. Therefore, the overreaching aim of this study was to investigate how EREG may contribute to the initiation and progression of lung fibrosis.

In particular, the specific aims of these studies were:

In vitro studies:

- To evaluate the effects of EREG on the morphology of human airway epithelial cells.
- To investigate the impact of EREG on airway epithelial cellular proliferation and senescence induction.

In vivo studies:

- To assess the effects of EREG exposure on development of lung fibrosis in bleomycin-treated mice, analyzing the effects on lung morphology, lung function and the expression of SASP-associated factors in murine BALF.
- To characterize the effects of EREG on cellular proliferation and senescence induction in airway epithelial cells from bleomycin-treated murine lungs.

2 Material and Methods

2.1 Material

2.1.1 Apparatuses and Equipment

Name	**Manufacturer / Company**
BD FACS Aria III	BD Biosciences, Franklin Lakes, NJ, USA
BioRad TC 20 Automated Cell Counter	Bio-Rad Laboratories, Hercules, CA, USA
ChemiDoc™ Touch Imaging System	Bio-Rad Laboratories, Hercules, CA, USA
CO_2 Incubator CB 170	Binder GmbH, Tuttlingen, Germany
CometAssay® Electrophoresis System II	Bio-Techne, Minneapolis, MA, USA
Compact Gas Anesthesia System 21100	Ugo Basile S.R.L., Gemonio, Italy
Eppendorf Multipette® Plus Pipet	Eppendorf AG, Hamburg, Germany
Eppendorf Research Plus Pipet	Eppendorf AG, Hamburg, Germany
Five Easy pH-Meter	Mettler Toledo, Columbus, OH, USA
FlexiVent FX	Emka Technologies, Paris, France
gentleMACS™ Dissociator	Miltenyi Biotec B.V. & Co. KG, Bergisch Gladbach, Germany
GFL 1004 Incubator Bath	Gesellschaft für Labortechnik mbH, Burgwedel, Germany
Gilson P2, P10 P20, P200 P1000 Pipet	Gilson, Middleton, WI, USA
Gilson Pipetman Classic P10 Pipet	Gilson, Middleton, WI, USA
Gilson Pipetman L P1000L Pipet	Gilson, Middleton, WI, USA

Heraeus Fresco 21 Microcentrifuge	Thermo-Fisher Scientific, Waltham, MA, USA
Heraeus Function Line Incubator	Thermo-Fisher Scientific, Waltham, MA, USA
Hettich Benelux AC 02 Vacuum System	Andreas Hettich GmbH & Co KG, Tuttlingen, Germany
HistoCore Autocut Automated Rotary Microtome	Leica Microsystems GmbH, Wetzlar, Germany
HLC Cooling-ThermoMixer MKR 13	DITABIS AG - Digital Biomedical Imaging Systems AG, Pforzheim, Germany
Holten Safe 2010 Laminar Air Flow	Thermo-Fisher Scientific, Waltham, MA, USA
Hybaid Shake 'n' Stack Hybridization Oven	Thermo-Fisher Scientific, Waltham, MA, USA
Integra PipetBoy 2 Automatic Pipet Pump	Integra Biosciences Corp., Hudson, NH, USA
Leica DMR 2000 Microscope	Leica Microsystems GmbH, Wetzlar, Germany
Leica HI1210 Water Bath	Leica Microsystems GmbH, Wetzlar, Germany
Leica HI1220 Flattening Table	Leica Microsystems GmbH, Wetzlar, Germany
Leica M80 Stereo Microscope	Leica Microsystems GmbH, Wetzlar, Germany
Leica SFL 4000 Stereo Microscope	Leica Microsystems GmbH, Wetzlar, Germany
Leica TCSSP5 Microscope	Leica Microsystems GmbH, Wetzlar, Germany
MCO-17-AIC CO_2 Incubator	Sanyo Denki. K.K., Moriguchi, Japan
Microcentrifuge 5415R	Eppendorf AG, Hamburg, Germany
MicroSprayer®Aerosolizer FMJ-250 High Pressure Syringe	Penn-Century Inc., Wyndmoor, PA USA
Mikro 185 Centrifuge	Andreas Hettich GmbH & Co KG, Tuttlingen, Germany
MiniVent Ventilator for Mice (Model 845)	Hugo Sachs Elektronik Harvard Apparatus GmbH, March-Hugstetten Germany
Mouse Restrainer Type A	G&P Kunststofftechnik GbR, Kassel, Germany

MR Hei-Standard Magnetic Stirrer	Heidolph Instruments, Schwabach, Germany
New Classic MF Precision Balance	Mettler Toledo, Columbus, OH, USA
Nikon Eclipse CI-L Microscope	Nikon, Tokio, Japan
Pannoramic DESK II DW Digital Slide Scanner	3DHISTECH, Budapest, Hungary
Philips XL30 ScEM (scanning electron microscope)	Philips / FEI, Hillsboro, OR, USA
Rotamax 120 Shaker	Heidolph Instruments, Schwabach, Germany
Rotina 35 Type 1705 Centrifuge	Andreas Hettich GmbH & Co KG, Tuttlingen, Germany
SP8 Lightning Confocal Microscope	Leica Microsystems, Wetzlar, Germany
Spectramax 190 Microplate Reader	San Jose, CA, USA
SpectraMax 190 Plate Reader	Molecular Devices, San José, CA, USA
Spot-RT Slider Digital Microscope Camera	Diagnostic Instruments Inc., Sterling Heights, MI, USA
SRT9 Roller Mixer	Cole-Parmer Ltd., Staffordshire, United Kingdom
StainTray™ Humidity Chamber	Carl Roth GmbH, Karlsruhe, Germany
Thriller Thermoshaker Incubator	PeQlab, Erlangen, Germany
Vortex Genie 2 G56OE Mixer	Electro Scientific Industries, Inc. Portland, OR, USA
YJ-2005S Microscope	Ningbo Tianyu Optoelectronic Technology, Beilun, Ningbo, China
Zeiss EM902 TEM (transmissions electron microscope)	Carl Zeiss Microscopy GmbH, Jena, Germany

2.1.2 Software

Software	**Manufacturer / Company**
BD FACS Diva Software 8.0.1	BD Biosciences, Franklin Lakes, NJ, USA

CometAssay® Analysis Software	Bio-Techne, Minneapolis, MA, USA
flexiWare™ 8	Emka Technologies, Paris, France
Graph Pad Prism 10.1.2	GraphPad Software Inc., Boston, MA, USA
Image Lab Software 7.0	Bio-Rad Laboratories Inc., Hercules, CA, USA
ImageJ 1.54j / "Fiji"	Wayne Rasband / National Institutes of Health / University of Wisconsin, Madison, WI, USA
LAS X Software 3.5.7	Leica Microsystems, Wetzlar, Germany
MetaMorph Software 5.0	Molocular Devices LLC, San José, CA, USA
NIS-Elements D Software 6.02.01	Nikon, Tokio, Japan

2.1.3 Chemicals, Reagents and Solutions

Acetic acid	Carl Roth GmbH, Karlsruhe, Germany
Agarose	Carl Roth GmbH, Karlsruhe, Germany
Airway Epithelial Cell Growth Medium	PromoCell GmbH, Heidelberg, Germany
Alexa Fluor 488 streptavidin	BioLegend, San Diego, CA, USA
Amphotericin B	Merck KGaA, Darmstadt, Germany
Antibody Diluent	Zytomed Systems GmbH, Berlin, Germany
BEBM (Bronchial Epithelial Cell Growth Basal Medium)	Lonza Group AG, Basel, Switzerland
Bleomedac® 15 mg, 15000 I.E., bleomycin sulfate	medac GmbH, Wedel, Germany
BSA (bovine serum albumin)	Sigma-Aldrich, St. Louis, MO, USA
Calcium chloride	Carl Roth GmbH, Karlsruhe, Germany
Collagen I	Merck KGaA, Darmstadt, Germany
cOmplete™ Protease Inhibitor Cocktail	Roche Holding, Basel, Switzerland
DAKO Fluorescent Mounting Medium	Dako, Glostrup, Denmark
DAPI (4',6-diamino-2-phenylindole)	Sigma-Aldrich, St. Louis, MA, USA
Desoxyribonuklease (DNase) I	Serva Electrophoresis GmbH, Heidelberg, Germany

D-glucose	Carl Roth GmbH, Karlsruhe, Germany
Disodium hydrogen phosphate	Carl Roth GmbH, Karlsruhe, Germany
Dispase II	Roche Holding, Basel, Switzerland
DMEM (Dulbecco's Modified Eagle Medium)	Invitrogen Life Technologies, Waltham, MA, USA
DMEM (Dulbecco's modified Eagle's Medium)/F-12	Invitrogen Life Technologies, Waltham, MA, USA
DMSO (dimethyl sulfoxide)	Carl Roth GmbH, Karlsruhe, Germany
Double-distilled water / Aqua Bidest	Carl Roth GmbH, Karlsruhe, Germany
Doxorubicin hydrochloride	Santa Cruz Biotechnology, Santa Cruz, CA, USA
DTT (dithiothreitol)	Carl Roth GmbH, Karlsruhe, Germany
ECL Western Blot Detection Reagent	GE Healthcare, Buckinghamshire, United Kingdom
EDTA (ethylendiamintetraacetate)	Invitrogen Life Technologies, Waltham, MA, USA
Eosin Y	Carl Roth GmbH, Karlsruhe, Germany
Epon 812, epoxy embedding medium	(Sigma-Aldrich, St. Louis, MA, USA)
Ethanol	Sigma-Aldrich, St. Louis, Missouri, USA
Fast Enzyme (ready-to-use)	Zytomed Systems GmbH, Berlin, Germany
Fetal calf serum (FCS)	PromoCell, Heidelberg, Germany
Fibronectin, human	Corning Inc., Amsterdam, Netherlands
Glycerol	Carl Roth GmbH, Karlsruhe, Germany
Glycine	Carl Roth GmbH, Karlsruhe, Germany
Halt^{TM} Protease Inhibitor Cocktail	Thermo-Fisher Scientific, Waltham, Massachusetts, USA
HBSS (Hank's Balanced Salt Solution)	Carl Roth GmbH, Karlsruhe, Germany
HEPES (2-(4-(2-hydroxyethyl)piperazin-1-yl)-ethane sulfonic acid)	Sigma-Aldrich, St. Louis, MA, USA

Hematoxylin solution A, according to Weigert	Carl Roth GmbH, Karlsruhe, Germany
Hematoxylin solution B, according to Weigert	Carl Roth GmbH, Karlsruhe, Germany
Heparin sodium 25000 I.U./5ml injectable solution	Ratiopharm GmbH, Ulm, Germany
IsoFlo 100% (isoflurane)	Zoetis, Parsippany, NJ, USA
Isopropanol	Sigma-Aldirch, St. Louis, MO, USA
Isotonic sodium chloride solution 0,9%	Braun, Melsungen, Germany
Ketamine 100mg/ml injectable solution	CP-Pharma GmbH, Burgdorf, Germany
Light Green SF (C.I. 42095)	Carl Roth GmbH, Karlsruhe, Germany
Low melting point agarose	Sigma-Aldrich, St. Louis, Missouri, USA
Magnesium chloride	Carl Roth GmbH, Karlsruhe, Germany
Magnesium sulfate	Carl Roth GmbH, Karlsruhe, Germany
Orange G (C.I. 16230)	Carl Roth GmbH, Karlsruhe, Germany
Osmium tetroxide	Carl Roth GmbH, Karlsruhe, Germany
Penicilline / streptomycine (1000U/ml)	Thermo-Fisher Scientific, Waltham, MA, USA
PFA (paraformaldehyde)	Carl Roth GmbH, Karlsruhe, Germany
PMSF (phenylmethylsulfonyl fluoride) protease inhibitor	Thermo-Fisher Scientific, Waltham, MA, USA
Potassium chloride	Carl Roth GmbH, Karlsruhe, Germany
Potassium dihydrogen phosphate	Carl Roth GmbH, Karlsruhe, Germany
Potassium phosphate	Carl Roth GmbH, Karlsruhe, Germany
ProLong™ Glass Antifade Mountant	Invitrogen Life Technologies, Waltham, MA, USA
PRONASE® Protease, Streptomyces griseus	Merck KGaA, Darmstadt, Germany
Proteinase K	Thermo-Fisher Scientific Inc., Waltham, MA, USA

PureCol® Type I Bovine Collagen Solution, 3 mg/ml	AdvancedBiomatrix Inc. Carlsbad, CA, USA
Recombinant Human Epiregulin (E. coli derived), 1195-EP/CF	Bio-Techne, Minneapolis, MA, USA
RNase-free water / Ampuwa	Fresenius Kabi, Bad Homburg, Germany
Rodent Block M	Zytomed Systems GmbH, Berlin, Germany
Rodent Decloaker	Zytomed Systems GmbH, Berlin, Germany
Roti Histo Kit II	Carl Roth GmbH, Karlsruhe, Germany
RPMI (Roswell Park Memorial Institute medium) 1640	Invitrogen Life Technologies, Waltham, MA, USA
SDS (sodium dodecyl sulfate)	Sigma-Aldrich, St. Louis, MA, USA
Skim milk powder (5%)	Sigma Aldrich, St. Louis, MO, USA
Sodium acetate	Carl Roth GmbH, Karlsruhe, Germany
Sodium bicarbonate	Carl Roth GmbH, Karlsruhe, Germany
Sodium chloride	Carl Roth GmbH, Karlsruhe, Germany
Sodium citrate	Carl Roth GmbH, Karlsruhe, Germany
Sodium hydrogen phosphate	Carl Roth GmbH, Karlsruhe, Germany
Sterile water	Braun, Melsungen, Germany
Sulfuric acid	Carl Roth GmbH, Karslruhe, Germany
TRIS (tris(hydroxymethyl)amin methane)	Carl Roth GmbH, Karlsruhe, Germany
Triton X-100 (octylphenoxypoly-ethoxyethanol)	Carl Roth GmbH, Karlsruhe, Germany
TriZol™	Invitrogen Life Technologies, Waltham, MA, USA
Trypan blue solution (0,4%)	Thermo-Fisher Scientific, Waltham, MA, USA
Trypsin	Sigma-Aldrich, St. Louis, Missouri, USA
Trypsin/EDTA	Thermo-Fisher Scientific, Waltham, MA, USA
Tween 20	Carl Roth GmbH, Karlsruhe, Germany
Ultracomp eBeads™ Compensa-tion Beads	Thermo-Fisher Scientific, Waltham, MA, USA
Uranyl acetate	Merck KGaA, Darmstadt, Germany

Xylasel 20mg/ml injection solution (xylazine)	Selectavet Dr. Otto Fischer GmbH, Munich, Germany
Xylene	Carl Roth GmbH, Karlsruhe, Germany
Xylidin de Ponceau 2R	Carl Roth GmbH, Karlsruhe, Germany

2.1.4 Expandable Materials

Name	**Manufacturer / Company**
35 mm cell culture dish	Merck KGaA, Darmstadt, Germany
96-well cell culture plates	Thermo-Fisher Scientific, Waltham, MA, USA
CometSlide™ slide	R&D Systems, Minneapolis, MN, USA
Costar Transwell Permeable Supports	Corning Inc., Amsterdam, Netherlands
Falcon® Cell Strainer, 20, 40, 70 µm	Corning Inc., Amsterdam, Netherlands
Falcon® 50ml tubes	Greiner Bio-One, Frickenhausen, Germany
Filter, 22 µm pore size	Carl Roth GmbH, Karlsruhe, Germany
gentleMACS™ C Tubes	Miltenyi Biotec B.V. & Co. KG, Bergisch Gladbach, Germany
Injekt® Luer Solo, 2, 5, 10 ml syringe	Braun, Melsungen, Germany
Injekt®-F Solo, 1 ml syringe	Braun, Melsungen, Germany
MS200 & 300 Microtome Blades	micros Austria, St. Veit/Glan, Austria
Petri dish 94x16mm	Greiner Bio-One GmbH, Frickenhausen, Germany
Pipet tips 1000 µl, 200 µl, 20 µl	Eppendorf, Hamburg, Germany
Precision Cover Glasses, thickness No. 1.5 (tol. ±5 µm)	Paul Marienfeld GmbH, Lauda-Königshofen, Germany
SafeSeal Reaction Tubes, 500, 1500, 2000 µl	Sarstedt, Nümbrecht, Germany
Sterican® 30G needle	Braun, Melsungen, Germany
Sterican® Gr. 1, G 20 needle	Braun, Melsungen, Germany
Sterican® Gr. 20, G 27 needle	Braun, Melsungen, Germany

Superfrost® Plus Gold Adhesion Slides	Carl Roth GmbH, Karlsruhe, Germany
Ted Pella Inc Carbon Tape, conductive adhesive tape	Thermo-Fisher Scientific, Waltham, MA, USA
Transwell® 6.5mm, 0.4 µm Pore Polyester Membrane Insert	Corning Inc., Amsterdam, Netherlands
Vasofix® Safety G 20, G24	Braun, Melsungen, Germany

2.1.5 Kits

Kit	**Manufacturer / Company**
Alexa Fluor™ 647 Tyramide Super Boost™ Kit - CAT-No.: #B40926	Invitrogen Life Technologies, Waltham, MA, USA
CometAssay® Kit - CAT-No.: #4250-050-K	R&D Systems, Minneapolis, MN, USA
CometAssay® Silver Staining Components Kit - CAT-No.: #4254-200-K	R&D Systems, Minneapolis, MN, USA
DuoSet® ELISA Kit Mouse IL-6 - CAT-No.: #DY406	R&D Systems, Minneapolis, MN, USA
DuoSet® Human TGF-α - CAT-No.: #DY239	R&D Systems, Minneapolis, MN, USA
DuoSet® Mouse Epiregulin - CAT-No.: #DY1068	R&D Systems, Minneapolis, MN, USA
DuoSet® Mouse TGF-β1 - CAT-No.: #DY1679	R&D Systems, Minneapolis, MN, USA
DuoSet® Mouse TweakR/TNFRSF12 - CAT-No.: #DY1610	R&D Systems, Minneapolis, MN, USA
eBioscience™ Foxp3/Transcription Factor Staining Buffer Set - CAT-No.: #00-5523-0	Thermo-Fisher Scientific, Waltham, MA, USA
MaxBlock™ Autofluorescence Reducing Reagent Kit - CAT-No.: #MB-L	MaxVision Biosciences Inc., Washington, D.C., USA

PeproTech® Murine TNF-α Standard TMB ELISA Development Kit - CAT-No.: #900-T54	Thermo-Fisher Scientific, Waltham, MA, USA
Permanent AP Red Kit - CAT-No.: #ZUC001-125	Zytomed Systems GmbH, Berlin, Germany
Quantikine® ELISA Kit Mouse IL-1a/IL-1F1 - CAT-No.: #MLA00	R&D Systems, Minneapolis, MN, USA
Quantikine® ELISA Kit Mouse CXCL2/MIP-2 - CAT-No.: #MM200	R&D Systems, Minneapolis, MN, USA
Quantikine® ELISA Kit Total MMP-2 - CAT-No.: #MMP200	R&D Systems, Minneapolis, MN, USA
Senescence beta-Galactosidase Staining Kit #9860 - CAT-No.: 9860S	Cell Signaling Technology, Leiden, Netherlands
TMB Substrate Kit - CAT-No.: #34021	Thermo-Fisher Scientific, Waltham, MA, USA
Zytochem Plus (AP) Polymer Kit POLAP-006 - CAT-No.: #POLAP-006	Zytomed Systems GmbH, Berlin, Germany

2.1.6 Antibodies

2.1.6.1 Primary Antibodies

Antibody	**Manufacturer / Company**
Anti-Ki67 antibody - Polyclonal rabbit IgG - CAT-No.: #ab15580	Abcam, Cambridge, United Kingdom
Anti-p21/WAF1/Cip1 antibody, clone CP74 - Monoclonal mouse IgG2bκ - CAT-No.: #05-655	Merck Millipore, Burlington, MA, USA
Anti-p63 antibody (4A4) - Monoclonal mouse IgG2a	Abcam, Cambridge, United Kingdom

- CAT-No.: #ab3239	
Anti-phospho-Histone H2A.X antibody (Ser139), clone JBW301 - Mouse monoclonal IgG1 - CAT-No.: #05-636	Merck Millipore, Burlington, MA, USA
p21 Waf1/Cip1 12D1 antibody - Monoclonal rabbit IgG - CAT-No.: #2947	Cell Signaling Technology, Leiden, Netherlands
p63 antibody (D-9) - Monoclonal mouse IgG2aκ - CAT-No.: #sc-25268	Santa Cruz Biotechnology, Santa Cruz, CA, USA
P63 SFI-6 antibody - Monoclonal mouse IgG - CAT-No.: #P1006T50	Innovative Diagnostik-Systeme (DCS), Haussee, Germany
PCNA (D3H8P) XPR antibody - Monoclonal rabbit IgG - CAT-No.: #13110	Cell Signaling Technology, Leiden, Netherlands
PCNA (PC10) antibody - Mouse monoclonal IgG2a - CAT-No.: #2586	Cell Signaling Technology, Leiden, Netherlands
Phospho-Histone H2A.X (Ser139) (20E3) antibody - Rabbit monoclonal Ab - CAT-No.: #9718	Cell Signaling Technology, Leiden, Netherlands
Recombinant anti-p63 antibody (EPR5701) - Monoclonal rabbit IgG - CAT-No.: #ab124762	Abcam, Cambridge, United Kingdom
ΔNp63: Purified anti-p63 (N) antibody Poly 6190 - Polyclonal rabbit IgG - CAT-No.: #619001	BioLegend, San Diego, CA, USA

2.1.6.2 Secondary Antibodies

Antibody	**Manufacturer / Company**
Alexa Fluor™ 488 antibody - F(ab')2-Goat anti-rabbit IgG (H+L) cross-adsorbed - CAT-No.: #A-1107	Invitrogen Life Technologies, Waltham, MA, USA

Alexa Fluor™ 488 cross-adsorbed antibody - Goat anti-mouse IgG (H+L) - CAT-No.: #A-11001	Invitrogen Life Technologies, Waltham, MA, USA
Alexa Fluor™ 488 cross-adsorbed antibody - Goat anti-rat IgG (H+L) - CAT-No.: #A-11006	Invitrogen Life Technologies, Waltham, MA, USA
Alexa Fluor™ 488 highly cross-adsorbed antibody - Donkey anti-rabbit IgG (H+L) - CAT-No.: #A-21206	Invitrogen Life Technologies, Waltham, MA, USA
Alexa Fluor™ 555 cross-adsorbed antibody - Goat anti-rabbit IgG (H+L) - CAT-No.: #A-21428	Invitrogen Life Technologies, Waltham, MA, USA
Alexa Fluor™ 555 cross-adsorbed antibody - Goat anti-mouse IgG (H+L) - CAT-No.: #A-21422	Invitrogen Life Technologies, Waltham, MA, USA
Alexa Fluor™ 647 antibody - Donkey anti-mouse IgG (H+L) - CAT-No.: #A31571	Invitrogen Life Technologies, Waltham, MA, USA
Alexa Fluor™ 647 Plus highly cross-absorbed antibody - Goat anti-rabbit IgG (H+L) - CAT-No.: #A32733	Invitrogen Life Technologies, Waltham, MA, USA

2.1.6.3 Fluorescence-Activated Cell Sorting Antibodies

Antibody	**Manufacturer / Company**
Alexa Fluor™ 488 isotype control antibody, clone MOPC-21 - Mouse IgG1κ - CAT-No.: #400129	BioLegend, San Diego, CA, USA
Alexa Fluor™ 647 isotype control antibody, eBioscience™, clone RbNP15 - Rabbit IgG2aκ - CAT-No.: #51-4616-82	Thermo-Fisher Scientific, Waltham, MA, USA

anti-21 A647 antibody, clone EPR18021 - Rabbit IgG - CAT-No.: #652411	Abcam, Cambridge, United Kingdom
Brilliant Violet 421™ isotype control antibody, clone RTK2758 - Rat IgG2aκ - CAT-No.: #400535	BioLegend, San Diego, CA, USA
CD31 PE-Dazzle antibody, clone 390 - Rat IgG2a, κ - CAT-No.: #102430	BioLegend, San Diego, CA, USA
CD326 BV605 antibody, clone G.8.8 - Rat IgG2aκ - CAT-No.: #118227	BioLegend, San Diego, CA, USA
CD45 APC-Cy7 antibody, clone 30-F11 - Rat IgG2aκ - CAT-No.: #104116	BioLegend, San Diego, CA, USA
CD54 PE antibody, clone YN1/1.7.4 - Rat IgG2a, κ - CAT-No.: #116107	BioLegend, San Diego, CA, USA
Ki67 BV421 antibody, clone 16A8 - Rat IgG2aκ - CAT-No.: #ab237265	BioLegend, San Diego, CA, USA
Live/Dead A700 antibody - Rat IgG2aκ - CAT-No.: #L34987	BioLegend, San Diego, CA, USA
MHC II BV 510 antibody, clone M5/114.15.2 - Rat IgG2aκ - CAT-No.: #107636	BioLegend, San Diego, CA, USA
SOX2 A488 antibody clone 14A6A34 - Mouse IgG1κ - CAT-No.: #656110	BioLegend, San Diego, CA, USA

2.1.7 Buffer

Buffer	Components
Blocking buffer (for ELISA)	1%BSA, 25 mM Tris-HCl, 150 mM NaCl, pH 7.5
Blocking solution (for ELISA)	1% bovine serum albumin (BSA) in PBS, pH 7.4
Coating buffer (for ELISA)	50 mM $NaHCO_3$, pH 9.6
Erythrocyte lysis buffer	0,1 mM Na_2EDTA, 0,154M NH_4CL, 10 mM $KHCO_3$, pH 7.4
HEPES buffer	150 mM NaCl, 50 mM HEPES, pH 7.4
PBS (phosphate buffered saline)	137 mM NaCl, 2,8 mM KCl, 8,1 mM Na_2HPO_4, 1,5 mM KH_2PO_4, pH 7.4
PBS-T (phosphate buffered saline with Tween)	137 mM NaCl, 2,7 mM KCl, 10 mM Na_2HPO_4, 2 mM KH_2PO_4, 0,1% Tween 20, pH 7.4
RIPA (radioimmunoprecipitation-assay buffer)	50 mM Tris-HCl, 150 mM NaCl,1 mM EDTA, 1% Triton X-100, 1% sodium deoxycholate, 0,1% SDS, 1 mM phenylmethylsulfonyl fluoride (PMSF) (Thermo-Fisher Scientific, Waltham, MA, USA), 1 µg/ml cOmplete™ Protease Inhibitor Cocktail (Roche Holding, Basel, Switzerland)
TBS (Tris buffered saline)	25 mM Tris-HCl, 150 mM NaCl, pH 7.5
TBS-T (Tris buffered saline with Tween)	25 mM Tris-HCl150 mM NaCl, 0,1% Tween 20, pH 7.5

2.1.8 Human and Murine Samples

2.1.8.1 Human Lung Sections / Cells for Air Liquid Interface

Lung tissue was provided by the Philipps-University Marburg. Experiments were approved by the ethics review committee of the faculty of medicine of the Philipps-University Marburg (Reference: AZ 161-17).

2.1.8.2 Murine Lung Sections, Bronchoalveolar Lavage Fluid

Mice of the genotype C57Bl/6J were used as littermates. The mice were 8 to 12 weeks old. Gender was stratified between the groups. The experiments were performed

according to national laws and guidelines for animal welfare. The project was approved by the local authorities (Regierungspräsidium Gießen, reference number: Gi 20/2 - 39/2018).

2.1.8.3 Cell Lines

The human adenocarcinoma epithelial cell line A549 is a tumor cell line derived from human alveolar adenocarcinoma (253). A549 cells were used to study the effect of EREG on ATII epithelial cells.

Immortalized human bronchial epithelial cell line BEAS-2B is a non-cell line derived from normal human bronchial epithelium (254). BEAS-2B cells were used to study EREG effects on bronchial epithelial cells.

2.2 Methods

2.2.1 Cell Culture

A549 cells were cultured on petri dishes (Greiner Bio-One GmbH, Frickenhausen, Germany) at 37°C under 5% CO_2. Dulbecco's Modified Eagle Medium (DMEM) (Invitrogen Life Technologies, Waltham, MA, USA) supplemented with 10% fetal calf serum (FCS, PromoCell, Heidelberg, Germany) and 1% penicillin/streptomycin (P/S) (1000U/ml, Thermo-Fisher Scientific, Waltham, MA, USA) was used as cell culture growth medium for A549 cells. BEAS-2B cells were cultured on precoated coated plates at 37°C under 5% CO_2. Precoating solution included 97 ml of Hank's Balanced Salt Solution (HBSS), 10µg/ml human fibronectin (Corning Inc., Amsterdam, Netherlands), 30µg/ml PureCol® Type I Bovine Collagen Solution (AdvancedBiomatrix Inc. Carlsbad, CA, USA) and 10µg/ml bovine serum albumin (BSA) (Sigma-Aldrich, St. Louis, MO, USA). A 1:6 ratio mixture of Bronchial Epithelial Cell Growth Basal Medium (BEBM) (Lonza Group AG, Basel, Switzerland) and Roswell Park Memorial Institute Medium (RPMI) (Invitrogen Life Technologies) supplemented with 10% FCS (PromoCell) was used as cell culture growth medium for BEAS-2B cells.

After reaching 90% confluence, cells were washed with phosphate buffered saline (PBS) buffer (2.1.7), following incubation with trypsin-ethylenediaminetetraacetate (EDTA) (Thermo-Fisher) for 3 min at 37°C. Next, supplemented medium was added to stop the enzymatic trypsin activity and cells were centrifuged at 300 g for 7 min at room

temperature. Cells were resuspended in growth medium and 6 x 10^4 cells/cm^2 were seeded onto a new cell culture plate or harvested for further analysis.
Cells were treated differently in three groups:

1. Cells treated with PBS buffer instead of EREG as a vehicle for 48 h.
2. Cells treated with 250 ng/ml Recombinant Human Epiregulin (Bio-Techne, Minneapolis, MA, USA) for 48 h.
3. Cells treated with 5 µM doxorubicin hydrochloride (Santa Cruz Biotechnology, Santa Cruz, CA, USA), a chemotherapeutic drug initiating DNA damage as a positive control for 48 h.

2.2.2 Senescence / β-Galactosidase Assay in Cell Culture

To detect senescence, Senescence beta-Galactosidase Staining Kit (#9860, Cell Signaling Technology, Leiden, Netherlands) was used according to manufacturer's instructions. All working solutions were prepared following manufacturer's instructions.
BEAS-2B cells were grown in 35 mm culture plates (Merck KGaA, Darmstadt, Germany) as described in 2.2.1 until they reached 90% confluence. Cell culture medium was then removed and the cells were rinsed with PBS buffer (see 2.1.7). To fixate the cells, 1ml of fixation solution was added and the cells were incubated for 15 min at room temperature. Afterwards, the cells were washed twice with PBS buffer. Next, 1ml of β-galactosidase solution was added. To prevent evaporation, plates were sealed with parafilm. The plates were then incubated at 37°C without CO_2 overnight. On the next day, staining was checked with a microscope and if sufficient, the staining solution was removed and the cells were covered with 1ml of 70% glycerol solution (Carl Roth GmbH, Karlsruhe, Germany) until image acquisition with a bright field Nikon Eclipse CI-L Microscope (Nikon, Tokio, Japan).

2.2.3 Comet Assay in Cell Culture

To evaluate DNA damage, a comet assay was performed using a CometAssay® Kit (CAT-No.: 4250-050-K, R&D Systems, Minneapolis, MN, USA) and a CometAssay® Silver Staining Kit (CAT-No.: 4254-200-K, R&D Systems). All reagents and buffers (lysis solution, tris-borate-EDTA (TBE) buffer, fixation solution, staining solution) were prepared and used according to manufacturer's instructions.
BEAS-2B cells were harvested as described in 2.2.1 and resuspended in PBS at a concentration of 1 x 10^5 cells per ml. Next, normal melting agarose (Carl Roth GmbH) was

melted in boiling water and cooled down to 37°C, before it was mixed with cells at a ratio of 1:10 and immediately applied onto CometSlide™ slides (R&D Systems). After incubation at 4°C for 10 min in the dark, agarose solidified and the slides were immersed in lysis solution for 1h at 4°C. After lysis of the cells, the buffer was washed off with TBE buffer and slides were immersed in TBE buffer for another 15 min at 4°C. Next, slides were transferred into the slide tray of the CometAssay® Electrophoresis System II (Bio-Techne) which was filled with TBE buffer. Electrophoresis was performed with 21V for 40 min and kept away from light to prevent DNA damage. After electrophoresis, TBE buffer was drained and slides were immersed in double-distilled water (Carl Roth GmbH) for 5 min. Slides were then transferred into 70% ethanol for 5 min to dehydrate and dry them afterwards at 37°C for 10 min. To stain DNA, silver staining was performed. Therefore, the sample area on the CometSlide™ slide was covered with 100 µl of fixation solution and incubated at room temperature for 20 min. Afterwards, slides were rinsed with double-distilled water for 30 min to remove all acetic acid from the fixation solution. Next, the sample area was covered with 100 µl of the staining solution for 5 to 20 min at room temperature. Staining was controlled under the Nikon Eclipse CI-L Microscope (Nikon) and stopped by adding 5% acetic acid (Carl Roth GmbH) for 15 min onto the sample area. After another rinsing step with double-distilled water slides were dried and kept away from light until further analysis. Images were acquired with the Nikon Eclipse CI-L Microscope (Nikon) and image analysis was performed using the CometAssay® Analysis Software (Bio-Techne). Damaged DNA was evaluated by the migration pattern of the DNA. Therefore, the length of the comet tail was measured and the percentage of silver-stained DNA in the comet tail was calculated. The tail moment, which correlates with DNA damage, was calculated by multiplying the percentage of DNA in the comet tail with the tail length. Data were statistical analyzed as described in 2.2.9.

2.2.4 Air Liquid Interface Cell Culture

Primary human bronchial epithelial cells (hBECs) were isolated from bronchial tissue that was provided by the faculty of medicine of the Philipps-University Marburg. The tissue was treated according to local ethics regulations (Permit-reference: 161-17, faculty of medicine Philipps-University Marburg). hBECs were retrieved from the tissue and cultured on 6,5 mm transwells with an underlying 0,4 µm pore polyester membrane (Corning Inc.). Isolation of the cells was started by separating the bronchus from the tissue sample with scalpel and scissors. The retrieved tissue was then washed once with PBS. To protect

the cells, the inner bronchial side was placed onto a petri dish (Greiner Bio-One GmbH) and DMEM (Invitrogen Life Technologies) added on top of the tissue. DMEM was supplemented with 0,15% dithiothreitol (DTT) (Carl Roth GmbH), 1% amphotericin B (Merck KGaA) and 1% P/S (Thermo-Fisher Scientific). The cells were incubated for 12 h at 4°C, before washing them gently with PBS and switching the medium to DMEM supplemented with amphotericin B, 1% PRONASE® Protease from Streptomyces priseus (Merck KGaA) and P/S mix. After another 24 h of incubation, the cells were washed gently with PBS, scraped from the inner layer of the bronchus and put in 1x PBS. Cells were then centrifuged for 10 min at 40 g in a Rotina 35 1705 (Andreas Hettich GmbH & Co KG, Tuttlingen, Germany). The retrieved cell pellet was dissolved in Airway Epithelial Cell Growth Medium (PromoCell) supplemented with amphotericin B and P/S mix and were incubated at 37°C and 5% CO_2. For differentiation, 6 x 10^4 cells per cm^2 were transferred to Costar Transwell Permeable Supports (Corning Inc.) that were collagenized with 0.1% collagen type I solution (Merck KGaA) according to manufacturer's instructions. When cells reached confluence, they were apically airlift for 28 days. Cells were washed carefully with PBS to remove apical secretion fluid and medium was frequently replaced on the basolateral side during cultivation. After 28 days of cultivation, stimulation was started. Therefore, 250 ng/ml Recombinant Human Epiregulin (Bio-Techne) or PBS was added to the basolateral medium. PBS was used as a vehicle control. After 24, 48 and 72 h, apical washing fluid was retrieved by pipetting 500 µl medium on top of the cells and recollecting it. Also, medium from the basolateral side was collected and both media were processed for further analysis. The cells were then washed with PBS from the apical and basolateral side and processed for further analysis.

2.2.5 Animal Experiments

To study the effect of EREG on experimental fibrosis in vivo, the bleomycin mice model was used (255, 256). Bleomycin has been associated with lung fibrosis in human patients receiving chemotherapy with bleomycin (255) and also mice receiving bleomycin develop lung injury and inflammation, which leads to remodeling processes in the lung and in the end induction of experimental pulmonary fibrosis after 21 days (255, 256). The experiments were performed under specific pathogen-free conditions and according to national and international laws and guidelines for animal welfare. The project was granted approval by the local authorities (Regierungspräsidium Gießen, reference number: GI 20/2 - 39/2018).

2.2.5.1 Mice Strains

Mice of the C57Bl/6J (Black6) genotype were used as littermates. C57Bl/6J mice were obtained from Charles River Laboratories (Charles River Laboratories, Erkrath, Germany). Breeding and experiments were performed at the animal husbandry of the Institute for Biochemistry of the Justus-Liebig-University Gießen, Germany. The mice used in the experiments were eight to 12 weeks old and sex was stratified between groups.

2.2.5.2 Bleomycin Instillation

Application of bleomycin was performed via intratracheal instillation of an aerosol of bleomycin on day 0. Bleomycin stock was prepared by dissolving bleomycin (Medac GmbH, Wedel, Germany) in 0,9% isotonic sodium chloride solution (Braun, Melsungen, Germany). Control-groups received 0.9% sodium chloride instead of bleomycin. Each mouse received a volume of 100 µl intratracheally. To perform the instillation, mice had to be intubated under analgosedation with isoflurane (Zoetis, Parsippany, NJ, USA). Isoflurane was administered with a Compact Gas Anesthesia System 21100 (Ugo Basile S.R.L., Gemonio, Italy). When mice were unconscious, they were intubated with a 20G Vasofix® plastic i.v. catheter (Braun) under visual control with a Leica DMR Microscope (Leica Microsystems GmbH). After verifying correct placement of the plastic catheter into the trachea with a dentist mirror, each mouse received 2,5U/kg bleomycin (Medac GmbH) with a MicroSprayer®Aerosolizer FMJ-250 High Pressure Syringe (Penn-Century Inc., Wyndmoor, USA).

2.2.5.3 Lung Function Measurement and Collection of Bronchoalveolar Lavage Fluid

At the end of the experiment (21 days after bleomycin instillation) lung function for each mouse was measured, BALF was collected before the mice lungs were extracted and processed for further analysis.

Lung function was measured using a FlexiVent FX (Emka Technologies, Paris, France). Therefore, a mixture of 16 mg/kg body weight xylazine hydrochloride (Selectavet, Dr. Otto Fischer GmbH, Munich, Germany) and 120 mg/kg body weight ketamine hydrochloride (Ketamine, CP-Pharma GmbH, Burgdorf, Germany) was injected intraperitoneally (i.p.) with a Sterican® 30G needle (Braun) to accomplish general anesthesia. After reaching surgical tolerance, tracheostomy was performed and a cannula (Emka Technologies) was inserted into the trachea. Lung function was then measured with the FlexiVent

FX using FlexiWare™ Software (Emka Technologies). To measure lung function, total lung capacity (TLC), resistance, dynamic compliance, elastance and static compliance were assessed 5 times. For statistical analysis, the mean of each parameter was used, and analysis was performed as described in 2.2.9.

After finishing the lung function measurement, mice were restrained on a surgical table and the abdomen was opened surgically via a midline incision. Then, animals were sacrificed by exsanguination after cutting the aorta abdominalis. Next, BALF was collected by washing the lungs with Hank's Balanced Salt Solution (HBSS) (Carl Roth GmbH) via a 20G Vasofix® plastic i.v. catheter (Braun) that was inserted into the tracheostoma. After washing the lungs with 500 µl HBSS, the fluid was retrieved and transferred into a SafeSeal Reaction Tube (Sarstedt, Nümbrecht, Germany). The lung was then washed 3 times with 400 µl HBSS and the retrieved fluid was pooled in a SafeSeal Reaction Tube. The samples were then put on ice until centrifugation at 150 g for 7 min at 4°C. After separating supernatant from cells, Halt™ Protease Inhibitor Cocktail (Thermo-Fisher Scientific) was added according to manufacturer's instructions to prevent degradation of proteins before it was stored at -80°C until further analysis. The cell pellet was resuspended well in 1:10 FCS/dimethyl sulfoxide (DMSO) and also stored at -80°C until further analysis.

2.2.5.4 Processing of Lung Tissue for Further Analysis

After measuring lung function and collection of BALF, the lungs were extracted for further analysis. Preparation for histology and FACS differed from each other and is described in the next subchapters.

2.2.5.5 Preparation for Histology

For histology, the diaphragm was opened with an incision from caudal and the ribcage was opened after the lungs collapsed completely. To remove the erythrocytes from the lung vessels, the heart's left ventricle was opened by a small incision and the right ventricle was punctured with a 20G Vasofix® plastic i.v. catheter (Braun). The catheter was then connected to an extension tube and HBSS was flushed from the right ventricle of the heart into the lung until it exited the vascular system via the incision in the left atrium. During the flushing procedure, the lungs were ventilated using a MiniVent Ventilator (Hugo Sachs Elektronik, March-Hugstetten, Germany) inserted into the tracheostomy stoma to ensure adequate lung perfusion and removal of erythrocytes. After infusion of

20 ml HBSS and visible removal of the blood, lungs were surgical removed by disconnecting the trachea and removing the surrounding connective tissue and vessels from the lungs. Lungs were then put into 4% paraformaldehyde (PFA) solution (Carl Roth GmbH) for 24 h at room temperature for fixation. PFA was exchanged to PBS after 24 h and the lungs were incubated for additional 24 h at 4°C before paraffin block preparation (see 2.2.8.1).

2.2.5.6 Preparation for Fluorescence-Activated Cell Sorting

As preparation for FACS analysis, the lung tissue was digested to receive a single cell suspension suitable for the cell sorter. Instead of flushing the lungs as for histology, 150 mg of Dispase II enzyme (Roche Holding, Basel, Switzerland) were dissolved in 5 ml of 2-(4-(2-hydroxyethyl)-1-piperazinyle)-ethane sulfonic acid (HEPES) buffer (2.1.7) and 2 ml of this solution were injected into the lungs via cannulation of the trachea with a 20G Vasofix® plastic i.v. catheter (Braun) to start the digestion process of the lung tissue. After 5 min of incubation at room temperature, the tracheostoma was closed and the lung was surgically disconnected from the cranial part of the trachea and the surrounding connective tissue. The lung was placed into the remaining Dipase II solution for 45 min at room temperature for further digestion. Next, the lung was put in DMEM/HEPES buffer (DMEM + 2.5% 1M HEPES) supplemented with 0.01% DNase I enzyme (Serva Electrophoresis GmbH, Heidelberg, Germany) and the solution was homogenized in a gentleMACS™ C Tube (Miltenyi Biotec B.V. & Co. KG, Bergisch Gladbach, Germany) with a gentleMACS™ Dissociator (Miltenyi Biotec B.V. & Co. KG, Bergisch Gladbach, Germany). The retrieved lung homogenate was incubated while being rocked gently for 8 min at room temperature. Afterwards, it was filtered sequentially through a Falcon® 70 µm, 40 µm and 20 µm cell strainer (Corning Inc.). Between all filtering steps, cells were washed with DMEM/HEPES buffer. After the last filtering step, the suspension was centrifuged at 500 g for 10 min at 4°C. The supernatant was removed and the cell pellet underwent another step where the remaining erythrocytes were lysed. Therefore, erythrocyte lysis buffer (2.1.7) was added and the cells were incubated at room temperature for another 2 min and 30 s and centrifuged at 500 g for 10 min. The lysis process was stopped by adding PBS and the solution was centrifuged at 500 g for another 10 min at 4°C before resuspending the pellet in HBSS buffer. 1 µl of the cell suspension was then mixed with an equal volume of 10% trypan blue (Thermo-Fisher Scientific) and the absolute cell

count was acquired with a BioRad TC 20 Automated Cell Counter (Bio-Rad Laboratories, Hercules, CA, USA).

2.2.6 Fluorescence-Activated Cell Sorting Analysis

Prior to cellular phenotyping, lungs were prepared with enzymatic digestion to receive a single cell suspension suitable for flow cytometric measurements as described in 2.2.5.6. Single cell suspension samples were aliquoted into 100 µl HBSS buffer at a concentration of 1 x 10^7 cells/ml. Cells were then stained in two separate staining series: One for the extracellular staining and another one for the intracellular staining.

For the extracellular staining series, cells were incubated with fluorescein-conjugated antibodies at a dilution of 1:100 for 45 min at room temperature in the dark. Following antibodies were used: Cluster of differentiation (CD) 31 (CD31) (PE Dazzle, CAT-No.: #102430), CD54 (PE, CAT-No.: #116107), CD45 (APC-Cy7, CAT-No.: #104116), MHCII (BV510, CAT-No.: #107636) and CD326 (BV605, CAT-No.: #118227, all from BioLegend, San Diego, CA, USA). Details of the antibodies for extracellular markers used in this study are listed in section 2.1.6.3. To determine the amount of living and dead cells, viability dye Live/Dead A700 (Rat IgG2aκ, CAT-No.: #L34987, Thermo-Fisher Scientific) was carried along with the staining at a dilution of 1:200 for later flow cytometric analysis. After incubation, cells were washed with HBSS to remove unbound antibodies. Flow cytometry was performed on a BD FACS Aria III Cell Sorter (BD Biosciences, San José, CA, USA). To accurately compensate for spectral overlap between fluorophores, compensation controls were prepared with Ultracomp eBeads Compensation Beads (Thermo-Fisher Scientific). One drop of the stained beads and 1 µl of the corresponding fluorophore-conjugated antibody used in the surface staining protocol were added to 100 µl HBSS buffer. A negative control with HBSS and unstained beads was also carried through. Stained and unstained bead controls were then incubated for 10 min at room temperature in the dark. After incubation, flow cytometry was performed and the compensations obtained from the settings were validated by comparing the fluorescence profiles of the beads with those of the actual samples. This provided precise compensation, ensuring accurate detection and quantification of the surface markers of interest and minimal spectral overlap.

For the intracellular staining series, cells were first treated as in the extracellular or surface staining protocol. Therefore, cells were incubated with the same surface fluoresceine-conjugated antibodies at a dilution of 1:100 for 45 min at room temperature in the

dark. After incubation, cells were washed with HBSS buffer to remove unbound antibodies. Next, the cells were fixated and washed with the eBioscience™ Foxp3/Transcription Factor Staining Buffer Set (Thermo-Fisher Scientific). Buffers were prepared according to manufacturer's instructions. First, the cells were incubated with fixation/permeabilization buffer for 30 min at room temperature in the dark. Following fixation, cells were centrifuged at 500 g for 5 min at 4°C. After centrifugation supernatant was removed and the cell pellet was vortexed well. Next, the cells were washed with permeabilization buffer from the eBioscience™ Foxp3/Transcription Factor Staining Buffer Set (Thermo-Fisher Scientific) before they were centrifuged again at 500 g for 5 min at 4°C. Supernatant was again removed after centrifugation and the cell pellet was vortexed well too. Before incubating the cell pellet with the antibodies for intracellular markers, 10 µl of mouse serum were added to the samples to block Fc-receptors and the samples were incubated for 10 min in the dark on ice. For intracellular staining, the following antibodies were used: p21 (A647, CAT-No.: #652411, Abcam, Cambridge, United Kingdom) as a marker of senescence, Ki67 (BV421, CAT-No.: #ab237265, BioLegend) as a marker for cell proliferation and SOX2 (A488, CAT-No.: #656110, BioLegend) as a marker for basal cells of airway epithelial cells. Details of the antibodies for extracellular markers used in this study are listed in section 2.1.6.3. Antibodies for intracellular markers were added to the samples in a dilution of 1:33 and incubated for another 30 min in the dark on ice. After incubation, another two washing steps with permeabilization buffer were performed as described above. After the last washing step and removal of the supernatant, 100 µl of HBSS buffer were added and the samples were processed for flow cytometry.

Isotype controls were included for all antibodies stainings. With this control, false-positive signals were reduced. Therefore, for each fluorophore-conjugated antibody, an additional aliquot of the single cell suspension was incubated with an isotype control antibody that matched the primary antibody's class and subclass (isotype) and conjugated fluorochrome. Iso controls were treated under identical conditions and same antibody dilutions were used. The following isotype controls were used: Alexa Fluor™ 647 isotype control (CAT-No.: #51-4616-82, Thermo-Fisher Scientific), Brilliant Violet 421™ isotype control (CAT-No.: #400129, BioLegend) and Alexa Fluor™ 488 isotype control (CAT-No.: #400129, BioLegend). Details of the isotype controls used in this study are listed in section 2.1.6.3. Flow cytometry was performed on a BD FACS Aria III Cell Sorter (BD Biosciences) for extracellular/surface staining, intracellular staining, compensation beads and isotype controls.

2.2.6.1 Epiregulin Instillation

Application of EREG was performed intravenously (i.v.) via injection and intratracheally (i.t.) via instillation. Recombinant Human Epiregulin (1195-EP/CF, Bio-Techne) was dissolved in 0.9% sodium chloride (Braun) under sterile conditions and 100 mg/kg body weight EREG was injected or instilled per mouse. Control-groups received 0.9% sodium chloride instead of EREG as a vehicle. Each mouse received a maximum volume of 100 µl per injection or instillation.

Intratracheal application was performed as described for bleomycin in 2.2.5.2. Intravenous injections were performed while the mice were kept in a Mouse Restrainer Type A (G&P Kunststofftechnik GbR, Kassel, Germany). EREG or 0.9% sodium chloride were injected into the tail veins. Together with the application of bleomycin or vehicle on day 0, application of EREG or vehicle was performed at four different time points:

1. i.t. bleomycin/vehicle on d0 and i.v. EREG/vehicle on day 0, 2, 4 to investigate the effect of EREG during lung injury and inflammatory phase.
2. i.t. bleomycin/vehicle on d0 and i.t. EREG/vehicle on day 0, 2, 4 to investigate the effect of EREG during lung injury and inflammatory phase.
3. i.t. bleomycin on d0 and i.v. EREG on day 8, 10, 12, 14, 16 to investigate the effect during the remodeling and fibrosis induction.
4. i.t. bleomycin on d0 and i.t. EREG on day 8, 10, 12, 14, 16 to investigate the effect during the remodeling and fibrosis induction.

2.2.7 ELISA of Bronchoalveolar Lavage Fluid

The levels of cytokines in BALF from mouse experiments were quantified using commercially available enzyme-linked immunosorbent assay (ELISA) kits from R&D Systems and Thermo-Fisher Scientific. ELISAs were performed according to manufacturer's instructions if not stated otherwise. All reagents included in the kits were prepared and used according to manufacturer's instructions. Cytokines of interest were: IL-1α / IL-1F1, IL-6, TGF-β, C-XC motif chemokine (CXCL2) / macrophage inflammatory protein 2 (MI2-2), MMP-2, tumor necrosis factor receptor superfamily member 12A (TNFRSF12A or TWEAKR), EREG and TNF-α. For IL-1α/IL-1F1 (CAT-No.: MLA00), CXCL2/MIP-2 (CAT-No.: MM200), MMP-2 (CAT-No.: MMP200) Quantikine® ELISA Kits (R&D Systems) were used. For IL-6 (CAT-No.: DY406), TGF-β1 (CAT-No.: DY1679), TWEAK Receptor/TNFRSF12A (CAT-No.: DY1610) and EREG (CAT-No.: DY1068), DuoSet® ELISA kits (R&D Systems) were used. For TNF-α (CAT-No.: 900-T54)

PeproTech® ELISA Kit (Thermo-Fisher Scientific) was used. Details of the ELISA kits used in this study are listed in section 2.1.52.1.7. ELISA assays were performed and solutions were prepared according to manufacturer's instructions. If solutions were not provided from the manufacturer, solutions were used as described in the following protocol and prepared as listed in section 2.1.7. If a range of volume or frequency is stated, the volume or frequency was used as noted in the manufacturer's protocol.

If no well plate was included in the ELISA kit, ELISA was performed in a 96-well cell culture plate (Thermo-Fisher Scientific) and coating was performed as followed:

In preparation for the ELISA, dependent on the used ELISA kit, 100 µl of capture antibody dilution (in PBS) was pipetted into each well and the plate was incubated overnight at 4°C. On the following day, the fluid was removed from the wells and the wells were washed three to 4 times with the provided washing solution or 400 µl phosphate buffered saline with Tween (PBS-T) (see 2.1.7). Then, the plate was blocked as recommended in the product datasheet with 300 µl of provided blocking solution or prepared blocking solution (see section 2.1.7) for 1 h at room temperature. Next, washing was repeated three to 4 times with the provided washing solution or 400 µl PBS-T.

After coating the plate or if the precoated plate was already provided by the manufacturer, 100 µl of undiluted BALF, control samples (PBS) and descending standard solution of known concentration diluted with provided assay/reagent diluent (1000 pg/ml, 500 pg/ml, 250 pg/ml, 125 pg/ml, 62.5 pg/ml, 31.25 pg/ml, 15.61 pg/ml) were added to the corresponding wells and incubated for 2 h at 37°C. If BALF had to be diluted, 50 µl was mixed with an equal volume of the provided assay/reagent diluent or blocking solution (see 2.1.7). Next, the wells were washed again three to 4 times with the provided washing solution or 400 µl PBS-T before adding 100 µl of the provided detection antibody at recommended dilution in provided conjugate/reagent dilution or 1% BSA in PBS-T. The wells were incubated for 2 h at 37°C. After washing off the antibody three to 4 times with provided washing solution or 400 µl PBS-T, 100 µl of provided substrate solution or streptavidin horseradish peroxidase (HRP) working dilution (diluted 1:40, BioLegend) was added to each well for 20-30 min and incubated at room temperature while protected from light. For some manufacturer's protocols, a washing step with provided washing solution or 400 µl PBS-T was performed before the next step to remove the unbound streptavidin peroxidase. If substrate solution was provided and used in the prior step, then no washing step was needed and the next step was skipped as well. Afterwards 100-200 µl of provided substrate solution or TMB substrate solution from the TMB Substrate Kit

(Thermo-Fisher Scientific) was pipetted into each well and the plate was incubated for another 20-30 min protected from light. The resulting chemical reaction of the remaining peroxidase and the TMB substrate turned the substrate into a blue colored solution. The enzymatic reaction was stopped by adding 50-100 µl of provided stop solution or 2M sulfuric acid (Carl Roth GmbH, Karlsruhe, Germany) to the wells and optical density was immediately measured photometrically at a wavelength of 450 nm using the SpectraMax190 plate reader (Molecular Devices, San José, CA, USA).
The standard curve was created by competing the standard levels against their corresponding optical density (OD) values. All samples were run in duplicate and the average of both measurements was taken for the following statistical analysis (see 2.2.9).

2.2.8 Histology and Cytology

2.2.8.1 Preparation of Lung Sections

Stainings were performed on murine tissue obtained from animal experiments as described in section 2.2.5.4 and 2.2.5.5.
Murine lungs were treated with the same protocol before performing individual staining protocols. After fixation (see 2.2.5.5), samples were dehydrated with increasing ethanol dilutions of 70%, 80%, 95% and 100%, each for 1 h. The samples were then processed to clearing steps in xylene before embedding them in paraffin. Following three clearing steps in xylene, samples were embedded into warm paraffin. After hardening of the paraffin, paraffin blocks were stored at 4°C until further preparation. Sections of 1-2 µm thickness were cut sequentially from the paraffin blocks with MS300 blades (Micros Austria, St. Veit/Glan, Austria) on a HistoCore Autocut Automated Rotary Microtome (Leica Microsystems GmbH) and transferred onto microscope slides. After drying for 24 h, sections were stained individually as described in 2.2.8.3 and 2.2.8.4.

2.2.8.2 Preparation of Air Liquid Interface Filter Sections

Bronchial epithelial cells from air liquid interface (ALI) cell cultures were fixed in a 4% PFA solution for 1 h at room temperature. Afterwards, PFA was exchanged to PBS. For further processing, the filter on which the cells grew was cut gently from the cell culture well walls with a scalpel. The filter was then processed through dehydration and clearing steps as described in 2.2.8.1. After dehydration and clearing steps, the filter was held in a vertical position with a forceps while embedding it into paraffin. Cutting of the paraffin blocks was performed as described in 2.2.8.1 for murine lung samples.

2.2.8.3 Hematoxylin and Eosin Staining

Lung sections were prepared as described in 2.2.8.1 and then deparaffinized at 60°C for 60 min and 3 times for 2 min in xylene solution (Carl Roth GmbH). Afterwards, the sections were rehydrated for 2 min in descending ethanol concentrations of 100%, 96%, 70%, 50%. Sections were then washed with distilled water to remove the rest of the ethanol before staining them with Hematoxylin solution according to Weigert (Carl Roth GmbH) for 3 min. Another washing procedure under tap water was performed for 3 min to elevate pH value to change the nuclear staining color from red to blue. Sections were then stained with eosin (Carl Roth GmbH) by dipping the slides 3 times in 1% eosin solution. Washing with distilled water for 3 min removed traces of eosin. The sections were then again dehydrated for 2 min each in ascending ethanol concentrations of 50%, 70%, 96%, 100%. Incubation for 3 min in xylene was then performed to remove the ethanol. In the last step, Roti Histo Kit II (Carl Roth GmbH) was administered onto the sections and a glass slide was set on top to finish mounting.

2.2.8.4 Immunohistochemistry

Immunohistochemistry (IHC) stainings were performed with ZytoChem Plus (AP) Polymer Kit POLAP-006 (Zytomed Systems GmbH, Berlin, Germany).

The sections were deparaffinized and rehydrated as described before for HE staining (2.2.8.3). After rehydration, the slides were washed with Tris buffered saline (TBS) with Tween (TBS-T) buffer for 5 min. For antigen retrieval, the sections were incubated either with Fast Enzyme solution (Zytomed Systems) for 10 min at room temperature or with a 0.1% Triton X-100 solution (Carl Roth GmbH) for 10 min at room temperature. After being washed 3 times for 5 min in TBS buffer, the sections were treated with blocking solution from the ZytoChem Plus (AP) Polymer Kit for 5 min in a StainTray^{TM} Humidity Chamber (Carl Roth GmbH). After blocking, the slides were washed 3 times for 5 min with TBS buffer. Next, a primary antibody was diluted in TBS buffer solution with 0.1% BSA (Sigma-Aldrich) and the sections were incubated with the antibody overnight at 4°C in the humidity chamber. The primary antibodies against the following markers were used in IHC stainings: p63 (ΔN) (CAT-No.: #619001, BioLegend) as a marker for basal cells of airway epithelial cells, PCNA (CAT-No.: #13110, Cell Signaling Technology) as a marker for cell proliferation and p21 (CAT-No.: #2947, Cell Signaling Technology) as a marker of senescence. Details of the primary antibodies used in this study are listed in section 2.1.6.1. The dilution of the primary antibody was chosen after establishment of

the staining on test sections of murine and humane tissue. All p63 antibodies used were diluted 1:100, PCNA antibodies were diluted 1:200 and p21 antibodies were diluted 1:100. After incubation with the primary antibodies, the sections were washed 3 times for 5 min in TBS buffer before they were treated with Post Block reagent from the ZytoChem Plus (AP) Polymer Kit for 30 min. After another three washing steps with TBS, the color development was performed. Therefore, the sections were treated with Permanent AP Red Kit (Zytomed Systems GmbH) according to manufacturer's instructions. The color development process was controlled under the microscope and stopped with double-distilled water (Carl Roth GmbH) when staining results were satisfactory. The sections were then counterstained with hematoxylin, followed by a rinse in tap water for 10 min. Afterwards, the stained slides were rehydrated by sequential immersion in graded ethanol (70%, 95%, 100%) 3 times for 30 seconds, followed by clearing in xylene twice for 5 min each. Finally, the slides were mounted with Roti Histo Kit II.

2.2.8.5 Immunocytochemistry / Immunofluorence

For immunofluorescence stainings, lung sections from mice and cells cultivated on a filter membrane in an ALI cell culture were cut from paraffin blocks into 1 µm-thick sections using MS300 Microtome Blades (Micros Austria) on a HistoCore Autocut Automated Rotary Microtome (Leica Microsystems GmbH). Afterwards, sections were transferred onto microscope slides. After drying for 24 h, sections were stained with the following protocols.

2.2.8.5.1 Paraffin Sections from Lung Tissue and Air Liquid Interface Cultures

The following protocol was performed for paraffin sections of murine lung tissue as well as for paraffin sections from cells harvested from ALI cell cultures (see section 2.2.4).
The sections were deparaffinized and rehydrated as described before for HE staining (see section 2.2.8.3). The paraffin sections from mouse lung samples were treated with MaxBlock™ Autofluorescence Reducing Reagent Kit (MaxVision Biosciences Inc. Washington, USA) to reduce autofluorescence. Therefore, after rehydration steps, MaxBlock™ Reagent A was put on top of the section with a pipette and incubated for 5 min at room temperature. The solution was then rinsed off with 60% ethanol before washing the slide with double-distilled water (Carl Roth GmbH). For all other samples, these steps were skipped. All samples were then processed using the same protocol. After three washing steps with PBS, the samples were then transferred into a decloaking buffer and cooked at

100°C for 30-45 min. For murine samples, Rodent Decloaker (Zytomed Systems GmbH) was used according to manufacturer's instructions, while human samples were cooked at 95% in citrate buffer at pH 6 for 30 min. After cooling down to room temperature in the buffer, the sections were washed 3 times for 5 min in double-distilled water on a shaker. Blocking of the unspecific antibody binding sites was performed with a solution of 10% BSA in PBS at pH 7.4 solution for 60 min in a StainTray™ Humidity Chamber. After four washing steps with PBS, murine samples were again blocked with Rodent Block M solution (Zytomed Systems GmbH) for another 30 min at room temperature in the humidity chamber. For human samples this step was skipped. After another two washing steps with PBS, the primary antibody was administered onto the tissue diluted with Antibody Diluent solution (Zytomed Systems GmbH). Primary antibodies against the following markers were used in IHC stainings:

- p63 was used as a marker for basal cells of airway epithelial cells:
  - CAT-No.: #b3239, mouse (Abcam)
  - CAT-No.: #sc-25268, mouse (Santa Cruz Biotechnology)
  - CAT-No.: #P1006T50, mouse (DCS, Chaussee, Germany)
  - CAT-No.: #ab124762, rabbit (Abcam)
- PCNA was used as a marker for cell proliferation:
  - CAT-No.: #13110, rabbit (Cell Signaling)
  - CAT-No.: #2586, mouse (Cell Signaling Technology)
- Ki67 antibody was used as an alternative marker for cell proliferation:
  - CAT-No.: #ab15580, rabbit (Abcam)
- p21 was used as a marker of senescence in cells:
  - CAT-No.: #2947, rabbit (Cell Signaling)
  - CAT-No.: #05-655, mouse (Merck Millipore, Burlington, MA, USA)
- Phospho-Histone H2Ax (γH2Ax) was used as a marker for DNA damage:
  - CAT-No.: #05-636, mouse (Merck Millipore)
  - CAT-No.: #9718, rabbit (Cell Signaling Technology)

Details of the primary antibodies used in this study are listed in section 2.1.6.1. The primary antibody was pipetted onto the section and incubated overnight at 4°C in the humidity chamber. The dilution of the primary antibodies was chosen as in IHC stainings (see 2.2.8.4). On the next day the antibody was washed off with PBS 3 times for 10 min. The sections were then incubated with the secondary antibody for 60 min in the humidity chamber. Secondary antibodies were diluted with Antibody Diluent solution. Dilution

was 1:500 for all samples. The secondary antibodies that were used are listed in section 2.1.6.2. Secondary antibodies were chosen according to the corresponding species of the primary antibody and incubated for 1 h in the humidity chamber. From this point on, the slides were kept away from light, even in between the incubation steps to protect weakening of the fluorescent signal. Secondary antibody was washed off with PBS 3 times for 5 min.

For antibodies that showed low signals in test stainings, the protocol was changed and Alexa Fluor™ 647 Tyramide Super Boost™ Kit (Invitrogen Life Technologies) was used according to manufacturer's instructions. Therefore, secondary antibody was replaced by provided poly-HRP-conjugated secondary antibody solution that was prepared according to manufacturer's instructions. After washing off the secondary antibody as described for the regular secondary antibodies, samples were treated with tyramide working solution for 10 min and the reaction was stopped with 100 µl of HRP reaction stop reagent. After three washing steps with PBS samples were treated in the same way as all other samples. To stain the nuclei, the sections were treated with 4',6-diamino-2-phenylindole (DAPI) (Sigma-Aldrich). For DAPI staining, sections were treated with 300 nM DAPI solution diluted 1:1000 in PBS for 5 min at room temperature and kept away from light. Afterwards, the slides were washed 3 times with PBS buffer for 5 min. Finishing MaxBlock™ autofluorescent reducing protocol, MaxBlock™ Reagent B was added on top of the section for another 5 min in the humidity chamber. After another three washing steps with double-distilled water, the staining protocol was complete. To prepare the slides for microscopy, the sections were mounted with ProLong™ Glass Antifade Mountant mounting medium (Invitrogen Life Technologies) and a cover glass with a thickness of 1.5 µm (Paul Marienfeld GmbH, Lauda-Königshofen, Germany) was put on top. In the final step, the slides were sealed around the glass slide with commercially available nail polish.

2.2.8.5.2 Whole Air Liquid Interface Cell Cultures (Not Paraffin-Embedded)

The cells were fixed inside the well plate with 4% PFA for 20 min prior to the staining procedure. All steps contained a treatment of the cells from the top and the bottom of the well plate. First, the cells were washed 3 times with PBS. Permeabilization was performed by incubating the cells with PBS solution that contained 0.5% Triton X-100 for 20 min at room temperature. After another 3 washing steps with PBS, the cells were blocked with a 3% BSA PBS solution for 1 h at room temperature. Following 3 washing steps with PBS, the cells were incubated with the primary antibody diluted in 1% BSA PBS solution

overnight at 4°C. Primary antibodies used are described in section 2.1.6.1. Dilution depended on the chosen antibody (2.1.6.1). After another 3 washing steps, corresponding secondary antibody was diluted with 1% BSA in PBS, pipetted onto the cells and incubated for 1 h at room temperature. From this step on, the well plate was kept away from light. Following the incubation with the secondary antibody, the cells were washed another 3 times for each 5 min each. To stain the nuclei, the sections were treated with 300 nM DAPI solution diluted 1:1000 in PBS for 10 min at room temperature. After another three washing steps with PBS, the staining protocol was complete. To prepare the slides for microscopy, slides were mounted as paraffin sections described in 2.2.8.5.1.

2.2.8.6 Light Microscopy Imaging

Light microscopy of lungs and cells stained with HE staining and IHC staining was performed with a Nikon Eclipse CI-L Microscope (Nikon) and slides were scanned with a Pannoramic DESK II DW Digital Slide Scanner (3DHISTECH, Budapest, Hungary) for virtual microscopy and to acquire digital images.

2.2.8.7 Immunofluorescence Microscopy Imaging

The processing and analysis of the images were carried out with the assistance of Dr. rer. nat. Ioannis Alexopoulos from the Multiscale Imaging Platform of the Institute for Lung Health of the Justus-Liebig-University, Gießen in Germany.

All images were captured using an inverted confocal laser scanning microscope SP8 Lightning Confocal Microscope (Leica Microsystems), operated by the LAS X Software version 3.7.5. Fluorescence emissions were recorded sequentially. Capturing z-stacks was performed using a 20xAir 0.75NA and a 63xOil 1.4NA objective. The same scanning settings (voxel size, excitation power, etc.) were used for all acquisitions to ensure comparability. Three-dimensional (3D) reconstructions of z-stacks was conducted using the 3D module of the LAS X Software version 3.7.5. For further analysis and cell counting, images of the whole length of the filter were acquired with the microscope and stitched together digitally.

2.2.8.8 Electron Microscopy

2.2.8.8.1 Transmission Electron Microscopy

Transmission electron microscopy (TEM) was performed with the help of Prof. Dr. Ulrich Gärtner in corporation with the Institute of Anatomy and Cell Biology of the Justus-Liebig-University Gießen in Germany.

Samples were fixed with a 1,5% PFA (Merck KGaA) and 1,5% glutaraldehyde (GDA) (Merck KGaA) solution in 0.15M HEPES buffer for 24 h at room temperature. Afterwards PFA and GDA were washed off with 0.15M HEPES buffer (Sigma-Aldrich) 3 times for 10 min. For stabilization, the sections were postfixed in 1% osmium tetroxide (Carl Roth GmbH) in distilled water for 2 h. Osmium tetroxide solution was washed off 3 times for 10 min before staining the samples with half saturated uranyl acetate solution (Merck KGaA) overnight and keeping them away from light. On the next day, the solution was washed off 3 times for 10 min with distilled water before the samples were dehydrated through graded ethanol washes (30%, 50%, 70%, 90%, 96%, 3x100%, 10 min each). Afterwards, the sections were degassed in a desiccator for 4 h before being treated with Epon 812 epoxy embedding medium (Sigma-Aldrich) for 48 h in a drying cabinet. Sections were examined with the Zeiss EM 902 TEM (Carl Zeiss AG, Oberkochen Germany).

2.2.8.8.2 Scanning Electron Microscopy

Scanning electron microscopy (ScEM) was performed with the help of Prof. Dr. Ulrich Gärtner in corporation with the Institute of Anatomy and Cell Biology of the Justus-Liebig-University Gießen in Germany.

Samples were fixed as described for TEM samples (see 2.2.8.8.1). The samples were postfixed in 1% osmium tetroxide (Merck KGaA) in distilled water for 2 h, washed 3 times in distilled for 10 min and were then dehydrated through graded ethanol washes (30%, 50%, 70%, 90%, 2x100%, 10 min each) and critical point dried by CO_2 treatment with the critical point drying machine CPD 030 (Evatec AG, Trübbach, Switzerland). Afterwards, the samples were pasted with conductive adhesive tape (Thermo-Fisher Scientific) and sputtered with gold. Examination of the samples was performed with a Philips XL30 ScEM (Philips / FEI, Hillsboro, OR, USA).

2.2.9 Data Analysis and Statistical Analysis

Statistical analysis of compliance data, cell counts, data from BALF analysis and tail moments was performed using the software Graph Pad Prism 9 (GradPad Software, Boston, MA, USA). Results are presented in dot plots with mean and standard error mean (SEM) or standard deviation (SD). Differences between two groups were analyzed with an unpaired Mann-Whitney t-test. For comparisons between multiple groups, an analysis of variance (ANOVA) test was performed. Differences were considered as statistically significant at a level of $p<0,05$.

Data acquired with FACS were analyzed and gated with BD FACS Diva Software version 8.0.1 (BD Biosciences). Statistical analysis was also performed with Graph Pad Prism 9 and presented in dot plots with mean and SEM or SD. Differences between groups were analyzed as described for compliance data, cell counts and tail moments.

Cell counts from IHC or immunofluorescence stainings were performed in an automatic manner using ImageJ / Fiji software (257). For every image upon thresholding, the positive cells (for all relevant markers) were counted with the "Analyze Particles" plugin of Fiji. Cell counts then underwent statistical analysis with Graph Pad Prism 9 as described earlier.

3 Results

3.1 Effects of Epiregulin on Airway Epithelial Cells

3.1.1 Epiregulin Stimulation Alters Epithelial Morphology and Cell Differentiation of Airway Epithelial Cells

To assess the effects of EREG on airway epithelial cells, hBECs were stimulated with EREG in an air liquid interface cell culture.

Fig. 1 shows that the morphology of the cultured epithelial cells is altered after EREG stimulation. On the one hand, the controls show a (semi-)differentiated airway epithelium (Fig. 1A, top two images, Fig. 1B, top image) with basal cells in the base layer and a top layer with iso- to high prismatic cells (Fig. 1A-B, top images) with ciliated cells and a few goblet cells (Fig. 1B, top image). On the other hand, EREG-treated cells show a heterogenous epithelial appearance with flat (Fig. 1A-C second images from below) and hyperplastic parts (Fig. 1C, bottom images). The base layer consists of flat basal cells with squamous appearance, while the top layer consists of hyperplastic cells with lower cellular volume, forming epithelial folds (Fig. 1C, bottom image). The EREG stimulated epithelium is overall less differentiated than the controls but still shows signs of differentiation including kinocilia (Fig. 1B, bottom image).

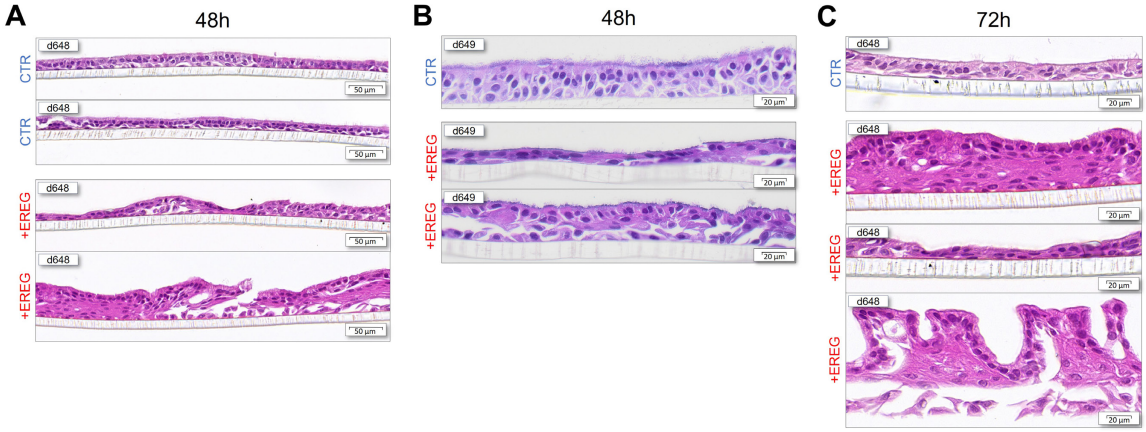


Fig. 1: EREG stimulation alters epithelial morphology and cellular differentiation in hBECs.
(A-C) Hematoxylin-eosin stainings of primary human bronchial epithelial cells (hBECs) cultured in an air liquid interface cell culture after stimulation for 48 h and 72 h with either PBS (CTR) or 250 ng/ml EREG. **(A)** Overview of the epithelial morphology (donor 648) in lower magnification. Representative pictures are shown. Scale bars = 50 µm. **(B)** Detailed view of the epithelial morphology (donor 649) after stimulation with EREG for 48 h. Representative pictures are shown. Scale bar = 20 µm. **(C)** Detailed view of epithelial morphology (donor 648) for 72 h. Representative pictures are shown. Scale bars = 20 µm.

EREG-triggered morphological changes were further investigated in transmission TEM and ScEM. In TEM (Fig. 2A), cells treated with vehicle control show a stratified epithelium consisting of secretory and ciliated cells in the top layer of the epithelium. The

ciliated cells have few long microvilli (Fig. 2A, m) and cilia (Fig. 2A, c) on their apical surface. In the basal region of the epithelium, basal cells (Fig. 2, BC) are in contact with the filter.

After EREG stimulation, the height of the epithelium is greater (Fig. 2A, right picture) than in vehicle controls (Fig. 2A, left picture). The cells form a stratified epithelium, predominantly composed of secretory cells (Fig. 2A, SC) in the top layer of the epithelium. The apical surface contains numerous long microvilli (Fig. 2A, m), but only few cilia (Fig. 2A, c). Beneath are intermediate cells with abundant protein synthesis, as indicated by stacks of rough endoplasmatic reticulum (Fig. 2A, rER) and cisternae (Fig. 2A, arrowheads), as signs of excessive protein export. In the lower half of the epithelium, cells exhibit specializations for withstanding mechanical stress including desmosomes (Fig. 2A, circles) and intracellular filament bundles (Fig. 2A, arrows).

In ScEM (Fig. 2B), cilia and microvilli are composed on the surface as signs of differentiation in both vehicle (Fig. 2B, top picture) and EREG-treated cells (Fig. 2B, bottom picture). After EREG stimulation, folding of the epithelium is seen on the surface of the epithelium (Fig. 2B, bottom picture), while in controls such folding is absent (Fig. 2B, top picture).

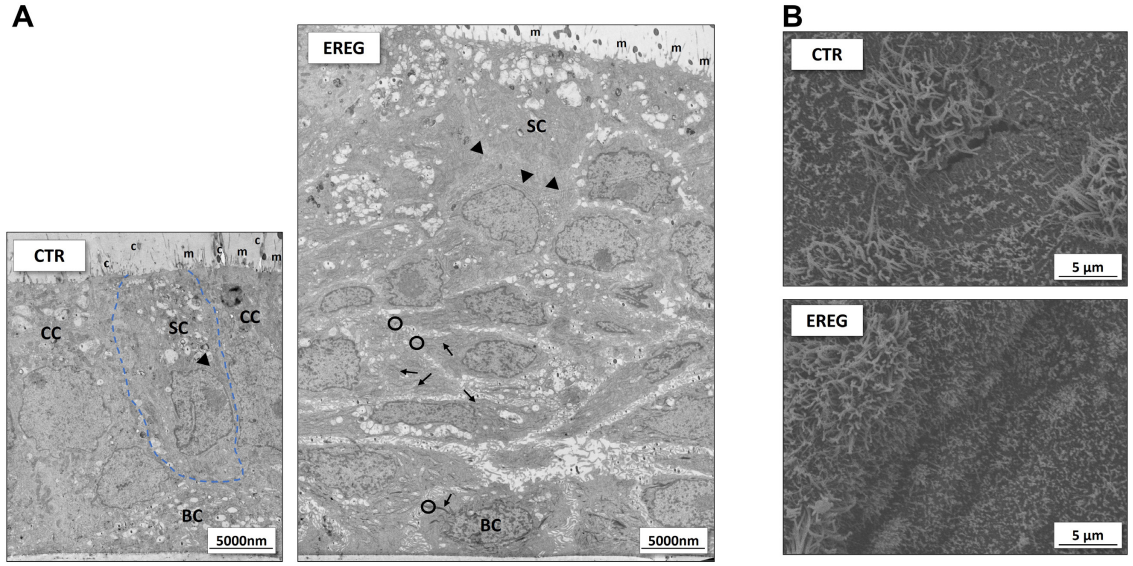


Fig. 2: EREG stimulation alters cellular morphology and differentiation in hBECs.
(A) Transmission electron microscopy and **(B)** scanning electron microscopy of air liquid interface cultures of primary human bronchial epithelial cells (hBECs) treated for 48 h with either vehicle (CTR) or 250 ng/ml EREG. **SC** indicates secretory cells (---), **BC** indicates basal cells, **CC** indicates ciliated cells, **m** indicates microvilli, **c** indicates (kino)cilia. Arrows (➞) indicate intracellular filament bundles, circles (**O**) indicate desmosomes. Arrowheads (▶) indicates stacks of rough endoplasmatic reticulum (rER)**.** Representative pictures are shown. Scale bar = 5000 nm **(A)** / 10 µm **(B)**.

3.1.2 Epiregulin Treatment Induces DNA Damage and Senescence in Airway Epithelial Cells

One of the cellular effects of the ErbB system overactivation is the induction of senescence. Therefore, it was anticipated that EREG may also trigger alterations in airway epithelial cells that can finally lead to their senescence. To investigate the effect of EREG on cellular DNA damage and senescence, comet assay (Fig. 3A-B) and β-galactosidase staining (Fig. 3C) were performed.

Fig. 3A shows that in comet assay, the tail length of EREG-treated cells (Fig. 3A, middle image) is longer than in vehicle-treated controls (Fig. 3A, top image). Treatment with doxorubicin (Fig. 3A, bottom image), a chemotherapeutic drug, was used as a positive control for DNA damage and shows the longest tail length, indicating the most DNA damage. To quantify the amount of DNA damage, the tail moment was calculated from the tail length and results are shown in Fig. 3B. Tail moments of EREG-treated cells were significantly higher than in controls ($p<0.0001$), while positive control with doxorubicin treatment showed the highest tail moment and amount of DNA damage (Fig. 3B).

Furthermore, Fig. 3C shows that β-galactosidase staining is more intense after EREG treatment (Fig. 3C, lower images) than in vehicle-treated controls (Fig. 3C, top images), representing increased activation of cellular senescence.

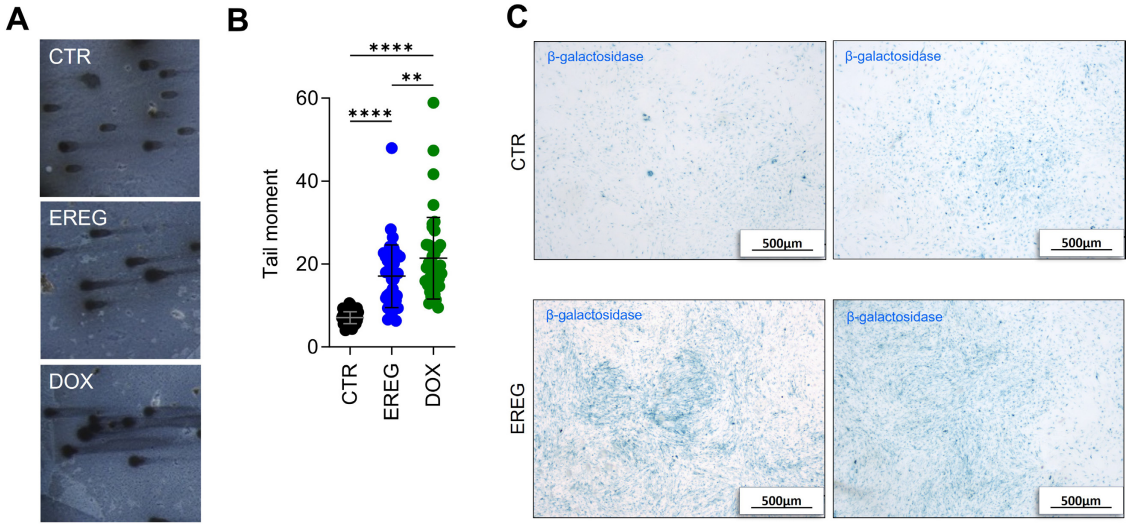
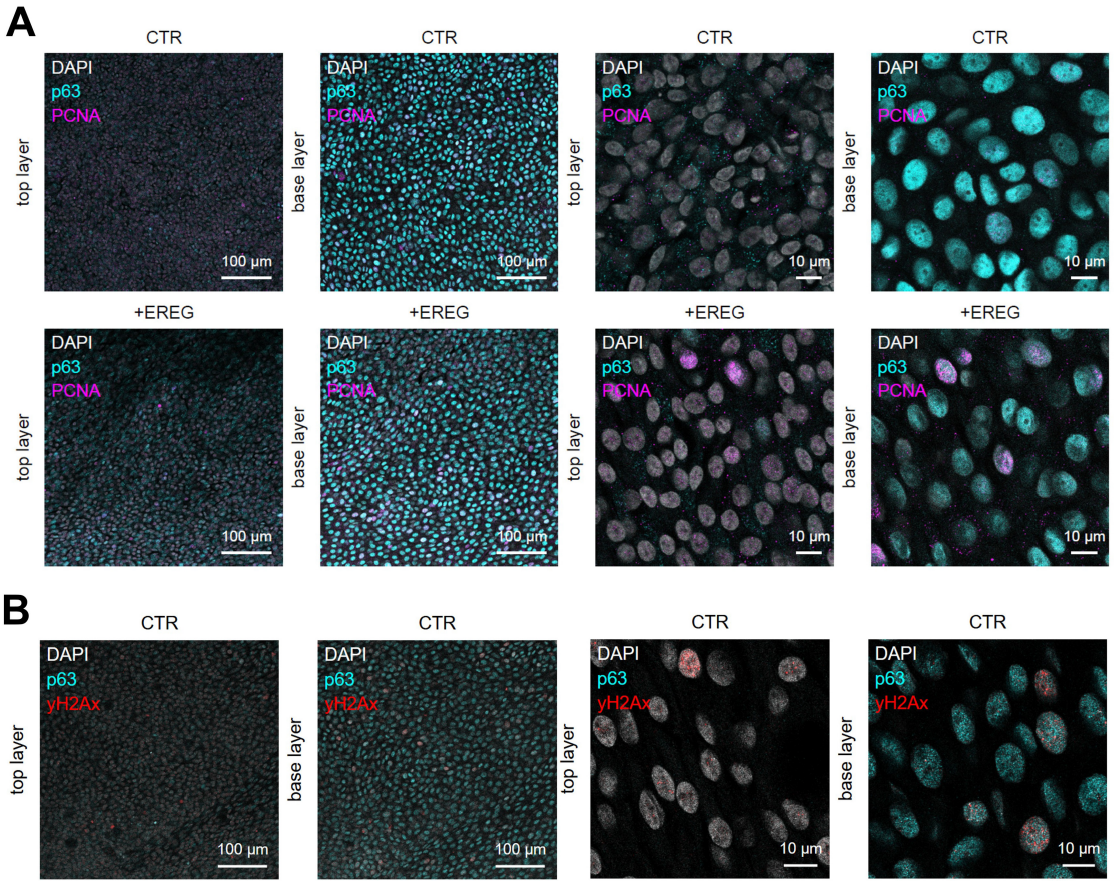


Fig. 3: EREG treatment of bronchial epithelial cells increases DNA damage and induces cellular senescence.
(A) Comet assay showing comet tails of cells indicating DNA fragmentation and damage in BEAS-2B cells treated either with vehicle (CTR) or 250 ng/ml EREG. 5µM doxorubicin (DOX) was used as a positive control for DNA damage. Representative pictures are shown. **(B)** Tail moment (tail length x DNA percentage) was calculated from 61 cells for CTR, 43 cells for EREG and 43 cells for doxorubicin-treated cells. Black dots represent vehicle controls (CTR), blue dots represent EREG-treated cells (EREG) and green dots represent doxorubicin controls (DOX). Data are presented in dot plots with mean and SD *$p<0.05$, **$p<0.01$, ***$p<0.001$, ****$p<0.0001$. **(C)** β-galactosidase staining of BEAS-2B cells that were treated for 48 h with either vehicle (PBS) or 250 ng/ml EREG. Blue staining indicates positive β-galactosidase staining. Representative pictures are shown. Scale bars = 500µm.

3.1.3 *Epiregulin Stimulation Enhances DNA Damage and Cellular Senescence in Basal Cells and Proliferation in Non-Basal Cells in the Respiratory Epithelium*

To decipher the underlying mechanisms of the effect of EREG stimulation on epithelial morphology, immunofluorescence stainings from air liquid interface cell cultures of airway epithelial cells were performed as described in section 2.2.8.5.2.

Fig. 4 shows that the EREG stimulation alters the expression of p21, PCNA and γH2Ax throughout the cultured epithelium. After EREG stimulation, PCNA is expressed in $p63^+$ basal cells but also in cells from the top layer that are $p63^-$, while in vehicle-treated controls, PCNA expression is rarely seen in both $p63^+$ and $p63^-$ cells (Fig. 4A). Figure 4B shows that in vehicle controls, γH2Ax is mainly detected in cells from the top layer, while after EREG stimulation, also $p63^+$ basal cells show γH2Ax expression, indicating DNA damage in these cells (Fig. 4B). Fig. 4C shows that p21 is only expressed in $p63^-$ cells of the epithelium in vehicle controls, while after EREG stimulation, $p63^+$ basal cells also express p21, showing activation of cellular senescence in basal cells (Fig. 4C).



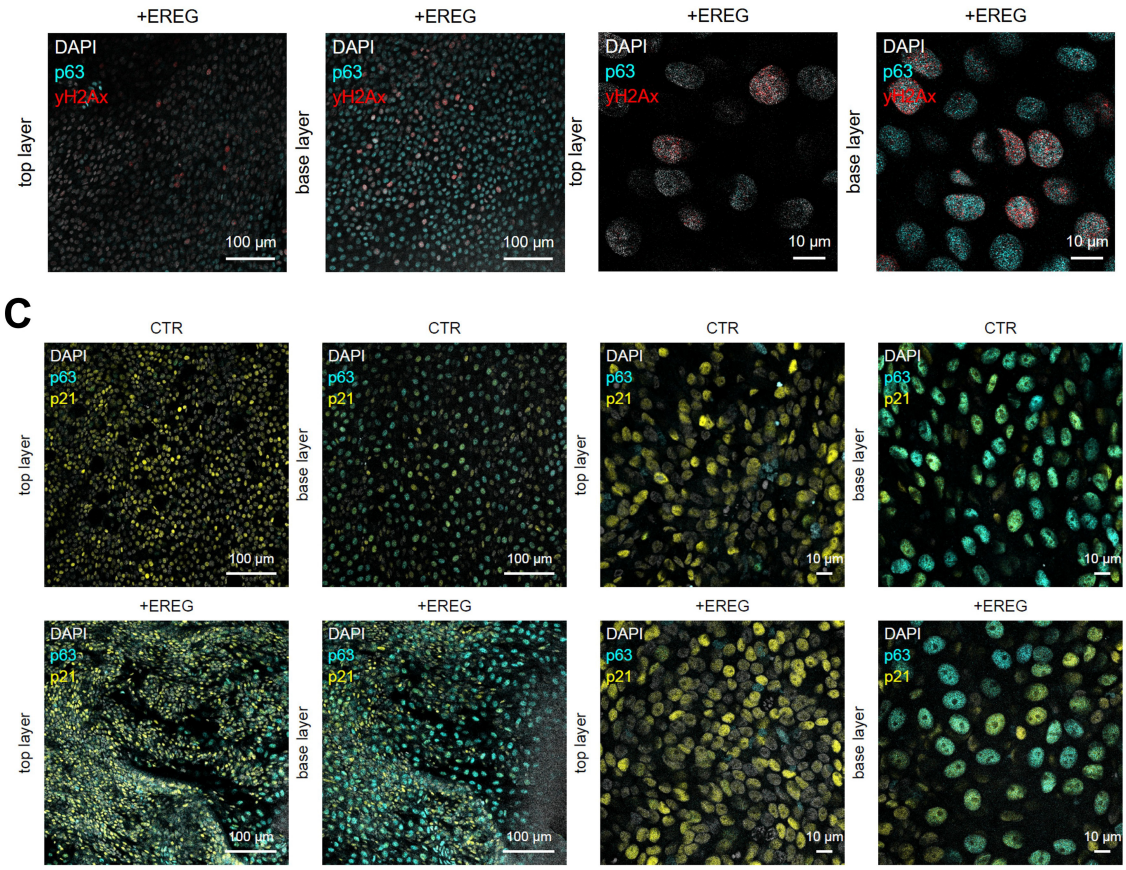


Fig. 4: Airway epithelial cells show altered expression patterns of PCNA, p21 and γH2Ax while p63 expression is unaltered.
(A-C) Immunocytofluorescence staining of airway epithelial cells cultured in an air liquid cell culture interface and treated with 250 ng/ml EREG or vehicle (CTR) for 48 hours. Immunofluorescence staining was performed using markers for p63 and PCNA **(A)**, p63 and γH2Ax **(B)** and p63 and p21 **(C)**. Nucleus staining was performed using DAPI-staining **(A-C)**. DAPI stained cell nuclei are shown in white, $p63^+$ cells in teal-blue, $PCNA^+$ cells in pink, $γH2AX^+$ cells in red and $p21^+$ cells in yellow. Representative pictures of different magnifications of the top layer, base layer and an interpolated sideview of the epithelium are shown for each staining. Scale bars = 100 µm (overview magnification top and base layer), 10 µm (high magnification top and base layer).

Since the reconstruction of z-stacks only covered either the top or the base layer of the airway epithelium, altered expression of markers was alternatively investigated in immunofluorescence stainings from paraffin sections, as described in 2.2.8.5.1, to show the expression of the top and base layer in one image together.

Fig. 5A shows that γH2Ax is occasionally found in $PCNA^+$ cells of the base layer of the epithelium. After EREG stimulation, also cells from the top layer are $PCNA^+$ and $γH2Ax^+$, suggesting that hyperproliferating cells may undergo DNA damage. As shown in Fig. 5A, PCNA staining is seen in both basal cells and non-basal cells.

In vehicle controls, γH2Ax staining is only seen in a few cells that are also stained positive for PCNA in the base layer (Fig. 5A, left images). After EREG stimulation, PCNA and γH2Ax are co-expressed in almost all cells over the epithelium (Fig. 5A, right images).

Fig. 5B shows that in vehicle controls, p21 expression is limited to the top layer of the

epithelium (Fig. 5B, left images), while PCNA expression is mainly located in cells from the base layer of the epithelium (Fig. 5B, left images). After EREG stimulation, PCNA and p21 staining is seen in almost all cells of the epithelium in the top and base layer (Fig. 5B, right images).

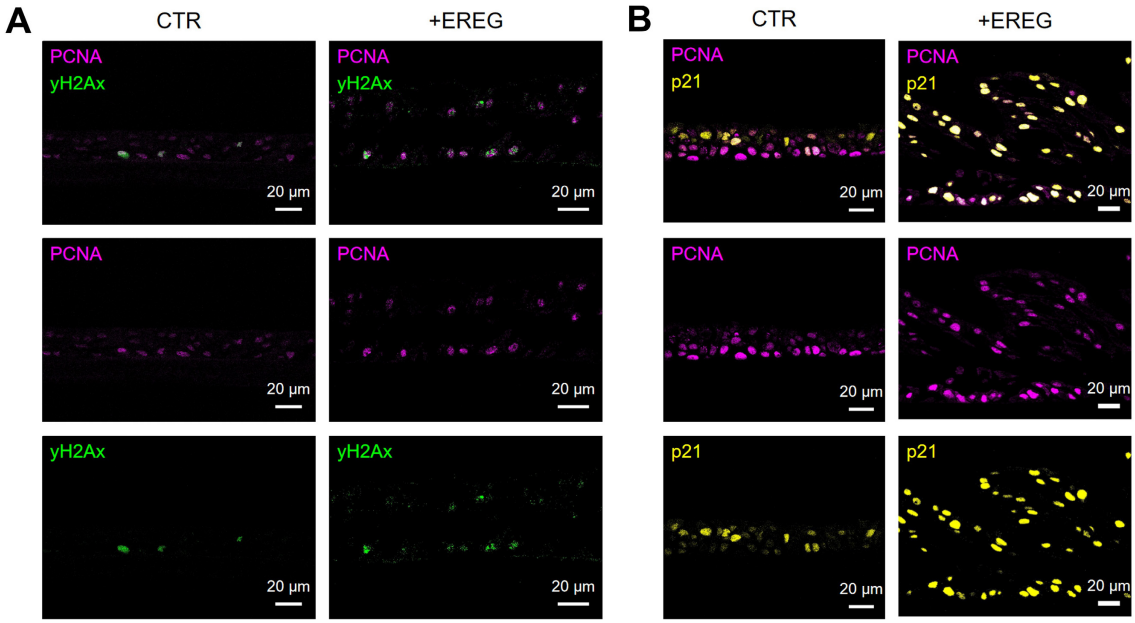


Fig. 5: Expression pattern of p21, γH2Ax and PCNA is altered in airway epithelial cells after EREG stimulation.
(A-B) Immunocytofluorescence staining of airway epithelial cells cultured in an air liquid cell culture interface and treated with 250 ng/ml EREG or vehicle (CTR) for 48 hours. Immunofluorescence staining was performed using markers for PCNA and γH2Ax **(A)** and PCNA and p21 **(B)**. **(A-B)** PCNA$^+$ cells in pink, γH2Ax$^+$ cells in green and p21$^+$ cells in yellow. Representative pictures are shown. Scale bars = 20 µm.

To quantify p63$^+$ basal cells co-expressing PCNA, p21 and γH2Ax after EREG stimulation, paraffin sections were stained accordingly and immunofluorescence-positive cells were counted in an automatic manner as described in 2.2.9. Fig. 6A shows the results for p63 and PCNA staining. In vehicle-treated controls, only a few p63$^+$ basal cells show co-staining of p63 and PCNA and almost no other cells show a PCNA signal. In EREG-treated cells, almost all cells (p63$^+$ basal cells and p63$^-$ cells) show a positive PCNA signal. Fig. 6B shows the staining of airway epithelial cells for p63 and p21. While in controls, p21 staining is only observed in a few p63$^+$ basal cells, cells stimulated with EREG show positive p21 staining in both p63$^+$ basal cells and p63$^-$ non-basal cells from the top layer of the epithelium. Fig. 6C shows the staining for p63 and γH2Ax. While in controls, only p63$^-$ non-basal cells show an occasional signal for γH2Ax, EREG stimulation triggered an increase in γH2Ax$^+$ signal in p63$^+$ and p63$^-$ cells.

Cell counting revealed an elevated number of p63$^+$, PCNA$^+$, p21$^+$ and γH2Ax$^+$ cells following stimulation with EREG (Fig. 6D). p63$^+$ and p21$^+$ as well as p63$^+$ and γH2Ax$^+$ cells were increased after EREG treatment, indicating augmented DNA damage and

senescence in basal cells. Only the numbers of $p63^+$ and $PCNA^+$ cells were not significantly altered after EREG stimulation, suggesting no change in the proliferation of basal cells upon exposure to the stimulus.

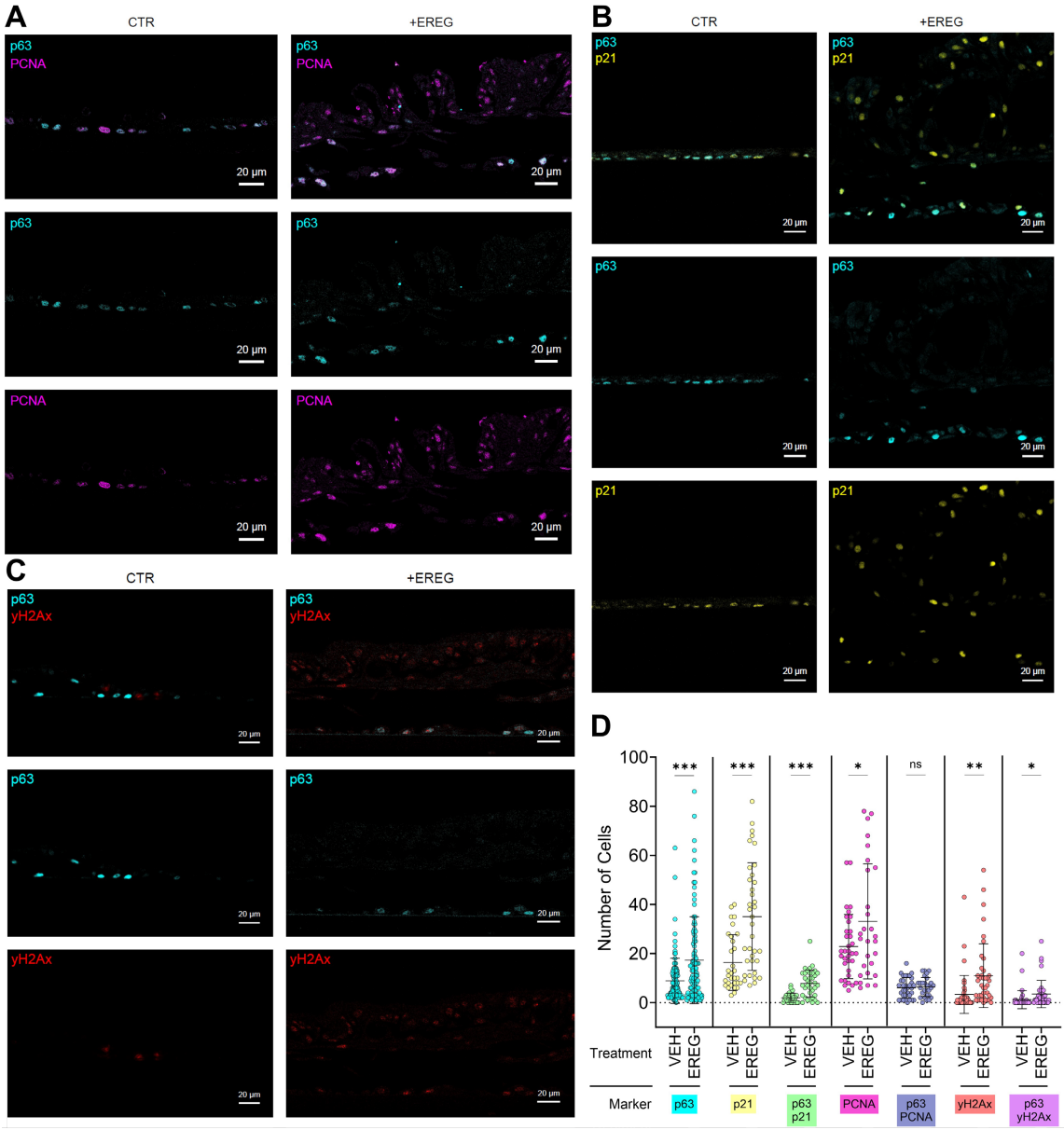


Fig. 6: Airway epithelial cells show upregulation of p63, p21, PCNA and γH2Ax in all cells, but only p21 and γH2Ax upregulation in $p63^+$ cells after EREG treatment.
(A-C) Immunocytofluorescence staining of paraffin sections from airway epithelial cells cultured in an air liquid cell culture interface and treated with 250 ng/ml EREG or vehicle (CTR/VEH) for 48 hours. Immunofluorescence staining was performed using markers for p63 and PCNA **(A)**, p63 and p21 **(B)** and p63 and γH2Ax **(C)**. $p63^+$ cells are shown in teal-blue, $PCNA^+$ cells in pink, $γH2Ax^+$ cells in red and $p21^+$ cells in yellow. Representative pictures are shown. Scale bars = 20 µm. **(D)** Cell counts were acquired from immunofluorescence stainings A-C from 3 different donors. The total length of the paraffin-embedded filter embedded was scanned, and all cells were counted for all four markers p63, PCNA, γH2Ax and p21. Data are represented as mean ± SD. *p<0.05, **p<0.01, ***p<0.001, ****p<0.0001, ns = not significant.

3.2 In vivo effects of Epiregulin Experimental Pulmonary Fibrosis in Mice

3.2.1 Histological Fibrosis and Lung Function Is Unaltered in Bleomycin Exposed Mice Treated with Epiregulin

To investigate if EREG has an effect on the pathogenesis of pulmonary fibrosis, mice receiving bleomycin were also treated intratracheally with EREG or saline as shown in Fig. 7A1 and Fig. 8A1. Pulmonary compliance was measured at the end of the experiment as a diagnostic marker for lung fibrosis. Additionally, hematoxylin and eosin staining of the lung tissue from affected animals was performed to determine the extent of fibrosis. Fig. 7 shows results of mice that received EREG intratracheally on day 0, 2 and 4 after bleomycin instillation, while Fig. 8 shows results of mice receiving EREG on day 8, 10, 12, 14 and 16 after bleomycin instillation.

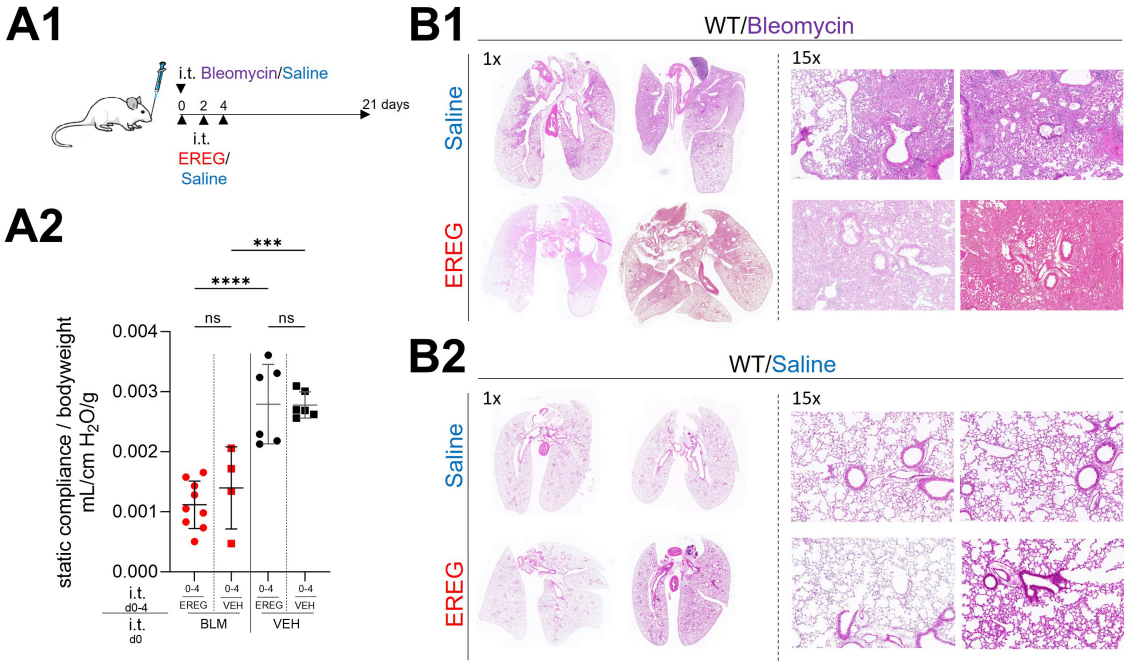


Fig. 7: Bleomycin treatment lowers static lung compliance and leads to histological lung fibrosis, while EREG administration on day 0, 2 and 4 does not aggravate the effect of bleomycin.
(A1) Mice received bleomycin or saline (NaCl) intratracheally on day 0 and were treated with EREG or saline intratracheally on day 0, 2, 4. **(A2)** Static lung compliance measurements from mice 21 days after bleomycin or saline (NaCl) instillation and treatment with EREG or saline on day 0, 2 and 4. Red dots and blocks represent bleomycin-treated mice, while black dots and blocks represent saline-treated mice. Dots represent EREG treatment, while blocks represent saline treatment during the experiment. Data are represented as mean ± SEM. *p<0.05, **p<0.01, ***p<0.001, ****p<0.0001, ns = not significant. **(B1-B2)** Hematoxylin and eosin stainings of lungs from mice 21 days after bleomycin **(B1)** or saline instillation **(B2)** and additional treatment with EREG or saline on day 0, 2 and 4. Representative pictures are shown in 1x magnification on the left and in 15x magnification on the right.

Fig. 7A2 and Fig. 8A2 show that static compliance of mice is reduced after bleomycin treatment. Neither early (day 0, 2 and 4) nor late application of EREG (day 8, 10, 12, 14 and 16) had an effect on lung function of bleomycin-treated mice. Furthermore, EREG

treatment didn't have any impact on the extend of fibrosis as assessed by the histological evaluation of lung tissue sections. In control mice, EREG alone didn't have an effect on the lung histology without bleomycin treatment (Fig. 7B2 and Fig. 8B2). Since saline groups were consistent for both early and late EREG application in previous studies, only one control group and time point of application (day 0, 2 and 4) was used as a control, in alignment with the 3R principles.

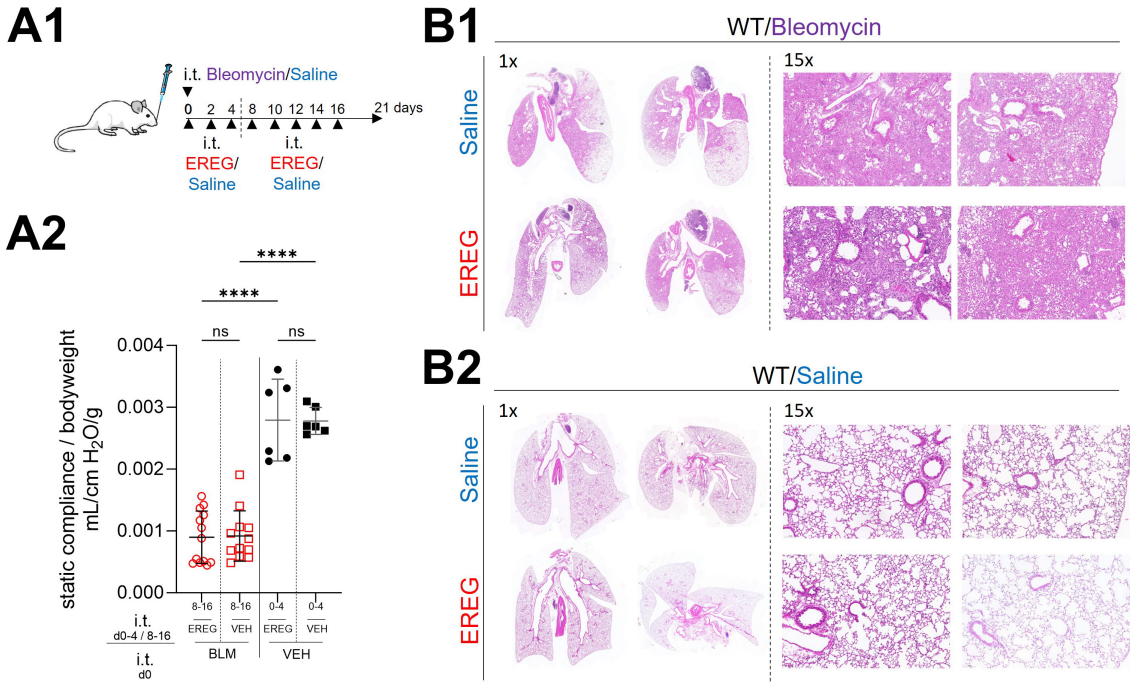


Fig. 8: Bleomycin treatment lowers static lung compliance and leads to histological lung fibrosis, while EREG administration on day 8, 10, 12, 14 and 16 does not aggravate the effect of bleomycin. **(A1)** Mice received bleomycin or saline (NaCl) intratracheally on day 0 and were treated with EREG or saline intratracheally on day 8, 10, 12, 14 and 16 or on day 0, 2 and 4 (only day 0 saline controls). **(A2)** Static lung compliance measurements on day 21 post-bleomycin treatment. EREG was administered on day 8, 10, 12, 14 and 16 post-bleomycin application. Red dots and blocks represent bleomycin-treated mice, while black dots and blocks represent saline-treated animals. Dots represent the EREG treatment of mice during the experiment, while blocks represent the saline treatment of mice during the experiment. Data are represented as mean ± SEM. *p<0.05, **p<0.01, ***p<0.001, ****p<0.0001, ns = not significant. **(B1-B2)** Hematoxylin and eosin stainings of lung tissue sections from mice 21 days after bleomycin **(B1)** or saline instillation **(B2)** and additional treatment with EREG on day 8, 10, 12, 14 and 16 or saline on day 0, 2 and 4. Representative pictures are shown in 1x magnification on the left and in 15x magnification on the right.

3.2.2 Senescence-Associated Secretory Phenotype Mediator Levels in Bronchoalveolar Lavage Fluid Are Altered after Bleomycin Treatment in Mice but Are Unaltered after Additional Epiregulin Application

In order to investigate whether EREG instillation in mice with lung fibrosis alters concentration of SASP-associated proteins, the levels of IL-6, MIP-2, MMP-25, EREG, MMP-2 and TWEAKR/TNFRSF12 were measured in BALF at day 21 post-bleomycin administration. While the overall protein levels were increased after bleomycin treatment, EREG application treatment did not alter this effect (Fig. 9A). Fig. 9B, Fig. 9C and Fig.

9E show that IL-6, MIP-2 and EREG levels were not increased after bleomycin treatment, while Fig. 9D, Fig. 9F and Fig. 9G show that MMP-2, MMP-25 and TNFRSF12/TWEAKR were elevated in BALF from bleomycin-treated mice. Overall, EREG treatment did not have an additional effect on bleomycin-associated upregulation of SASP mediator levels.

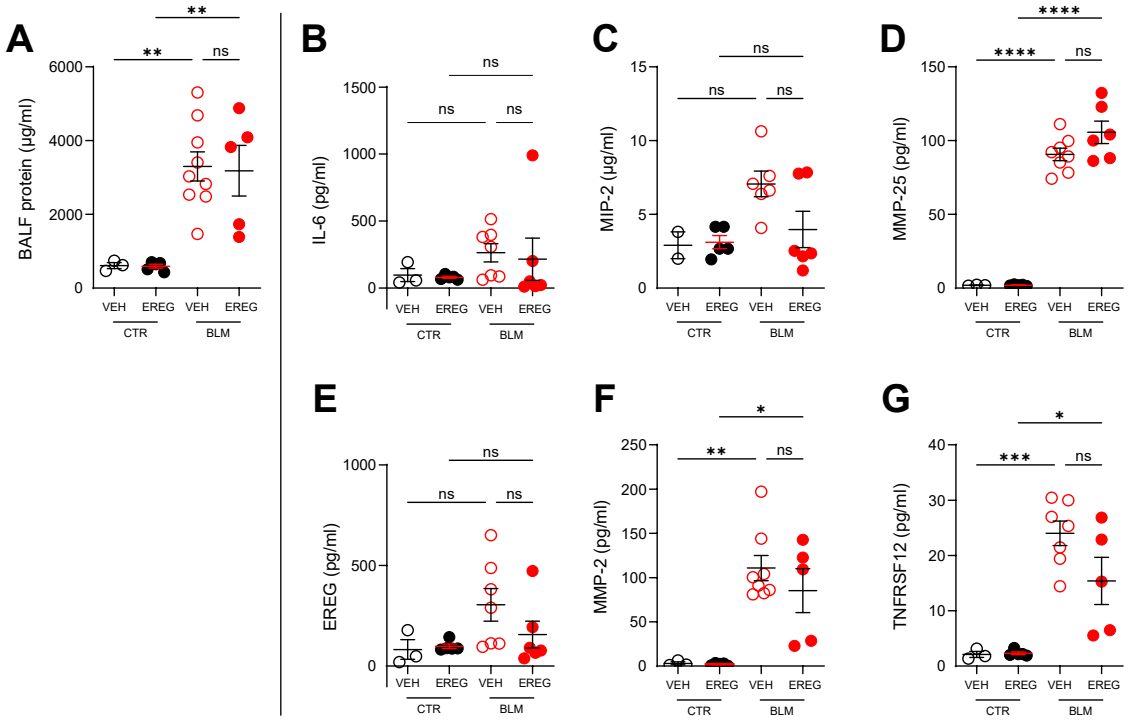


Fig. 9: Total protein levels and SASP mediators MMP-2, TNFRSF12/TWEAKR and MMP25 are upregulated in BALF from mice after bleomycin treatment, while EREG treatment does not augment the effect.
(A) Total protein levels and **(B-G)** levels of SASP mediators (IL-6, MIP-2, MMP-25, EREG, MMP-2, TNFRSF12/ TWEAKR) in BALF at day 21 post-bleomycin administration. Red dots and circles represent the bleomycin-treated mice while black dots and circles represent the saline-treated mice. Dots represent animals treated with EREG at day 8, 10, 12, 14, 16 or saline at day 0, 2, 4 respectively. Data are represented as mean ± SEM. *p<0.05, **p<0.01, ***p<0.001, ****p<0.0001, ns = not significant.

3.2.3 Administration of Epiregulin Promotes Proliferation and Senescence in Bleomycin Exposed Mice

In order to investigate whether the in vitro effects of EREG shown in 3.1 are transferable to the in vivo model of lung fibrosis, expression of ΔNp63, PCNA and p21 was assessed by means of IHC staining of lungs from mice that received bleomycin or saline and additionally EREG or saline. Because none of the tested antibodies against p63 yielded a specific IHC signal, an antibody against the p63 isoform ΔNp63 was used. Both p63 and ΔNp63 are expressed in basal cells (258). Additionally, PCNA was used as a marker for cell proliferation, while p21 was used as a marker for cellular senescence as in previous experiments.

Fig. 10 shows that the signal for ΔNp63 (Fig. 10, left images), PCNA (Fig. 10, middle images) and p21 (Fig. 10, right images) is enhanced in the lungs from bleomycin-treated animals that received EREG intratracheally. The signal of PCNA was found to be massively increased, while the signal of ΔNp63 and p21 was only slightly increased after EREG administration (Fig. 10A-B). EREG treatment alone only showed an enhanced signal for p21 in epithelial cells of the bronchi, but not in the alveoles or interstitial regions (Fig. 10C). Saline alone did not have an effect on ΔNp63-, PCNA- or p21 staining (Fig. 10D).

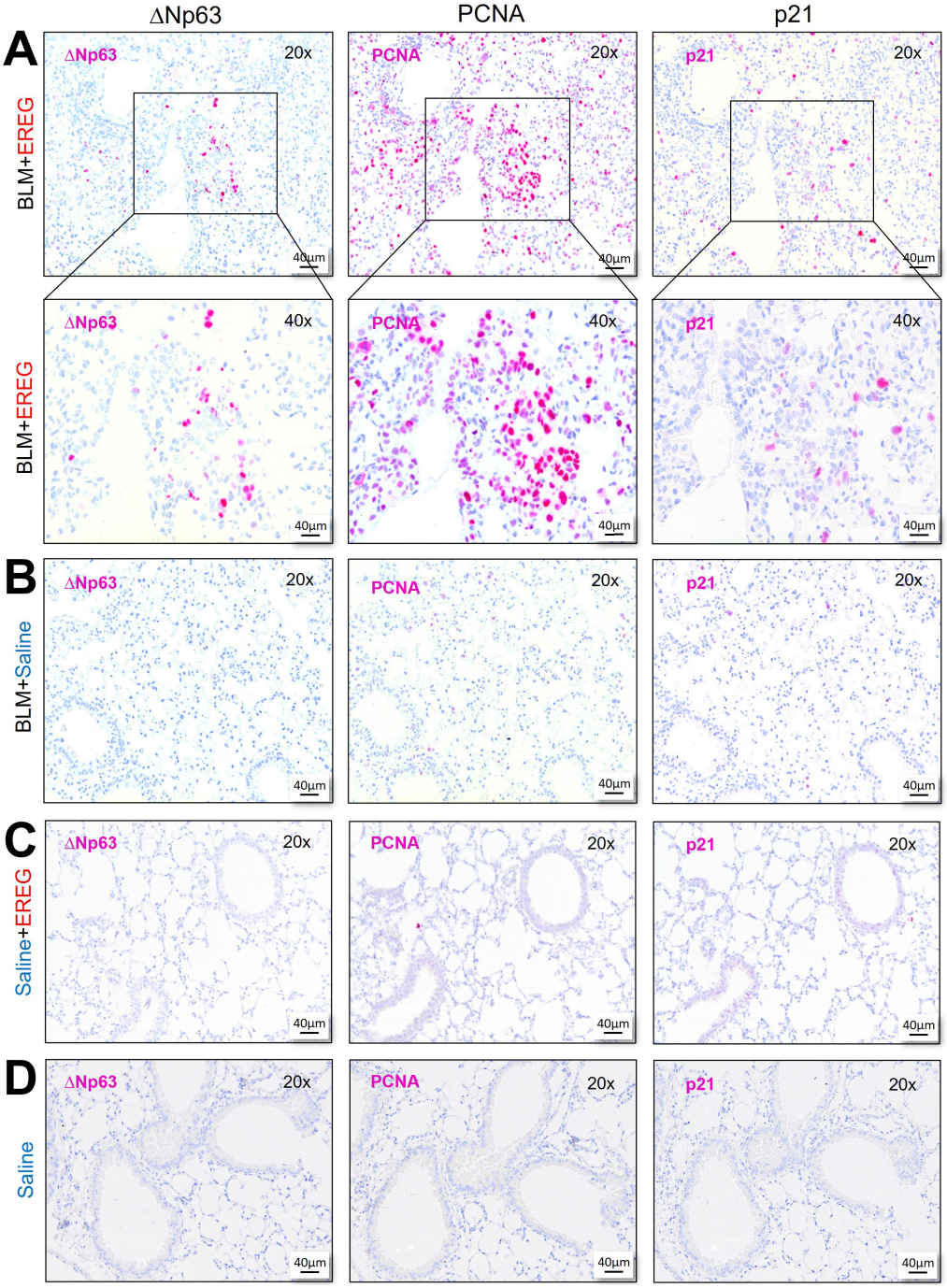
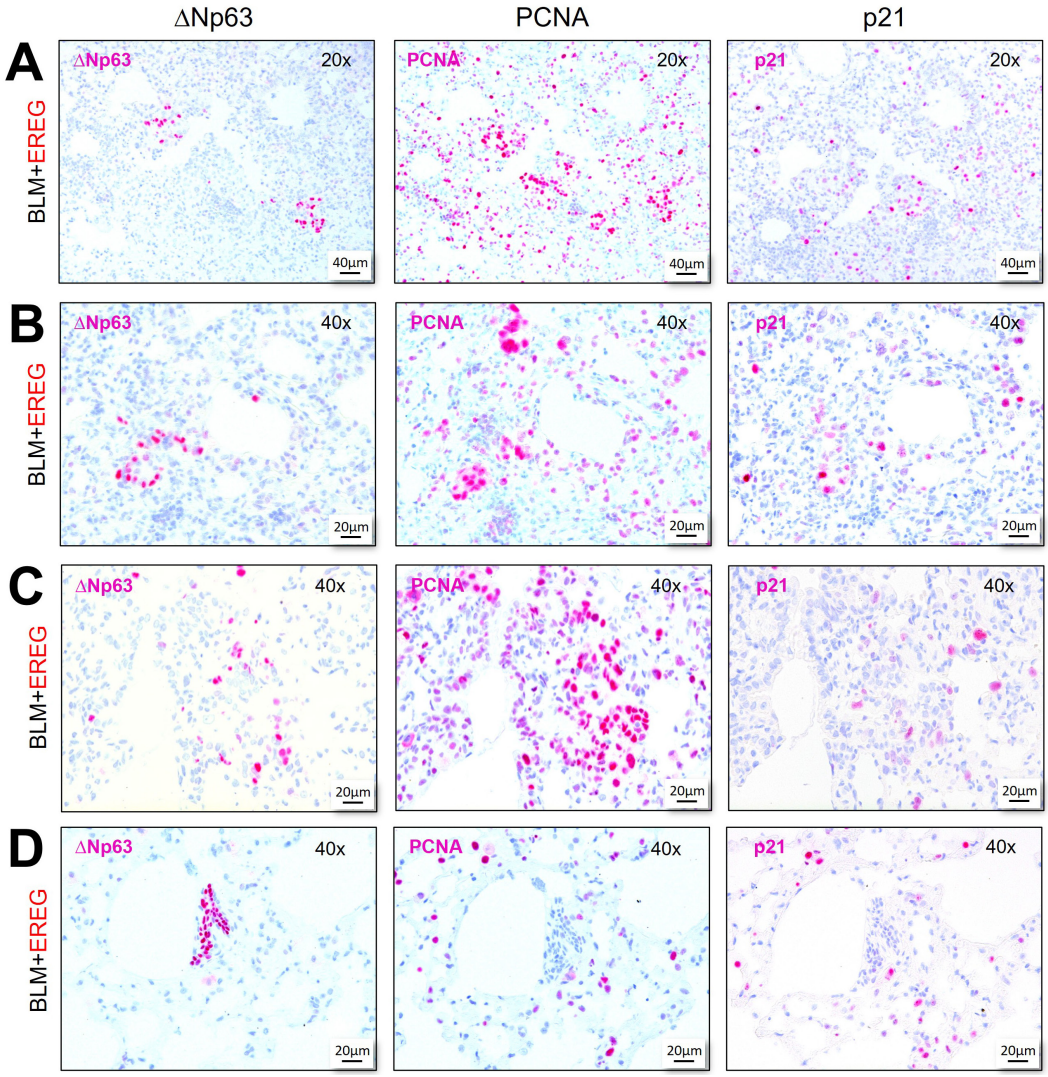


Fig. 10: EREG application amplifies ΔNp63-, PCNA- and p21-signals in bleomycin-treated mice.

(A-D) Immunohistochemistry stainings of ΔNp63-, PCNA- and p21 in lungs from mice at day 21 post-bleomycin (BLM, **A-B**) or saline instillation and additional treatment with EREG on day 8, 10, 12, 14, 16 (**A, C**) or saline on day 0, 2 and 4 (**B, D**). Representative pictures are shown in 20x and 40x magnification. Scale bars = 40µm **(A-D)**.

Fig. 11 presents higher magnification images of lungs treated with bleomycin and EREG that were stained with ΔNp63, PCNA and p21. Notably, $\Delta Np63^+$ cells appeared in clusters within dense fibrotic regions of the lung parenchyma, indicating their ectopic localization in areas of tissue injury (Fig. 11A-E, left panels). Some $\Delta Np63^+$ cells clusters exhibited co-staining with PCNA and p21 (Fig. 11A-C), whereas other clusters lacked co-staining of these markers (Fig. 11D). Co-localization of PCNA and p21 was observed only in a small subset of cells, predominantly within interstitial regions that showed histological fibrosis (Fig. 11A-E, center and right panels).



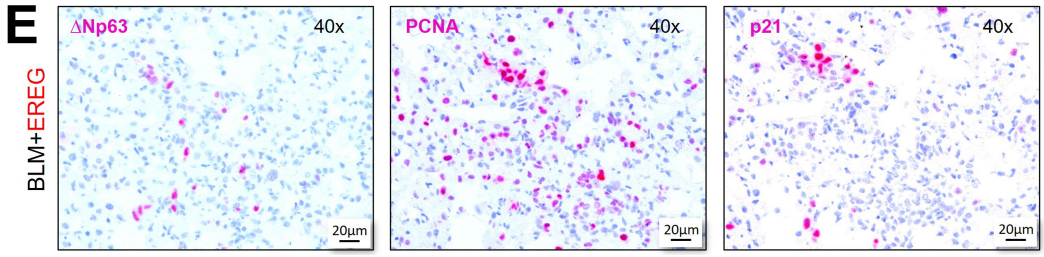


Fig. 11 Distribution of ΔNp63$^+$, PCNA$^+$ and p21$^+$ cells in the lungs of bleomycin- and EREG-treated mice.
(A-E) Immunohistochemistry stainings of ΔNp63-, PCNA- and p21 in lungs from mice at day 21 post bleomycin (BLM) administration and additional treatment with EREG on day 8, 10, 12, 14, 16. Representative pictures are shown in 20x and 40x magnification. Scale bars = 40µm **(A)**. Scale bars = 20µm **(B-E)**.

Next, ΔNp63$^+$ cells were counted in murine lungs that were treated with bleomycin and EREG or saline. While a significant difference in the total number of ΔNp63$^+$ cells was observed (Fig. 12A), no significant difference was found in the number ΔNp63$^+$ cells per mm² between EREG-treated animals and controls treated with saline (Fig. 12B).

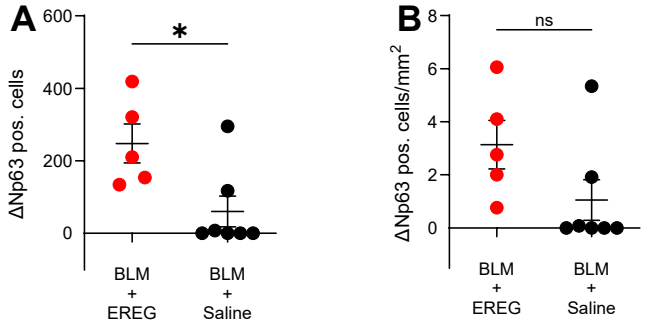


Fig. 12: ΔNp63$^+$ cell counts are higher in bleomycin-treated mice after EREG treatment.
(A-B) Cell counts of ΔNp63$^+$ cells in lung parenchyma from mice at day 21 post-bleomycin (BLM) or saline instillation and additional intratracheal treatment with EREG on day 8, 10, 12, 14, 16 **(A)** or saline on day 0, 2 ,4 **(B)** respectively. Data are represented as mean ± SEM. *p<0.05, **p<0.01, ***p<0.001, ****p<0.0001, ns = not significant.

Finally, FACS analysis was performed to identify and quantify the cell types exhibiting altered proliferation and senescence in the lungs of bleomycin-treated mice that received either EREG or saline. First, inflammatory cells (CD45$^+$ cells) and endothelial cells (CD31$^+$ cells) as well as mesenchymal cells (remaining CD326$^-$ cells) were excluded from the analysis as shown in Fig. 13A. CD326$^+$ epithelial cells were then divided into subpopulations of CD326$^+$/MHCII$^+$ and CD326$^+$/MHCII$^-$ cells. Here, MHCII was used to distinguish between alveolar epithelial cells (ATI- and ATII-cells, MHCII$^+$ cells) and other respiratory epithelial cells (MHCII$^-$ cells) (259) (Fig. 13B). Next, the two subpopulations of CD326$^+$/MHCII$^+$ and CD326$^+$/MHCII$^-$ cells were gated for Ki67$^+$, PCNA$^+$ and SOX2$^+$ cells. SOX2 was used to identify epithelial cells with progenitor function (basal cells or modified ATII cells = SOX2$^+$ cells) (260). Ki67 was used as a proliferation

marker and p21 was used as a marker of cellular senescence (Fig. 13B) to further investigate epithelial cell fate following bleomycin and EREG administration.

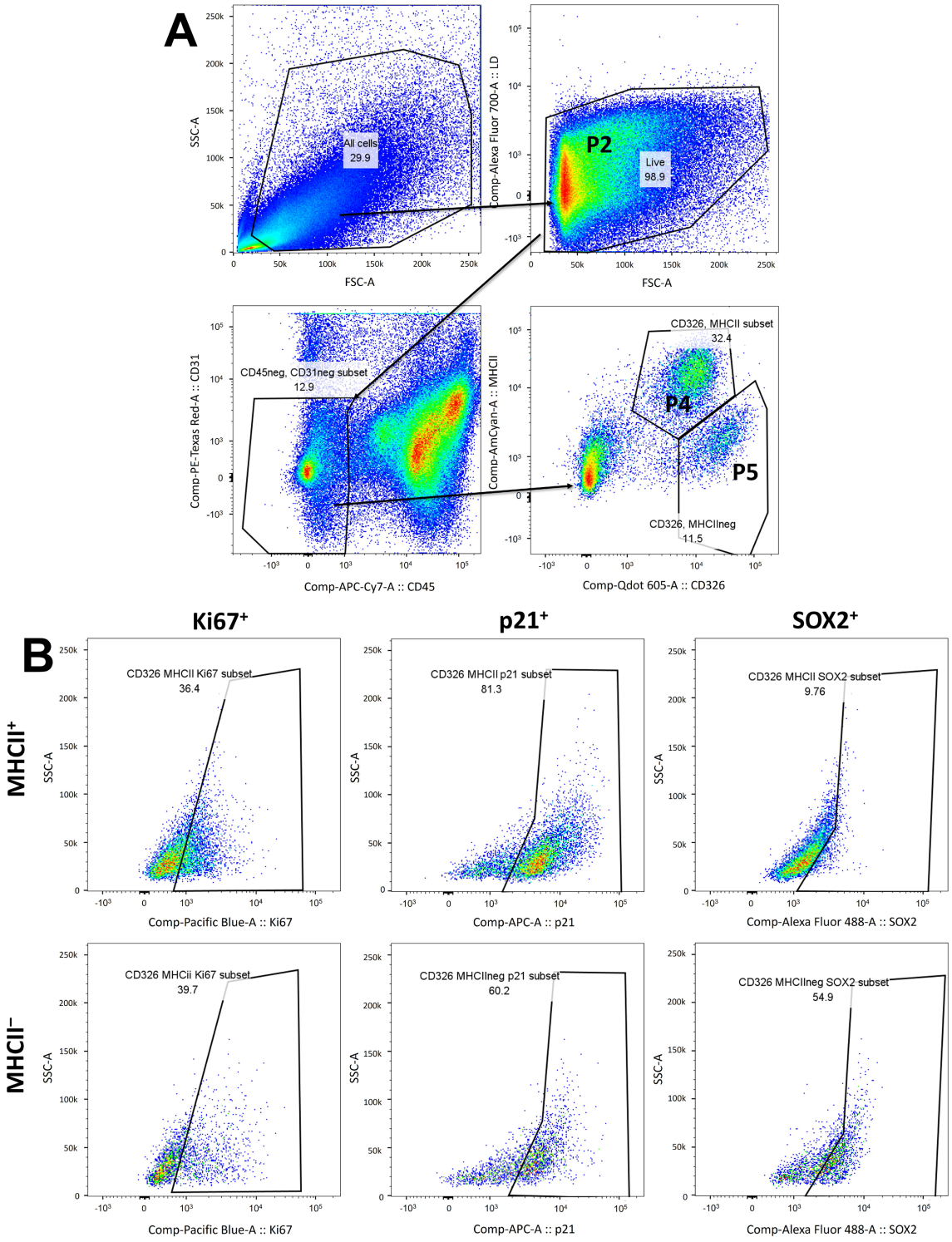


Fig. 13: Gating strategy for murine lung epithelial cells.
(A-B) Representative gating strategy for alveolar and airway epithelial cells from the lungs of mice 21 days after bleomycin or saline (NaCl) instillation and treatment with EREG on day 8, 10, 12, 14, 16 or saline on day 0, 2 4. **(A)** Cells from single cell suspensions **(P1)** were gated to exclude dead cells **(P2)**, $CD45^+$-cells (immune cells) and $CD31^+$-cells (endothelial cells) **(P3)**. ATI, ATII cells ($CD326^+$ & $MHCII^+$ = **P4**) and airway epithelial cells ($CD326^+$ & $MHCII^-$ = **P5**) were sorted by MHCII expression from $CD326^+$-population **(P3)**. **(B)** $MHCII^+$ and $MHCII^-$ subpopulations of epithelial cells P4 and P5 were differentiated by Ki67, p21 and SOX2 expression.

Fig. 14 shows that p21 signal is increased after bleomycin treatment in both MHCII$^+$ (AT I and II) and MHCII$^-$ cells (airway epithelial cells), while EREG treatment had no effect on the upregulated p21 expression (Fig. 14A1, Fig. 14B1 right images). After bleomycin treatment, SOX2 expression was also upregulated, but only in MHCII$^+$ cells, while this increase was not affected by additional EREG treatment (Fig. 14A2, Fig. 14B2). In MHCII$^+$/SOX2$^+$ cells, p21 was upregulated, while MHCII$^-$/SOX2$^+$ cells didn't show increased p21 expression (Fig. 14A3, Fig. 14B3, right images). Again, application of EREG didn't have any effect on the bleomycin-triggered increase in the p21 signal (Fig. 14A3, Fig. 14B3, right images). Ki67 expression remained unchanged in both MHCII$^+$ and MHCII$^-$ cells (Fig. 14A1, Fig. 14B1, left images) as well as in all SOX2$^+$ cell subpopulations after bleomycin and/or EREG treatment (Fig. 14A3, Fig. 14B3, left images).

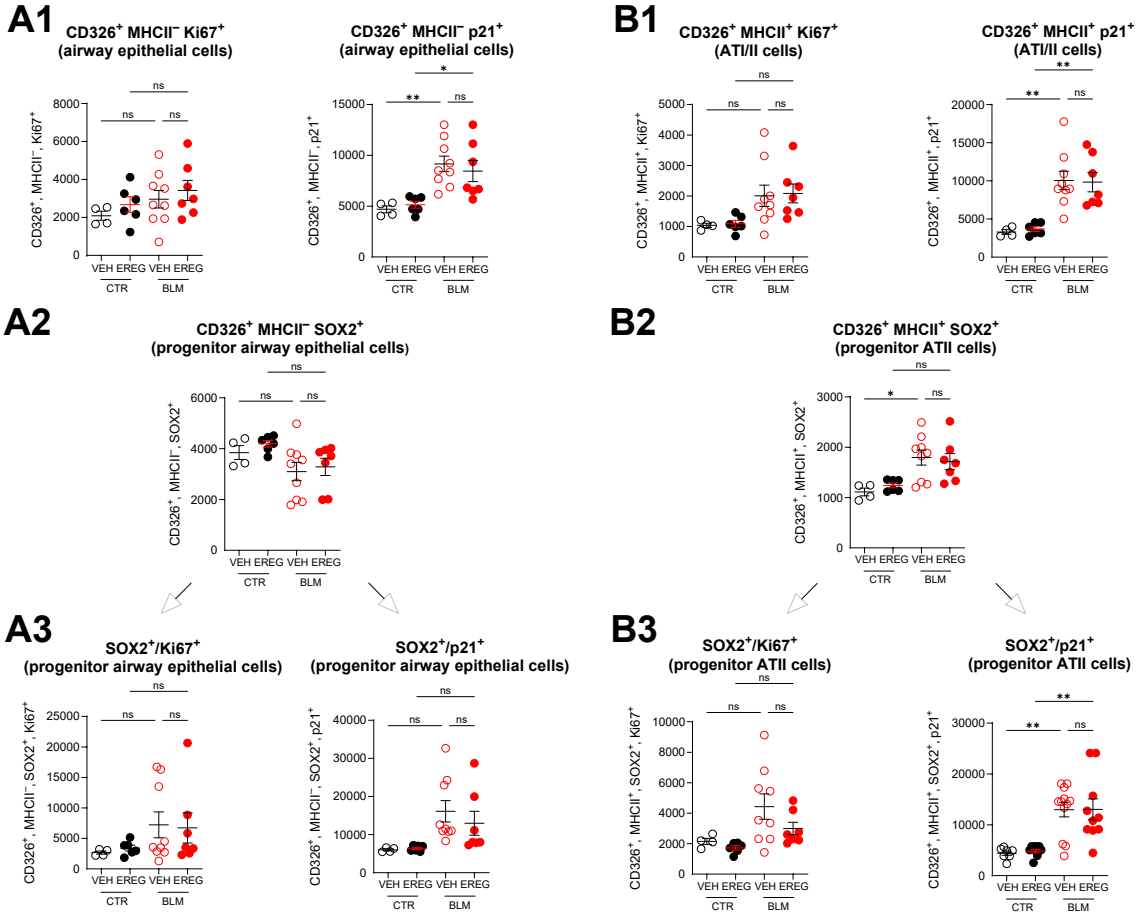


Fig. 14: Bleomycin treatment in mice alters p21- but not Ki67 expression in MHCII$^+$ and MHCII$^-$ epithelial cells. EREG treatment doesn't have an additional effect on p21-, Ki67- or SOX2 expression. Cell counts from FACS analysis of the lungs of mice 21 days after bleomycin or saline (NaCl) instillation and treatment with EREG on day 8, 10, 12, 14, 16 or saline on day 0, 2, 4. Red dots and circles represent the bleomycin-treated mice while black dots and circles represent the saline-treated mice. Dots represent the EREG-treated mice, while circles represent the saline-treated mice. **(A1-A3)** Cells that are CD326$^+$ but MHCII$^-$ were sorted for Ki67-, p21- and SOX2 expression. SOX2$^+$ cells were also counted for p21- and Ki67 expression **(B1-B3)** Cells that are CD326- and MHCII$^+$ were sorted for Ki67-, p21- and SOX2 expression. SOX2$^+$ cells were also counted for p21- and Ki67 expression. Data are represented as mean ± SEM. *p<0.05, **p<0.01, ***p<0.001, ****p<0.0001, ns = not significant.

4 Discussion

4.1 Epiregulin-Induced Morphological Changes in Airway Epithelial Cells

Despite the use of the antifibrotic substances pirfenidone (77) and nintedanib (76), IPF has a very poor prognosis (29) and finding other targetable key players in the pathogenesis has been topic of recent studies. Therapeutic administration of inhibitors of various components of the ErbB pathway has been reported to be associated with promising results in several animal models (160). Despite many findings for several other ErbB signaling pathway components, ErbB ligand EREG's role in IPF etiology has not been investigated intensively yet. Therefore, EREG was chosen to be investigated in this doctoral work.

The first approach to identify EREG's role in the pathogenesis of IPF focused on its effects on the morphology of the respiratory epithelium. Under physiological conditions, the pseudostratified respiratory epithelium consists of basal cells, club cells, goblet and ciliated cells, which together ensure epithelial integrity (261, 262). In the distal airways, the pseudostratified epithelium transitions into a cuboidal epithelium lining the alveolar spaces. This epithelium is composed of ATI and ATII cells (262). In both epithelial formations, progenitor cells serve as a reservoir for differentiation, maintaining epithelial structure and function. In the proximal airways, basal cells act as such progenitors (263), whereas in the distal airways, ATII cells fulfill this role (261, 264). In IPF, the airways undergo profound remodeling including the formation of honeycomb cysts, which result from aberrant repair processes, a phenomenon referred to as honeycombing (13). These cysts are lined by a mucociliary epithelium that replaces the alveolar epithelium, a process termed bronchiolization (13, 34). This epithelium contains abnormal basal cells, ciliated cells and mucus-producing cells, predominantly MUC5B-expressing cells (13, 15, 34). Interestingly, the abnormal basal cells resemble those of the proximal airway epithelium, expressing markers such as Keratin 5 (13), SOX2 (34), p63 (265) and its isoform ΔNp63 (266). A comparative study demonstrated that patients with ILD, including IPF, exhibit significant shifts in epithelial cell populations (261). Here, the subpopulations of ATI and ATII cells are reduced, while the subpopulation of proximal airway cell types including ciliated, secretory and basal cell populations is expanded (261).

Several theories have been proposed to explain the origin of abnormal basal cells that serve as progenitor cells in bronchiolized regions. Broadly, three concepts exist regarding the origin of these progenitors of the bronchiolized epithelium:

- **Migration from proximal airways:** Following injury, progenitor cells from the proximal airways ($p63^+$ and $SOX2^+$ progenitor cells) migrate to damaged lung tissue and form clusters of Keratin 5 (KRT5) positive ($KRT5^+$) cells (267).
- **Differentiation from ATII cells:** ATII cells in the alveoli give rise to a $KRT5^+$ progenitor cell population under the influence of mesenchymal signals like TGF-β (268).
- **Contribution from bronchioalveolar stem cells (BASCs):** Progenitors of the murine bronchioalveolar duct junctions were shown to express markers of club cells and ATII cells. They are activated upon injury and may contribute to bronchiolization and fibrogenesis (269).

Further studies identified another cell type of basal cells that was found in IPF: aberrant basaloid cells (ABCs). These cells originate from injured ATII cells or club cells that pass through a transitional $KRT8^+$ alveolar differentiation intermediate state (ADI) (32, 270). ABCs acquire proximal airway epithelial markers such as SOX2, TP63 and KRT17, but unlike classical basal cells, lack KRT5 expression, which distinguishes them from proximal respiratory epithelial cells (270). In addition, other studies showed that these basaloid cells express developmental markers of the respiratory epithelium like SOX9 and simultaneously express mesenchymal markers like vimentin, N-cadherin, fibronectin and collagen as well as senescence markers p21 and p16 (32). These cells are frequently located near fibroblasts foci and also line honeycomb cysts (32, 271).

Initially, EREG's effect on airway epithelial cells was investigated in vitro. Here, EREG stimulation disrupted the typical stratified and differentiated architecture of airway epithelial cells and induced a shift in epithelial cell fate towards a more proliferative and hyperplastic phenotype, especially in the top layers of the epithelium. These findings are consistent with the study by Vermeer et al., where stimulation with ErbB ligand HRG-α led to increased epithelial height (159). Contrary to this study, stimulation with EREG showed a hyperplastic and less differentiated epithelium in the top layer. This might be explained by excessive proliferation, which prevents cells from having enough time to differentiate as they migrate from the base layer to the top. Vermeer et al. further discussed that the ErbB signaling system is crucial for maintenance and repair of the epithelium (159). EREG has also been associated with such roles in other tissues (190–193). Similar alteration of the epithelium in ALI cell cultures has been described for studies that investigated AREG in this context. Here, AREG was able to induce cellular hyperplasia by stimulation of ErbB receptors in basal cells of the respiratory epithelium in vitro

(272). In general, in the pseudostratified epithelium, ErbB1 is mainly expressed in basal cells (273, 274). Under pathological conditions in metaplastic and remodeled epithelium of smokers, ErbB1 expression is present throughout the whole epithelium and overall elevated (273). Further analysis showed, that smoking induces activation of the ErbB signaling system in ciliated cells, which reprograms the differentiation of basal cells to a more squamous phenotype and the downregulation of genes of ciliated or mucin producing cells (272, 274). Interestingly, in IPF, hyperplastic epithelial cells in fibrotic areas also show elevated ErbB1 expression (251). Furthermore, ABCs from fibrotic lungs were found to exhibit an increased expression of the ErbB ligands AREG and HB-EGF as well as sheddases ADAM17 and ADAM9, which are responsible for the release of AREG and other ErbB ligands like EREG (112, 275).

The origin of EREG in IPF lungs has been topic of recent studies. Odell et al. were able to show that the EREG-ErbB1 axis is generally elevated in the lungs of IPF patients and in bleomycin-treated mice (227). They also found that EREG is mainly expressed in antigen-presenting cells, including dendritic cells in the lungs of patients with systemic sclerosis-associated ILD. Here, $EREG^{+}$ dendritic cells were distributed throughout the fibrotic lung tissue, while they were absent in healthy tissue (227). Additionally, Odell et al. were able to show that interferon type I induces the expression of EREG from the inflammatory subgroup of dendritic cells, which then induces proliferation of fibroblasts and production of ECM proteins by these cells (227).

My results show that EREG is a strong driver of airway epithelial hyperproliferation, a phenomenon that may also contribute to the maladaptive remodeling in IPF, particularly since hyperplasia of airway epithelial cells is one of the characteristics of IPF lung histology (28). This entire process might be driven by fibroblasts stimulated by dendritic cell-derived EREG to produce excessive ECM, resembling the proposed profibrotic mechanisms in IPF pathogenesis mediated by other signals, such as TGF-β released from myofibroblasts (61).

Co-culturing (myo)fibroblasts with airway epithelial cells in this setting, together with quantification of EREG levels and antibody-mediated disruption of EREG/ErbB signaling could help clarify the link between ErbB ligands and alterations in the respiratory epithelium, as well as the role of EREG in this process.

4.2 DNA Damage and Cellular Senescence Are Driven by Epiregulin in Airway Epithelial Cells

A process that recently drew much attention in IPF pathogenesis is cellular senescence. Based on our first results (see 3.1.1), cells treated with EREG showed signs of hyperproliferation. In general, excessive proliferation induces replication stress in affected cells, leading to the accumulation of DNA damage due to insufficient DNA repair. Such excessive DNA damage is a well-known trigger of cell cycle arrest and the induction of senescence (232). Senescence markers such as p21, along with the senescence-activating events like the accumulation of DNA damage, have been identified in fibroblast foci and hyperplastic airway epithelial cells of IPF lungs (57, 58, 60). Consequently, this doctoral thesis also focused on the potential induction of senescence by EREG. Airway epithelial cells were therefore treated with EREG, followed by analysis of senescence and DNA damage.

The results demonstrate that EREG is capable of significantly inducing senescence in bronchial epithelial cells, as shown by comet assays and β-galactosidase staining. Next, the studies focused on identifying the underlying trigger through which EREG induces senescence and understanding how basal cells, the progenitor cells of the epithelium, are involved in this process. The results show that EREG increases the number of $PCNA^+$, $\gamma H2Ax^+$ and $p21^+$ cells in ALI cultures. While non-basal cells from the top layer ($p63^-$) show enhanced proliferation, as indicated by enhanced PCNA staining, basal cells ($p63^+$) seem to not exhibit any alteration in proliferation upon EREG stimulation. Instead, they display an increased number of $\gamma H2Ax^+$ and $p21^+$ cells, indicating DNA damage and senescence respectively. $p63^+$ basal cells have previously been reported to express senescence markers in aging and in diseases such as IPF (276). However, the missing statistical significance of an increased number of $PCNA^+$ basal cells might already be a sign of full cell cycle arrest after EREG stimulation. Non-basal cells in the top layer, on the other hand, still exhibit positive staining for PCNA, as well as for p21 and γH2Ax. Normally, non-basal cells do not proliferate once their progenitors have differentiated into specialized cell types of the respiratory epithelium. This finding supports the observation of reduced differentiation seen in HE stainings, with top layers appearing less differentiated compared to the normal respiratory epithelium. The persistence of PCNA staining in these cells may indicate that the cell cycle arrest is not yet fully established and the cells are in an early stage of senescence induction. It should also be noted that, although PCNA is

commonly used as a marker of proliferation, its upregulation may also reflect ongoing DNA repair processes (277). Therefore, an increased number of $PCNA^+$ cells in the top layer should be interpreted with caution, as it may not exclusively indicate proliferative activity but rather a cellular response to replication stress or DNA damage, particularly in cells that previously exhibited EREG-induced increased proliferation and replication stress, as observed in this study.

Overall, EREG-induced hyperproliferation creates replicative stress in airway epithelial cells, which then leads to increased DNA damage by exhausting DNA-repair capacity. Excessive amount of DNA damage then triggers the cell cycle arrest and senescence induction. While basal cells seem to have mostly reached the state of cellular senescence already after 48 hours of EREG stimulation, other non-basal cells of the epithelium are still in a transition phase. Nevertheless, while the total number of cells is increased by EREG stimulation, also the amount of $p63^+$ basal cells that show signs of DNA damage ($\gamma H2Ax^+$ staining) and senescence ($p21^+$ staining) is increased. Comparing earlier and later time points may reveal the kinetics of this process, in which basal cells hyperproliferate, while non-basal cells show no signs of proliferation, DNA damage and senescence induction. Additionally, analyzing the expression of SASP-associated mediators could help clarify the relevance of autoamplification loops, whereby senescent cells induce other adjacent cells to enter senescence and the potential role of EREG in this process.

4.3 Limited Role of Epiregulin in Pulmonary Fibrosis Progression and Senescence Induction in Mice after Bleomycin Instillation and Novel Insights into the Pathogenesis of Fibrosis

To further explore the role of ErbB signaling and EREG in pulmonary fibrosis, the effect of EREG was examined in vivo using the bleomycin mouse model of lung fibrosis. The aim was to evaluate whether the in vitro findings were transferable to an in vivo setting. While ErbB ligands such as TGF-α have been shown to exert profibrotic effects in various mouse models (168, 170, 172), inhibition of ErbB receptors with specific TKIs has yielded promising results in the treatment of fibrosis. To assess whether EREG produces a similar effect, it was administered to bleomycin-treated mice at two different time points: once early to evaluate the inflammatory response and once later to examine its impact on the fibrotic phase of the bleomycin-induced injury.

The in vivo studies revealed that EREG's direct impact on the progression of pulmonary fibrosis is limited. Neither early nor late intratracheal administration of EREG affected

lung compliance or histological fibrosis severity in bleomycin-treated mice. Histological analysis also did not show significant changes in fibrotic lesions or lung architecture, suggesting that EREG alone does not potentiate or mitigate fibrosis in this experimental model. Contrary to this findings, ErbB ligand TGF-α showed a strong profibrotic potential in different mouse models with an impact on histology and lung function. (168, 170, 172). While all these studies used transgenic overexpression models for TGF-α, a similar overexpression model for EREG will be needed in future studies to enhance the effect on clinical symptoms and histological patterns in mice. Another limitation of the approach is the route of EREG administration. I.t. instillation primarily delivers EREG to the apical surface of the respiratory epithelium. However, ErbB receptors are predominantly localized on basal cells (133, 134). Thus, the approach may underestimate the true effect of EREG in experimental lung fibrosis.

Next, the aim was to identify if EREG treatment had an impact on the induction of cellular senescence in vivo as shown in the in vitro studies (see 3.1). The challenge was to distinguish whether EREG has an additional effect on senescence induction beyond the effect already caused by bleomycin. While the in vitro results of this thesis already demonstrated that EREG stimulation alone increases p21 expression in airway epithelial cells, the influence of bleomycin on senescence has been described in the literature both in vitro and in vivo. For example, ATII cells exhibit increased β-galactosidase activity and elevated p21 levels in vitro after bleomycin treatment (244), while bleomycin treatment in mice likewise induces senescence (60).

First, SASP mediator levels were assessed in BALF. Although the overall protein concentration was elevated after bleomycin treatment, most SASP mediator levels showed high variability. For example, IL-6 levels, which are reported to be elevated in the BALF of bleomycin-treated mice (60, 278), were not elevated. Only MMP-25, MMP-2 and TNFRSF12/TWEAKR levels were significantly increased after bleomycin treatment, whereas EREG had no additional effect on the total protein concentration or on specific SASP mediator levels. The elevation of MMP-2 and MMP-25 may be relevant since ErbB ligands such as EREG require proteolytic shedding of their precursors by metalloproteases like ADAMs and MMPs (111). Here, it has to be mentioned, that BALF was collected only at day 21 post-bleomycin administration. Thus, it cannot be excluded that SASP mediator levels were higher during the inflammatory phase and the early stages of fibrotic remodeling, subsequently decreasing once fibrogenesis was largely completed. Follow up studies may investigate the kinetics of SASP mediators in this experimental

setting. The high variability observed in the results may be explained by the BALF preparation itself. Collection in a fixed volume of 500µl likely diluted soluble mediators, markedly reducing detection sensitivity. In addition, individual variation among mice, due to differences in anatomy, body weight, fibrosis severity or the collection technique, may have further contributed to the variability of the results. Moreover, BALF reflects global changes in the lung and does not capture local alterations in mediator expression.
IHC staining results show that EREG treatment markedly increased positive staining of PCNA and p21. In addition, total $\Delta Np63^+$ cell counts in the lung parenchyma were significantly elevated after EREG administration, consistent with the in vitro immunofluorescence findings. Regarding the histological distribution of $\Delta Np63^+$ cells, it is noteworthy to mention that these cells appeared in clusters rather than being evenly distributed throughout the tissue. Ray et al. described a similar clustering of $p63^+/SOX2^+$ (and $KRT5^+$) cells in H1N1 influenza virus induced lung injury (267). However, the occurrence of such clustering of cells in fibrotic tissue, either in a murine lung fibrosis models or in IPF, has not been reported to date. According to the study of Ray et al., such cells are thought to migrate from the proximal airways to the alveolar region in response to injury (267), which could also explain the presence of such cells in fibrotic tissue. While total cell counts showed an increase in $\Delta Np63^+$ cells, the number of $\Delta Np63^+$ per mm^2 was not elevated, which may be explained by their uneven distribution and restriction of clustering to fibrotic regions. The presence of $\Delta Np63^+$ cells in IHC stainings in clusters may represent a phenotype of airway epithelial cells associated with dysfunctional repair processes, bronchiolization, repopulation of the distal airways and further fibrogenesis.
Co-staining of ΔNp63 and PCNA was not consistently observed. Accordingly, other studies reported that proliferation markers are absent in epithelial cells covering fibroblast foci (266). This may indicate a reduced repair capacity of these cells, a feature often seen in advanced stages of IPF (58). Moreover, the $\Delta Np63^+$ cells may also represent the subpopulation of abnormal basal or aberrant basaloid cells (32, 261, 270). These cells typically express markers of proximal epithelial cells, such as p63 and SOX2, and are thought to repopulate the lung and fibrotic regions in response to epithelial injury. Interestingly, such cells have been reported to express the senescence markers p21 and p16 in other studies (32) and are typically associated with fibroblast foci and the lining of honeycomb cysts (32, 271). In IHC, some $\Delta Np63^+$ cells were also found to be $p21^+$. However, since only serial sections were made, it was difficult to determine co-staining within the same cell with certainty. To further investigate and quantify potential co-localization of ΔNp63

and p21, immunofluorescence double staining was performed on the same section. Unfortunately, both antibodies used in IHC and alternative antibodies resulted in high background signal and non-specific signals, preventing reliable detection of the target. Consequently, these experiments were not included in this thesis. As further optimization of the staining protocols did not yield satisfactory results, FACS analysis was used to assess possible co-staining and quantification of the basal cell subpopulation previously identified by IHC. Unfortunately, FACS compatible antibodies that provide specific signals for p63 or ΔNp63 were not found. Therefore, SOX2 was used as an alternative marker. SOX2 is also a marker of basal cell and ABC subpopulations appearing in the lung tissue following injury (267). SOX2 is particularly interesting, because ErbB ligand NRG1-α has been associated with increased SOX2 expression in airway epithelial cells in regions of bronchiolization, suggesting a potential contributory role in IPF pathogenesis (34).

FACS analysis revealed that p21 expression was altered after bleomycin treatment in both airway epithelial cells and alveolar epithelial cells, but was not further affected by additional EREG treatment. The most notable finding here is the differential response of $MHCII^-$ (airway epithelial cells) and $MHCII^+$ cell populations (alveolar epithelial cells) to the bleomycin-induced injury. While bleomycin did not affect the number of $SOX2^+$ cells within the proximal airway epithelium, it significantly increased the amount of $SOX2^+$ alveolar epithelial cells upon injury. SOX2 has been shown to induce both proliferation and differentiation of epithelial cells in the lung as well as reprogramming of alveolar epithelial cells into epithelial cells resembling those of the conducting airways (279). This process may contribute to the remodeling of the airways and bronchiolization of the alveolar regions in IPF (34). Based on this hypothesis, SOX2 has been shown to also induce p63 expression (280), linking it to the previously described clustering of $\Delta Np63^+$ cells in fibrotic regions observed in IHC. The basal cell subpopulations of abnormal basal cells and ABCs both express markers of the proximal airway epithelium including p63 (265) and its isoform ΔNp63 (266) as well as SOX2 (34). As discussed earlier, the origin of the basal cell subpopulations remains controversial in the literature. Following initial injury, they may derive from basal cells that have migrated from the proximal airways (267) or from dedifferentiated ATII cells (268, 269). Further, the subpopulation of ABCs has been reported to originate specifically from ATII cells (32, 271). Since SOX2 was particularly increased in $MHCII^+$ cells, it seems likely that the $MHCII^+/SOX2^+$ cells identified by FACS analysis originate from ATII cells. One may further speculate, that the $SOX2^+$ cells detected by FACS and the $\Delta Np63^+$ cells observed

in IHC belong to the same subpopulation. In contrast, Ray et al. reported that $p63^+$ and $SOX2^+$ progenitor cells that have migrated from the proximal airways upon injury, form clusters of $KRT5^+$ cells (267). To clarify the origin and identity of these basal cells, distinguishing between subpopulations is essential. Beyond Ki67 and p21, further classification was not performed in this study and remains a focus of future investigations. Abnormal basal cells express KRT5 (267), whereas ABCs lack KRT5 but express KRT17 (270). Therefore, assessing KRT5 and KRT17 expression could help identify the underlying subpopulations and their progenitors. Additionally, as ABCs reportedly express mesenchymal markers such as vimentin, N-cadherin, fibronectin and collagen, along with senescence markers p21 and p16 (32), analysis of these markers could further help to characterize these cells in this context (32, 271).

EREG treatment did not produce an additional effect on p21 expression in these $MHCII^+/SOX2^+$ cells in FACS analysis. As noted earlier, the lack of an in vivo effect may be related to the method of EREG administration. An EREG overexpression model might have been more suitable to demonstrate EREG's effects, as observed in vitro, particularly given that TGF-α overexpression models have demonstrated the profibrotic potential of TGF-α in vivo (168, 170, 172). As discussed previously in the context of in vitro results, proliferation (represented by Ki67 in vivo versus PCNA in vitro) was also unaltered in FACS analysis of the in vivo experiments. It is important to note a key difference between PCNA and Ki67: PCNA reflects both proliferation and DNA repair following DNA damage (277), whereas Ki67 specifically marks cells in G1, S, G2 as well as M phases and is absent in G0 (281). In contrast, PCNA can be detected in G0 due to its role in DNA repair. Therefore, PCNA levels may be overestimated when addressing proliferation compared with Ki67, particularly in the context of DNA damage indicated by γH2AX in in vitro studies. Additionally, as previously pointed out for in vitro studies, comparing mice at different stages of fibrogenesis (day 7 to day 21), since all mice were sacrificed at day 21, could reveal a kinetic change in Ki67 expression. Contrary to the FACS analysis results, IHC revealed increased PCNA levels, which were further enhanced by EREG. Therefore, further investigation of the origin of $\Delta Np63^+$ cell clusters and assessment of their proliferative characteristics in combination with DNA damage marker levels may help clarify their contribution to fibrogenesis.

4.4 Limitations of the Study and Future Outlook

This thesis has several limitations that warrant consideration:

First, i.t. instillation of EREG may have influenced the outcomes of the in vivo studies. Following lung injury, EREG might not have adequately reached the ErbB1 expressing basal cells located at the bottom of the epithelium. As a result, potential effects on lung mechanics and histological outcomes could have been underestimated, given that basal cells are thought to play a key role in the epithelial remodeling and bronchiolization observed in IPF. Transgenic mouse models based on cell-specific EREG expression may offer an option to clarify and strengthen its effect on epithelial cell behavior in lung fibrosis.

Second, the limited complexity of the in vitro model, consisting solely of human airway epithelial cells, as well as cross-species differences, may have contributed to the observed discrepancies. The absence of interactions with other cell types such as fibroblasts could have influenced the results. Moreover, differences between murine and human senescence pathways, such as the p19-Arf dependency (282), may have impacted the findings.

Third, there are inherent limitations of the preclinical bleomycin model of lung fibrosis, which lacks features of IPF such as bronchiolization and honeycomb cyst formations (283), processes previously shown to be driven by abnormal epithelial cells of either alveolar or bronchial origin. A potential solution for this limitation could be the use of human lung organoid models, precision-cut lung slices from IPF patients or humanized mouse xenograft models in which mice receive human IPF basal cells i.t. (275) to recapitulate epithelial-driven fibrosis in future studies. The observed clusters of $\Delta Np63^+$ cells in IHC may correspond to the clustered basal cells described by Ray et al., which additionally showed $SOX2^+$ and $KRT5^+$ staining (267). However, BASCs, which are proposed to act as progenitors in murine lungs, have only been described in mice so far. Thus, subpopulations of basal cells and epithelial progenitors may differ between bleomycin-induced fibrosis in mice and human IPF (269). To further identify the underlying cell population, measuring additional epithelial and mesenchymal markers (e.g., SFTPC, Uteroglobin, SOX2, KRT5, KRT8, KRT17, N-cadherin, fibronectin and collagen) could help classify the $\Delta Np63^+$ and $MHCII^+/SOX2^+$ cell populations.

Fourth, in the vivo experiments, cellular senescence was assessed solely by p21 positivity. Including additional markers of cellular senescence like β-Galactosidase and $p16^{Ink4a}$, together with a detailed analysis of the specific cell subpopulations undergoing this phenotypic switch, would further strengthen the robustness of the findings.

5 Summary

Idiopathic pulmonary fibrosis (IPF) remains a progressive and fatal disease despite current antifibrotic therapies, highlighting the need for the identification of novel targetable pathways. This thesis investigated the role of the ErbB ligand epiregulin (EREG) in IPF pathogenesis, focusing on its effects on airway epithelial cell morphology, proliferation and senescence.

In vitro, EREG promoted proliferation and differentiation of human airway epithelial cells, causing replication stress and DNA damage in basal cells, as shown by increased numbers of $p63^+/PCNA^+$ and $p63^+/\gamma H2Ax^+$ cells, finally leading to senescence indicated by $p21^+$ co-staining. In vivo, intratracheal administration of EREG in bleomycin-treated mice had little effect on pulmonary fibrosis, as lung function, histology and senescence-associated secretory phenotype (SASP) mediators in bronchoalveolar lavage fluid (BALF) remained largely unchanged. Immunohistochemistry (IHC) revealed increased numbers of $\Delta Np63^+$, $PCNA^+$ and $p21^+$ cells after bleomycin instillation, further augmented by EREG treatment. Notably, clusters of $\Delta p63^+$ cells were detected in lung parenchyma in dense fibrotic regions, suggesting expansion of specific basal cell subsets, including abnormal basal or aberrant basaloid cells (ABCs) following injury. Fluorescence-activated cell sorting (FACS) analysis revealed no additional effect of EREG beyond those induced by bleomycin. However, distinct responses emerged between $MHCII^-$ proximal airway and $MHCII^+$ alveolar epithelial cells. In the latter, SOX2 and p21 signal increased following bleomycin exposure, suggesting the induction of senescence and a partial reversion toward a progenitor-like state. These observations underscore the cellular plasticity and complexity of basal cell dynamics in lung injury and repair. Future studies using additional epithelial and mesenchymal markers will be essential to define these cell populations more precisely and clarify their roles in fibrotic remodeling. Overall, these findings indicate that EREG promotes hyperproliferation, DNA damage and senescence in vitro, whereas its direct impact in vivo appears limited, highlighting the need for more refined animal models. Nevertheless, the in vivo results offer new insights into epithelial cell dynamics during injury response and their contribution to bronchiolization, maladaptive remodeling and senescence, processes also observed in IPF. Future studies should investigate species-specific differences, employ transgenic models with EREG overexpression and further characterize basal cell subpopulations to entangle the complex interplay between EREG signaling, epithelial remodeling and fibrogenesis.

6 Zusammenfassung

Die idiopathische Lungenfibrose (IPF) bleibt trotz antifibrotischer Therapien eine progressive und tödliche Erkrankung. Dies unterstreicht die Notwendigkeit neuer Therapieansätze. Diese Doktorarbeit untersucht die Rolle von Epiregulin (EREG), einem Liganden des ErbB-Rezeptor Systems, in der Pathogenese der IPF. Dabei liegt der Fokus der Arbeit auf den Effekten auf die epitheliale Morphologie, Proliferation und Induktion von zellulärer Seneszenz.

In vitro steigerte EREG die Proliferation, veränderte die Differenzierung von humanen Atemwegsepithelien und führte zu Replikationsstress sowie DNA-Schäden, erkennbar an einer erhöhten Anzahl von $p63^+/PCNA^+$ sowie $p63^+/\gamma H2Ax^+$ Zellen, was zur Induktion von Seneszenz führte, nachgewiesen durch gleichzeitige p21 Färbung. In vivo zeigte die Behandlung von Mäusen mit EREG nur geringe Auswirkungen auf die bleomycininduzierte Fibrose, da Lungenfunktion, Histologie sowie die Konzentration von Mediatoren des seneszenzassoziierten sekretorischen Phänotyps (SASP) in der bronchoalveolären Lavageflüssigkeit (BALF) unverändert blieben. Die Immunhistochemie (IHC) zeigte jedoch eine erhöhte Anzahl von $\Delta Np63^+$, $PCNA^+$ und $p21^+$ Zellen nach der Bleomycin-Behandlung, welche durch EREG sogar zusätzlich verstärkt wurde. Besonders hervorzuheben ist die Clusterbildung von $\Delta Np63^+$ Zellen in stark fibrotischen Bereichen des Lungenparenchyms, was auf eine Expansion spezifischer Basalzell-Subpopulationen hinweist, einschließlich abnormaler Basalzellen und aberranter basaloider Zellen (ABCs). In der fluorescence-activated cell sorting (FACS) Analyse zeigte EREG keine zusätzlichen Effekte über die durch Bleomycin bereits ausgelösten Veränderungen hinaus, wohl aber Veränderungen in $MHCII^-$ Atemwegsepithelien und $MHCII^+$ Alveolarepithelien. Letztere wiesen eine erhöhte SOX2- und p21-Expression auf, was auf die Induktion von Seneszenz und eine Dedifferenzierung mit Wiedererlangen von stammzellähnlichen Eigenschaften hindeutet. Dies verdeutlicht die Fähigkeit zur Plastizität und dynamischen Komplexität der Basalzellsubpopulationen nach Schädigung des Lungengewebes und anschließenden Reparaturmaßnahmen.

Zukünftige Studien sollten die Subpopulation mithilfe zusätzlicher epithelialer und mesenchymaler Marker genauer klassifizieren und ihre Rolle beim fibrotischem Umbau klären. Insgesamt zeigen die Ergebnisse, dass EREG in vitro eine Hyperproliferation, DNA-Schäden und Seneszenz induziert, während die Wirkung in vivo jedoch begrenzt zu sein scheint, was die Notwendigkeit anderer experimenteller Modelle unterstreicht.

Nichtsdestotrotz liefern die in vivo Ergebnisse wichtige Einblicke in die Dynamik von Lungenepithelzellen nach Gewebsschädigung und ihren Einfluss auf die Bronchiolisierung, Umbauprozesse und Seneszenz, alles Prozesse, die auch bei der Entstehung der IPF relevant sind. Zukünftige Studien sollten artspezifische Unterschiede berücksichtigen, transgene Mausmodelle mit EREG-Überexpression reevaluieren sowie die beteiligten Basalzell-Subpopulationen genauer charakterisieren, um die komplexen Wechselwirkungen zwischen EREG-Signalwegen, epithelialem Umbau und Fibrosierung besser verstehen zu können.

7 List of Abbreviations

3D	Three-dimensional
ABCs	Aberrant basaloid cells
ADAM	A disintegrin and metalloproteinases
ADI	Alveolar differentiation intermediate state
AIP	Acute interstitial pneumonia
AKT	Protein kinase B
ALI	Air liquid interface
AREG	Amphiregulin
ARIA	Acetylcholine receptor-inducing activity
ATI	Alveolar type I cells
ATII	Alveolar type II cells
BALF	Bronchoalveolar lavage fluid
BASCs	Bronchioalveolar stem cells
BC	Betacellulin
BEBM	Bronchial Epithelial Cell Growth Medium
BRAF	B-Raf proto-oncogene
BSA	Bovine serum albumin
C57Bl/6J	Black 6 mice genotype
CAF	Cancer associated fibroblast
CD	Cluster of differentiation
CDK	Cyclin dependent kinase
COP	Cryptogenic organizing pneumonia
COPD	Chronic obstructive pulmonary disease
COX-2	Cyclooxygenase-2
CXCL2	C-XC motif chemokine
DAPI	4’,6-diamino-2-phenylindole
DDR	DNA damage response
DIP	Desquamative interstitial pneumonia
DMEM	Dulbecco’s Modified Eagle Medium
DMSO	Dimethylsulfide
dox-CCSP	Doxycycline-controlled transactivator Clara cell secretory protein

DPLD	Diffuse parenchymal lung diseases
DPP9	Dipeptidyl peptidase 9
DSP	Desmoplakin
DTT	Dithiothreitol
e.g.	For example / exempli gratia
ECM	Extracellular matrix
EDTA	Ethylenediaminetetraacetate
EGF	Epidermal growth factor
EGFR	Epidermal growth factor receptors
ELISA	Enzyme-linked immunosorbent assay
EMT	Epithelial-mesenchymal transition
EPG	Epigen
ER	Endoplasmatic reticulum
ErbB	Erythroblastic leukemia viral oncogene homolog
EREG	Epiregulin
ERK	Extracellular signal-regulated kinase
ET-1	Endothelin 1
etc.	Et cetera / and so on
f12-/-	Factor XII knockout mouse genotype
FACS	Fluorescence-activated cell sorting
FCS	Fetal calf serum
FGF-2	Fibroblast growth factor 2
FXII	Coagulation factor XII
GDA	Glutaraldehyde
GGFs	Glial growth factors
hBECs	Primary human bronchial epithelial cells
HB-EGF	Heparin-binding EGF-like growth factor
HBSS	Hank’s Balanced Salt Solution
HE	Hematoxylin and eosin
HEPES	2-(4-(2-hydroxyethyl) piperazin-1-yl)-ethane sulfonic acid
HER	Human epidermal growth factor receptors
HRCT	High-resolution computed tomography
HRG	Heregulins

HRP	Horseradish peroxidase
i.t.	Intratracheal / intratracheally
i.v.	Intravenously
IGF-II	Insulin-like growth factor 2
IHC	Immunocytochemistry
IIPs	Idiopathic interstitial pneumonias
IL-18	Interleukin-18
IL-1α	Interleukin-1-α
IL-1β	Interleukin-1-β
IL-6	Interleukin-6
IL-8	Interleukin-8
ILD	Interstitial lung diseases
IPF	Idiopathic pulmonary fibrosis
JAK/STAT	Janus-kinase/signal transducer and activator of transcription (pathway)
KRAS	Kirsten rat sarcoma viral oncogene homolog
KRT5	Keratin 5
KRT8	Keratin 8
LPS	Lipopolysaccharide
m	Microvilli
MAPK/ERK	Mitogen-activated protein kinase/extracellular signal-regulated kinase (pathway)
MCP-1	Monocyte chemotactic protein 1
MI2-2	Macrophage inflammatory protein 2
MMP	Matrix metalloproteases
MUC5B	Mucin-5B
NDF	Neu differentiation factor
NF-κB	Nuclear factor kappa-light-chain-enhancer of activated B cells
NRGs	Neuregulins
NSAIDs	Non-steroidal anti-inflammatory drugs
NSCLC	Non-small cell lung cancer
NSIP	Non-specific interstitial pneumonia
NTAK	Neural- and thymus-derived activator for ErbB kinase
OBFC1	Oligonucleotide / oligosaccharide-binding fold-containing protein 1

OD	Optical density
OSCC	Oral squamous cell
P/S	Penicillin/streptomycin
PAI-1	Plasminogen activator inhibitor 1
PAI-2	Plasminogen activator inhibitor 2
PAR-1	Protease-activated receptor 1
PBS	Phosphate buffered saline
PBS-T	Phosphate buffered saline with Tween
PCNA	Proliferating cell nuclear antigen
PDGF	Platelet-derived growth factor
PEDF	Pigment epithelium-derived factor
PFA	Paraformaldehyde
PGE2	Prostaglandin E2
PGN	Peptidoglycan
PI3K/AKT	Phosphoinositide 3-kinase/protein kinase B (pathway)
PLCγ	Phospholipase Cγ (pathway)
Rb	Retinoblastoma protein
RB-ILD	Respiratory bronchiolitis-associated interstitial lung disease
rER	Rough endoplasmatic reticulum
RIPA	Radioimmunoprecipitation
RPMI	Roswell Park Memorial Institute Medium
rtTA-CCSP	Reverse tetracycline-controlled transactivator Clara cell secretory protein
SASP	Senescence-associated secretory phenotype
SC	Secretory cells
ScEM	Scanning electron microscopy
SCLC	Small cell lung cancer
SD	Standard deviation
SDF-1α	Stromal cell-derived factor-1-α
SDS	Sodium dodecyl sulfate
SEM	Standard error of the mean
SFTPC	Surfactant protein C
SFTRPA2	Surfactant protein A2

SMDF	Sensory and motor derived factor
TAF	Telomere associated foci
TBE	Tris-borate EDTA
TBS	Tris buffered saline
TBS-T	Tris buffered saline with Tween
TEM	Transmission electron microscopy
TERC	Telomerase RNA component
TERT	Telomerase reverse transcriptase
TGF-α	Transforming growth factor-α
TGF-β	Transforming growth factor-β
TKIs	Tyrosine kinase inhibitors
TLR	Toll like receptor
TNFRSF12A	Tumor necrosis factor receptor superfamily member receptor
TNF-α	Tumor necrosis factor-α
tPA	Tissue plasminogen activator
TRIS	Tris(hydroxymethyl)aminomethane
Triton X	Octylphenoxypolyethoxyethanol
TWEAKR	Tumor necrosis factor receptor superfamily member 12A
UIP	Usual interstitial pneumonia
uPA	Urokinase plasminogen activator
VEGF	Vascular endothelial growth factor
VSMCs	Vascular smooth muscle cells
YAP	Yes-associated protein
α-SMA	α-actin-2 / smooth muscle actin 2
γH2Ax	Phosphorylated histone H2Ax

8 List of Figures and Tables

Fig. 1: EREG stimulation alters epithelial morphology and cellular differentiation in hBECs.....61
Fig. 2: EREG stimulation alters cellular morphology and differentiation in hBECs.....62
Fig. 3: EREG treatment of bronchial epithelial cells increases DNA damage and induces cellular senescence. 63
Fig. 4: Airway epithelial cells show altered expression patterns of PCNA, p21 and γH2Ax while p63 expression is unaltered. 65
Fig. 5: Expression pattern of p21, γH2Ax and PCNA is altered in airway epithelial cells after EREG stimulation. 66
Fig. 6: Airway epithelial cells show upregulation of p63, p21, PCNA and γH2Ax in all cells, but only p21 and γH2Ax upregulation in $p63^+$ cells after EREG treatment. .67
Fig. 7: Bleomycin treatment lowers static lung compliance and leads to histological lung fibrosis, while EREG administration on day 0, 2 and 4 does not aggravate the effect of bleomycin. 68
Fig. 8: Bleomycin treatment lowers static lung compliance and leads to histological lung fibrosis, while EREG administration on day 8, 10, 12, 14 and 16 does not aggravate the effect of bleomycin. 69
Fig. 9: Total protein levels and SASP mediators MMP-2, TNFRSF12/TWEAKR and MMP25 are upregulated in BALF from mice after bleomycin treatment, while EREG treatment does not augment the effect. 70
Fig. 10: EREG application amplifies ΔNp63-, PCNA- and p21-signals in bleomycin-treated mice. 71
Fig. 11 Distribution of $\Delta Np63^+$, $PCNA^+$ and $p21^+$ cells in the lungs of bleomycin- and EREG-treated mice. 73
Fig. 12: $\Delta Np63^+$ cell counts are higher in bleomycin-treated mice after EREG treatment. 73
Fig. 13: Gating strategy for murine lung epithelial cells. 74
Fig. 14: Bleomycin treatment in mice alters p21- but not Ki67 expression in $MHCII^+$ and $MHCII^-$ epithelial cells. EREG treatment doesn't have an additional effect on p21-, Ki67- or SOX2 expression. 75

9 References

1. American Thoracic Society. American Thoracic Society/European Respiratory Society International Multidisciplinary Consensus Classification of the Idiopathic Interstitial Pneumonias. Am J Respir Crit Care Med 2002; 165(2):277–304.

2. Griese M. Etiologic Classification of Diffuse Parenchymal (Interstitial) Lung Diseases. J Clin Med 2022; 11(6).

3. Travis WD, Costabel U, Hansell DM, King TE, Lynch DA, Nicholson AG et al. An official American Thoracic Society/European Respiratory Society statement: Update of the international multidisciplinary classification of the idiopathic interstitial pneumonias. Am J Respir Crit Care Med 2013; 188(6):733–48.

4. Hutchinson J, Fogarty A, Hubbard R, McKeever T. Global incidence and mortality of idiopathic pulmonary fibrosis: a systematic review. Eur Respir J 2015; 46(3):795–806.

5. Hopkins RB, Burke N, Fell C, Dion G, Kolb M. Epidemiology and survival of idiopathic pulmonary fibrosis from national data in Canada. Eur Respir J 2016; 48(1):187–95.

6. Richeldi L, Collard HR, Jones MG. Idiopathic pulmonary fibrosis. Lancet 2017; 389(10082):1941–52.

7. Johnston ID, Prescott RJ, Chalmers JC, Rudd RM. British Thoracic Society study of cryptogenic fibrosing alveolitis: current presentation and initial management. Fibrosing Alveolitis Subcommittee of the Research Committee of the British Thoracic Society. Thorax 1997; 52(1):38–44.

8. Baumgartner KB, Samet JM, Stidley CA, Colby TV, Waldron JA. Cigarette smoking: a risk factor for idiopathic pulmonary fibrosis. Am J Respir Crit Care Med 1997; 155(1):242–8.

9. Baumgartner KB, Samet JM, Coultas DB, Stidley CA, Hunt WC, Colby TV et al. Occupational and environmental risk factors for idiopathic pulmonary fibrosis: a multicenter case-control study. Collaborating Centers. Am J Epidemiol 2000; 152(4):307–15.

10. Lederer DJ, Martinez FJ. Idiopathic Pulmonary Fibrosis. N Engl J Med 2018; 378(19):1811–23.

11. Hubbard R, Venn A, Smith C, Cooper M, Johnston I, Britton J. Exposure to commonly prescribed drugs and the etiology of cryptogenic fibrosing alveolitis: a case-control study. Am J Respir Crit Care Med 1998; 157(3 Pt 1):743–7.

12. Wuyts WA, Dahlqvist C, Slabbynck H, Schlesser M, Gusbin N, Compere C et al. Baseline clinical characteristics, comorbidities and prescribed medication in a real-world population of patients with idiopathic pulmonary fibrosis: the PROOF registry. BMJ Open Respir Res 2018; 5(1):e000331.

13. Seibold MA, Smith RW, Urbanek C, Groshong SD, Cosgrove GP, Brown KK et al. The idiopathic pulmonary fibrosis honeycomb cyst contains a mucocilary pseudostratified epithelium. PLoS One 2013; 8(3):e58658.

14. Fingerlin TE, Murphy E, Zhang W, Peljto AL, Brown KK, Steele MP et al. Genome-wide association study identifies multiple susceptibility loci for pulmonary fibrosis. Nat Genet 2013; 45(6):613–20.

15. Nakano Y, Yang IV, Walts AD, Watson AM, Helling BA, Fletcher AA et al. MUC5B Promoter Variant rs35705950 Affects MUC5B Expression in the Distal Airways in Idiopathic Pulmonary Fibrosis. Am J Respir Crit Care Med 2016; 193(4):464–6.

16. Nogee LM, Dunbar AE, Wert SE, Askin F, Hamvas A, Whitsett JA. A mutation in the surfactant protein C gene associated with familial interstitial lung disease. N Engl J Med 2001; 344(8):573–9.

17. Wang Y, Kuan PJ, Xing C, Cronkhite JT, Torres F, Rosenblatt RL et al. Genetic defects in surfactant protein A2 are associated with pulmonary fibrosis and lung cancer. Am J Hum Genet 2009; 84(1):52–9.

18. Markart P, Ruppert C, Wygrecka M, Schmidt R, Korfei M, Harbach H et al. Surfactant protein C mutations in sporadic forms of idiopathic interstitial pneumonias. Eur Respir J 2007; 29(1):134–7.

19. Lawson WE, Grant SW, Ambrosini V, Womble KE, Dawson EP, Lane KB et al. Genetic mutations in surfactant protein C are a rare cause of sporadic cases of IPF. Thorax 2004; 59(11):977–80.

20. Mushiroda T, Wattanapokayakit S, Takahashi A, Nukiwa T, Kudoh S, Ogura T et al. A genome-wide association study identifies an association of a common variant in TERT with susceptibility to idiopathic pulmonary fibrosis. Journal of medical genetics 2008; 45(10):654–6.

21. Tsakiri KD, Cronkhite JT, Kuan PJ, Xing C, Raghu G, Weissler JC et al. Adult-onset pulmonary fibrosis caused by mutations in telomerase. Proceedings of the National Academy of Sciences 2007; 104(18):7552–7.

22. Alder JK, Chen JJ-L, Lancaster L, Danoff S, Su S, Cogan JD et al. Short telomeres are a risk factor for idiopathic pulmonary fibrosis. Proceedings of the National Academy of Sciences 2008; 105(35):13051–6.

23. Armanios MY, Chen JJ-L, Cogan JD, Alder JK, Ingersoll RG, Markin C et al. Telomerase mutations in families with idiopathic pulmonary fibrosis. N Engl J Med 2007; 356(13):1317–26.

24. Antoniades HN, Bravo MA, Avila RE, Galanopoulos T, Neville-Golden J, Maxwell M et al. Platelet-derived growth factor in idiopathic pulmonary fibrosis. J. Clin. Invest. 1990; 86(4):1055–64.

25. Nash JR, McLaughlin PJ, Butcher D, Corrin B. Expression of tumour necrosis factor-alpha in cryptogenic fibrosing alveolitis. Histopathology 1993; 22(4):343–7.

26. Selman M, Pardo A. Role of epithelial cells in idiopathic pulmonary fibrosis: from innocent targets to serial killers. Proceedings of the American Thoracic Society 2006; 3(4):364–72.

27. Khalil N, Greenberg AH. The role of TGF-beta in pulmonary fibrosis. Ciba Found Symp 1991; 157:194-207; discussion 207-11.

28. Selman M, King TE, Pardo A. Idiopathic pulmonary fibrosis: prevailing and evolving hypotheses about its pathogenesis and implications for therapy. Ann Intern Med 2001; 134(2):136–51.

29. King TE, Pardo A, Selman M. Idiopathic pulmonary fibrosis. The Lancet 2011; 378(9807):1949–61.

30. Gabbiani G, Ryan GB, Majne G. Presence of modified fibroblasts in granulation tissue and their possible role in wound contraction. Experientia 1971; 27(5):549–50.

31. Tomasek JJ, Gabbiani G, Hinz B, Chaponnier C, Brown RA. Myofibroblasts and mechano-regulation of connective tissue remodelling. Nat Rev Mol Cell Biol 2002; 3(5):349–63.

32. Adams TS, Schupp JC, Poli S, Ayaub EA, Neumark N, Ahangari F et al. Single-cell RNA-seq reveals ectopic and aberrant lung-resident cell populations in idiopathic pulmonary fibrosis. Sci Adv 2020; 6(28):eaba1983.

33. Hancock LA, Hennessy CE, Solomon GM, Dobrinskikh E, Estrella A, Hara N et al. Muc5b overexpression causes mucociliary dysfunction and enhances lung fibrosis in mice. Nat Commun 2018; 9(1):5363.

34. Plantier L, Crestani B, Wert SE, Dehoux M, Zweytick B, Guenther A et al. Ectopic respiratory epithelial cell differentiation in bronchiolised distal airspaces in idiopathic pulmonary fibrosis. Thorax 2011; 66(8):651–7.

35. Cook DN, Brass DM, Schwartz DA. A matrix for new ideas in pulmonary fibrosis. Am J Respir Cell Mol Biol 2002; 27(2):122–4.

36. Phan SH. The myofibroblast in pulmonary fibrosis. Chest 2002; 122(6 Suppl):286S-289S.

37. Scotton CJ, Chambers RC. Molecular targets in pulmonary fibrosis: the myofibroblast in focus. Chest 2007; 132(4):1311–21.

38. Moore BB, Kolodsick JE, Thannickal VJ, Cooke K, Moore TA, Hogaboam C et al. CCR2-mediated recruitment of fibrocytes to the alveolar space after fibrotic injury. The American Journal of Pathology 2005; 166(3):675–84.

39. Roy SG, Nozaki Y, Phan SH. Regulation of alpha-smooth muscle actin gene expression in myofibroblast differentiation from rat lung fibroblasts. The International Journal of Biochemistry & Cell Biology 2001; 33(7):723–34.

40. Marmai C, Sutherland RE, Kim KK, Dolganov GM, Fang X, Kim SS et al. Alveolar epithelial cells express mesenchymal proteins in patients with idiopathic pulmonary fibrosis. American Journal of Physiology-Lung Cellular and Molecular Physiology 2011; 301(1):L71-8.

41. Kim KK, Kugler MC, Wolters PJ, Robillard L, Galvez MG, Brumwell AN et al. Alveolar epithelial cell mesenchymal transition develops in vivo during pulmonary fibrosis and is regulated by the extracellular matrix. Proceedings of the National Academy of Sciences 2006; 103(35):13180–5.

42. Wu Z, Yang L, Cai L, Zhang M, Cheng X, Yang X et al. Detection of epithelial to mesenchymal transition in airways of a bleomycin induced pulmonary fibrosis model derived from an alpha-smooth muscle actin-Cre transgenic mouse. Respir Res 2007; 8(1):1.

43. Hay ED. An overview of epithelio-mesenchymal transformation. Acta Anat (Basel) 1995; 154(1):8–20.

44. Hua W, Dijke P ten, Kostidis S, Giera M, Hornsveld M. TGFβ-induced metabolic reprogramming during epithelial-to-mesenchymal transition in cancer. Cellular and Molecular Life Sciences 2019; 77(11):2103–23.

45. Kiemer AK, Takeuchi K, Quinlan MP. Identification of genes involved in epithelial-mesenchymal transition and tumor progression. Oncogene 2001; 20(46):6679–88.

46. Desmoulière A, Geinoz A, Gabbiani F, Gabbiani G. Transforming growth factor-beta 1 induces alpha-smooth muscle actin expression in granulation tissue myofibroblasts and in quiescent and growing cultured fibroblasts. J Cell Biol 1993; 122(1):103–11.

47. Kalluri R, Neilson EG. Epithelial-mesenchymal transition and its implications for fibrosis. J Clin Invest 2003; 112(12):1776–84.

48. Fan JM, Ng YY, Hill PA, Nikolic-Paterson DJ, Mu W, Atkins RC et al. Transforming growth factor-beta regulates tubular epithelial-myofibroblast transdifferentiation in vitro. Kidney Int 1999; 56(4):1455–67.

49. Araya J, Nishimura SL. Fibrogenic reactions in lung disease. Annu Rev Pathol 2010; 5:77–98.

50. Gauldie J, Bonniaud P, Sime P, Ask K, Kolb M. TGF-beta, Smad3 and the process of progressive fibrosis. Biochem Soc Trans 2007; 35(Pt 4):661–4.

51. Okada H, Danoff TM, Kalluri R, Neilson EG. Early role of Fsp1 in epithelial-mesenchymal transformation. Am J Physiol 1997; 273(4):F563-74.

52. Morali OG, Delmas V, Moore R, Jeanney C, Thiery JP, Larue L. IGF-II induces rapid beta-catenin relocation to the nucleus during epithelium to mesenchyme transition. Oncogene 2001; 20(36):4942–50.

53. Strutz F, Zeisberg M, Ziyadeh FN, Yang C-Q, Kalluri R, Müller GA et al. Role of basic fibroblast growth factor-2 in epithelial-mesenchymal transformation. Kidney Int 2002; 61(5):1714–28.

54. Willis BC, Borok Z. TGF-beta-induced EMT: mechanisms and implications for fibrotic lung disease. American Journal of Physiology-Lung Cellular and Molecular Physiology 2007; 293(3):L525-34.

55. Willis BC, Liebler JM, Luby-Phelps K, Nicholson AG, Crandall ED, Du Bois RM et al. Induction of Epithelial-Mesenchymal Transition in Alveolar Epithelial Cells by Transforming Growth Factor-β1. The American Journal of Pathology 2005; 166(5):1321–32.

56. Kulasekaran P, Scavone CA, Rogers DS, Arenberg DA, Thannickal VJ, Horowitz JC. Endothelin-1 and transforming growth factor-beta1 independently induce fibroblast resistance to apoptosis via AKT activation. Am J Respir Cell Mol Biol 2009; 41(4):484–93.

57. Kuwano K, Kunitake R, Kawasaki M, Nomoto Y, Hagimoto N, Nakanishi Y et al. P21Waf1/Cip1/Sdi1 and p53 expression in association with DNA strand breaks in idiopathic pulmonary fibrosis. Am J Respir Crit Care Med 1996; 154(2 Pt 1):477–83.

58. Lomas NJ, Watts KL, Akram KM, Forsyth NR, Spiteri MA. Idiopathic pulmonary fibrosis: immunohistochemical analysis provides fresh insights into lung tissue remodelling with implications for novel prognostic markers. Int J Clin Exp Pathol 2012; 5(1):58–71.

59. van Deursen JM. The role of senescent cells in ageing. Nature 2014; 509(7501):439–46.

60. Schafer MJ, White TA, Iijima K, Haak AJ, Ligresti G, Atkinson EJ et al. Cellular senescence mediates fibrotic pulmonary disease. Nat Commun 2017; 8:14532.

61. Wipff P-J, Rifkin DB, Meister J-J, Hinz B. Myofibroblast contraction activates latent TGF-beta1 from the extracellular matrix. J Cell Biol 2007; 179(6):1311–23.

62. Villiger PM, Kusari AB, Dijke P ten, Lotz M. IL-1 beta and IL-6 selectively induce transforming growth factor-beta isoforms in human articular chondrocytes. J Immunol 1993; 151(6):3337–44.

63. Frangogiannis N. Transforming growth factor-β in tissue fibrosis. J Exp Med 2020; 217(3):e20190103.

64. O'Reilly S, Ciechomska M, Cant R, van Laar JM. Interleukin-6 (IL-6) trans signaling drives a STAT3-dependent pathway that leads to hyperactive transforming growth factor-β (TGF-β) signaling promoting SMAD3 activation and fibrosis via Gremlin protein. J Biol Chem 2014; 289(14):9952–60.

65. Epstein Shochet G, Brook E, Bardenstein-Wald B, Shitrit D. TGF-β pathway activation by idiopathic pulmonary fibrosis (IPF) fibroblast derived soluble factors is mediated by IL-6 trans-signaling. Respir Res 2020; 21(1).

66. Hinz B. Mechanical Aspects of Lung Fibrosis. Proceedings of the American Thoracic Society 2012; 9(3):137–47.

67. Cosgrove GP, Brown KK, Schiemann WP, Serls AE, Parr JE, Geraci MW et al. Pigment epithelium-derived factor in idiopathic pulmonary fibrosis: a role in aberrant angiogenesis. Am J Respir Crit Care Med 2004; 170(3):242–51.

68. Kotani I, Sato A, Hayakawa H, Urano T, Takada Y, Takada A. Increased procoagulant and antifibrinolytic activities in the lungs with idiopathic pulmonary fibrosis. Thromb Res 1995; 77(6):493–504.

69. Panos RJ, Mortenson RL, Niccoli SA, King TE. Clinical deterioration in patients with idiopathic pulmonary fibrosis: causes and assessment. Am J Med 1990; 88(4):396–404.

70. Raghu G, Collard HR, Egan JJ, Martinez FJ, Behr J, Brown KK et al. An official ATS/ERS/JRS/ALAT statement: idiopathic pulmonary fibrosis: evidence-based guidelines for diagnosis and management. Am J Respir Crit Care Med 2011; 183(6):788–824.

71. Kato E, Takayanagi N, Takaku Y, Kagiyama N, Kanauchi T, Ishiguro T et al. Incidence and predictive factors of lung cancer in patients with idiopathic pulmonary fibrosis. ERJ Open Res 2018; 4(1).

72. Deutsche Gesellschaft für Pneumologie und Beatmungsmedizin e.V. S2k-Leitlinie Diagnostik der Idiopathischen Lungenfibrose: Version 3.0. AWMF-Register-Nr.: 020-101. Arbeitsgemeinschaft der Wissenschaftlichen Medizinischen Fachgesellschaften; 2019 2019.

73. Raghu G, Remy-Jardin M, Myers JL, Richeldi L, Ryerson CJ, Lederer DJ et al. Diagnosis of Idiopathic Pulmonary Fibrosis. An Official ATS/ERS/JRS/ALAT Clinical Practice Guideline. Am J Respir Crit Care Med 2018; 198(5):e44-e68.

74. Akira M, Kozuka T, Yamamoto S, Sakatani M. Computed tomography findings in acute exacerbation of idiopathic pulmonary fibrosis. Am J Respir Crit Care Med 2008; 178(4):372–8.

75. Raghu G, Remy-Jardin M, Richeldi L, Thomson CC, Inoue Y, Johkoh T et al. Idiopathic Pulmonary Fibrosis (an Update) and Progressive Pulmonary Fibrosis in Adults: An Official ATS/ERS/JRS/ALAT Clinical Practice Guideline. Am J Respir Crit Care Med 2022; 205(9):e18-e47.

76. Richeldi L, Du Bois RM, Raghu G, Azuma A, Brown KK, Costabel U et al. Efficacy and safety of nintedanib in idiopathic pulmonary fibrosis. N Engl J Med 2014; 370(22):2071–82.

77. Noble PW, Albera C, Bradford WZ, Costabel U, Du Bois RM, Fagan EA et al. Pirfenidone for idiopathic pulmonary fibrosis: analysis of pooled data from three multinational phase 3 trials. Eur Respir J 2016; 47(1):243–53.

78. Didiasova M, Singh R, Wilhelm J, Kwapiszewska G, Wujak L, Zakrzewicz D et al. Pirfenidone exerts antifibrotic effects through inhibition of GLI transcription factors. FASEB J 2017; 31(5):1916–28.

79. Cohen S, Carpenter G, King L. Epidermal growth factor-receptor-protein kinase interactions. Co-purification of receptor and epidermal growth factor-enhanced phosphorylation activity. Journal of Biological Chemistry 1980; 255(10):4834–42.

80. Ullrich A, Coussens L, Hayflick JS, Dull TJ, Gray A, Tam AW et al. Human epidermal growth factor receptor cDNA sequence and aberrant expression of the amplified gene in A431 epidermoid carcinoma cells. Nature 1984; 309(5967):418–25.

81. Yamamoto T, Ikawa S, Akiyama T, Semba K, Nomura N, Miyajima N et al. Similarity of protein encoded by the human c-erb-B-2 gene to epidermal growth factor receptor. Nature 1986; 319(6050):230–4.

82. Kraus MH, Issing W, Miki T, Popescu NC, Aaronson SA. Isolation and characterization of ERBB3, a third member of the ERBB/epidermal growth factor receptor family: evidence for overexpression in a subset of human mammary tumors. Proceedings of the National Academy of Sciences 1989; 86(23):9193–7.

83. Plowman GD, Culouscou JM, Whitney GS, Green JM, Carlton GW, Foy L et al. Ligand-specific activation of HER4/p180erbB4, a fourth member of the epidermal growth factor receptor family. Proceedings of the National Academy of Sciences 1993; 90(5):1746–50.

84. Cohen S. Isolation of a Mouse Submaxillary Gland Protein Accelerating Incisor Eruption and Eyelid Opening in the New-born Animal. Journal of Biological Chemistry 1962; 237(5):1555–62.

85. Jones S, Rappoport JZ. Interdependent epidermal growth factor receptor signalling and trafficking. The International Journal of Biochemistry & Cell Biology 2014; 51:23–8.

86. Salomon DS, Brandt R, Ciardiello F, Normanno N. Epidermal growth factor-related peptides and their receptors in human malignancies. Crit Rev Oncol Hematol 1995; 19(3):183–232.

87. Normanno N, Bianco C, Luca A de, Salomon DS. The role of EGF-related peptides in tumor growth. Front Biosci 2001; 6:D685-707.

88. Marquardt H, Hunkapiller MW, Hood LE, Todaro GJ. Rat transforming growth factor type 1: structure and relation to epidermal growth factor. Science 1984; 223(4640):1079–82.

89. Shoyab M, Plowman GD, McDonald VL, Bradley JG, Todaro GJ. Structure and function of human amphiregulin: a member of the epidermal growth factor family. Science 1989; 243(4894 Pt 1):1074–6.

90. Higashiyama S, Abraham JA, Miller J, Fiddes JC, Klagsbrun M. A Heparin-Binding Growth Factor Secreted by Macrophage-Like Cells That Is Related to EGF. Science 1991; 251(4996):936–9.

91. Shing Y, Christofori G, Hanahan D, Ono Y, Sasada R, Igarashi K et al. Betacellulin: a mitogen from pancreatic beta cell tumors. Science 1993; 259(5101):1604–7.

92. Komurasaki T, Toyoda H, Uchida D, Morimoto S. Epiregulin binds to epidermal growth factor receptor and ErbB-4 and induces tyrosine phosphorylation of epidermal growth factor receptor, ErbB-2, ErbB-3 and ErbB-4. Oncogene 1997; 15(23):2841–8.

93. Strachan L, Murison JG, Prestidge RL, Sleeman MA, Watson JD, Kumble KD. Cloning and biological activity of epigen, a novel member of the epidermal growth factor superfamily. Journal of Biological Chemistry 2001; 276(21):18265–71.

94. Yarden Y, Sliwkowski MX. Untangling the ErbB signalling network. Nat Rev Mol Cell Biol 2001; 2(2):127–37.

95. Chang H, Riese II DJ, Gilbert W, Stern DF, McMahan UJ. Ligands for ErbB-family receptors encoded by a neuregulin-like gene. Nature 1997; 387(6632):509–12.

96. Zhang D, Sliwkowski MX, Mark M, Frantz G, Akita R, Sun Y et al. Neuregulin-3 (NRG3): A novel neural tissue-enriched protein that binds and activates ErbB4. Proceedings of the National Academy of Sciences 1997; 94(18):9562–7.

97. Harari D, Tzahar E, Romano J, Shelly M, Pierce JH, Andrews GC et al. Neuregulin-4: a novel growth factor that acts through the ErbB-4 receptor tyrosine kinase. Oncogene 1999; 18(17):2681–9.

98. Holmes WE, Sliwkowski MX, Akita RW, Henzel WJ, Lee J, Park JW et al. Identification of heregulin, a specific activator of p185erbB2. Science 1992; 256(5060):1205–10.

99. Wen D, Peles E, Cupples R, Suggs SV, Bacus SS, Luo Y et al. Neu differentiation factor: A transmembrane glycoprotein containing an EGF domain and an immunoglobulin homology unit. Cell 1992; 69(3):559–72.

100. Peles E, Bacus SS, Koski RA, Lu HS, Wen D, Ogden SG et al. Isolation of the NeuHER-2 stimulatory ligand: A 44 kd glycoprotein that induces differentiation of mammary tumor cells. Cell 1992; 69(1):205–16.

101. Falls D. ARIA, a protein that stimulates acetylcholine receptor synthesis, is a member of the neu ligand family. Cell 1993; 72(5):801–13.

102. Ho WH, Armanini MP, Nuijens A, Phillips HS, Osheroff PL. Sensory and motor neuron-derived factor. A novel heregulin variant highly expressed in sensory and motor neurons. Journal of Biological Chemistry 1995; 270(24):14523–32.

103. Yarden Y, Schlessinger J. Self-phosphorylation of epidermal growth factor receptor: evidence for a model of intermolecular allosteric activation. Biochemistry 1987; 26(5):1434–42.

104. Batzer. Hierarchy of binding sites for Grb2 and Shc on the epidermal growth factor receptor. Mol. Cell. Biol. 1994; 14:5192.

105. Rodrigues GA, Falasca M, Zhang Z, Ong SH, Schlessinger J. A novel positive feedback loop mediated by the docking protein Gab1 and phosphatidylinositol 3-kinase in epidermal growth factor receptor signaling. Mol Cell Biol 2000; 20(4):1448–59.

106. Margolis B, Rhee SG, Felder S, Mervic M, Lyall R, Levitzki A et al. EGF induces tyrosine phosphorylation of phospholipase C-II: A potential mechanism for EGF receptor signaling. Cell 1989; 57(7):1101–7.

107. Cantley LC. The phosphoinositide 3-kinase pathway. Science 2002; 296(5573):1655–7.

108. Klapper LN, Glathe S, Vaisman N, Hynes NE, Andrews GC, Sela M et al. The ErbB-2/HER2 oncoprotein of human carcinomas may function solely as a shared coreceptor for multiple stroma-derived growth factors. Proceedings of the National Academy of Sciences 1999; 96(9):4995–5000.

109. Tzahar E, Levkowitz G, Karunagaran D, Yi L, Peles E, Lavi S et al. ErbB-3 and ErbB-4 function as the respective low and high affinity receptors of all Neu differentiation factor/heregulin isoforms. Journal of Biological Chemistry 1994; 269(40):25226–33.

110. Sliwkowski MX, Schaefer G, Akita RW, Lofgren JA, Fitzpatrick VD, Nuijens A et al. Coexpression of erbB2 and erbB3 proteins reconstitutes a high affinity receptor for heregulin. Journal of Biological Chemistry 1994; 269(20):14661–5.

111. Harris R. EGF receptor ligands. Experimental cell research 2003; 284(1):2–13.

112. Suzuki M, Raab G, Moses MA, Fernandez CA, Klagsbrun M. Matrix metalloproteinase-3 releases active heparin-binding EGF-like growth factor by cleavage at a specific juxtamembrane site. Journal of Biological Chemistry 1997; 272(50):31730–7.

113. Sahin U, Weskamp G, Kelly K, Zhou H-M, Higashiyama S, Peschon J et al. Distinct roles for ADAM10 and ADAM17 in ectodomain shedding of six EGFR ligands. J Cell Biol 2004; 164(5):769–79.

114. Neufert C, Becker C, Türeci Ö, Waldner MJ, Backert I, Floh K et al. Tumor fibroblast-derived epiregulin promotes growth of colitis-associated neoplasms through ERK. J Clin Invest 2013; 123(4):1428–43.

115. Zeng F, Harris RC. Epidermal growth factor, from gene organization to bedside. Semin Cell Dev Biol 2014; 28:2–11.

116. Fukuyama R, Shimizu N. Expression of epidermal growth factor (EGF) and the EGF receptor in human tissues. J Exp Zool 1991; 258(3):336–43.

117. Wei Z, Park KW, Day BN, Prather RS. Effect of epidermal growth factor on preimplantation development and its receptor expression in porcine embryos. Mol Reprod Dev 2001; 60(4):457–62.

118. Dadi TD, Li M-W, Lloyd KCK. EGF and TGF-alpha supplementation enhances development of cloned mouse embryos. Cloning Stem Cells 2007; 9(3):315–26.

119. Lee KF, Simon H, Chen H, Bates B, Hung MC, Hauser C. Requirement for neuregulin receptor erbB2 in neural and cardiac development. Nature 1995; 378(6555):394–8.

120. Gassmann M, Casagranda F, Orioli D, Simon H, Lai C, Klein R et al. Aberrant neural and cardiac development in mice lacking the ErbB4 neuregulin receptor. Nature 1995; 378(6555):390–4.

121. Birchmeier C. ErbB receptors and the development of the nervous system. Experimental cell research 2009; 315(4):611–8.

122. Miettinen PJ, Warburton D, Bu D, Zhao JS, Berger JE, Minoo P et al. Impaired lung branching morphogenesis in the absence of functional EGF receptor. Dev Biol 1997; 186(2):224–36.

123. Schroeder JA, Lee DC. Dynamic expression and activation of ERBB receptors in the developing mouse mammary gland. Cell Growth Differ 1998; 9(6):451–64.

124. Sebastian J, Richards RG, Walker MP, Wiesen JF, Werb Z, Derynck R et al. Activation and function of the epidermal growth factor receptor and erbB-2 during mammary gland morphogenesis. Cell Growth Differ 1998; 9(9):777–85.

125. Miettinen PJ, Berger JE, Meneses J, Phung Y, Pedersen RA, Werb Z et al. Epithelial immaturity and multiorgan failure in mice lacking epidermal growth factor receptor. Nature 1995; 376(6538):337–41.

126. Duh G, Mouri N, Warburton D, Thomas DW. EGF regulates early embryonic mouse gut development in chemically defined organ culture. Pediatr Res 2000; 48(6):794–802.

127. Barberán S, Fraguas S, Cebrià F. The EGFR signaling pathway controls gut progenitor differentiation during planarian regeneration and homeostasis. Development 2016; 143(12):2089–102.

128. Desai TJ, Brownfield DG, Krasnow MA. Alveolar progenitor and stem cells in lung development, renewal and cancer. Nature 2014; 507(7491):190–4.

129. Baskin LS, Sutherland RS, Thomson AA, Nguyen HT, Morgan DM, Hayward SW et al. Growth factors in bladder wound healing. J Urol 1997; 157(6):2388–95.

130. Abe S, Sasano H, Katoh K, Ohara S, Arikawa T, Noguchi T et al. Immunohistochemical studies on EGF family growth factors in normal and ulcerated human gastric mucosa. Dig Dis Sci 1997; 42(6):1199–209.

131. Brown GL, Nanney LB, Griffen J, Cramer AB, Yancey JM, Curtsinger LJ et al. Enhancement of wound healing by topical treatment with epidermal growth factor. N Engl J Med 1989; 321(2):76–9.

132. Kobayashi K, Kashima K, Higuchi K, Arakawa T. The mechanisms of gastrointestinal mucosal injury and repair. Nihon Rinsho 1998; 56(9):2215–22.

133. Vermeer PD, Einwalter LA, Moninger TO, Rokhlina T, Kern JA, Zabner J et al. Segregation of receptor and ligand regulates activation of epithelial growth factor receptor. Nature 2003; 422(6929):322–6.

134. Dempsey PJ, Meise KS, Yoshitake Y, Nishikawa K, Coffey RJ. Apical enrichment of human EGF precursor in Madin-Darby canine kidney cells involves preferential basolateral ectodomain cleavage sensitive to a metalloprotease inhibitor. J Cell Biol 1997; 138(4):747–58.

135. Cohen MH, Williams GA, Sridhara R, Chen G, Pazdur R. FDA Drug Approval Summary: Gefitinib (ZD1839) (Iressa®) Tablets. Oncologist 2003; 8(4):303–6.

136. Yun C-H, Boggon TJ, Li Y, Woo MS, Greulich H, Meyerson M et al. Structures of Lung Cancer-Derived EGFR Mutants and Inhibitor Complexes: Mechanism of Activation and Insights into Differential Inhibitor Sensitivity. Cancer Cell 2007; 11(3):217–27.

137. Slamon DJ, Clark GM, Wong SG, Levin WJ, Ullrich A, McGuire WL. Human breast cancer: correlation of relapse and survival with amplification of the HER-2/neu oncogene. Science 1987; 235(4785):177–82.

138. Slamon DJ, Godolphin W, Jones LA, Holt JA, Wong SG, Keith DE et al. Studies of the HER-2/neu proto-oncogene in human breast and ovarian cancer. Science 1989; 244(4905):707–12.

139. Gravalos C, Jimeno A. HER2 in gastric cancer: a new prognostic factor and a novel therapeutic target. Ann Oncol 2008; 19(9):1523–9.

140. Tanner M, Hollmén M, Junttila TT, Kapanen AI, Tommola S, Soini Y et al. Amplification of HER-2 in gastric carcinoma: association with Topoisomerase IIalpha gene amplification, intestinal type, poor prognosis and sensitivity to trastuzumab. Ann Oncol 2005; 16(2):273–8.

141. Ueda S, Ogata S, Tsuda H, Kawarabayashi N, Kimura M, Sugiura Y et al. The correlation between cytoplasmic overexpression of epidermal growth factor receptor and tumor aggressiveness: poor prognosis in patients with pancreatic ductal adenocarcinoma. Pancreas 2004; 29(1):e1-8.

142. Ekstrand AJ, Sugawa N, James CD, Collins VP. Amplified and rearranged epidermal growth factor receptor genes in human glioblastomas reveal deletions of sequences encoding portions of the N- and/or C-terminal tails. Proceedings of the National Academy of Sciences 1992; 89(10):4309–13.

143. Hynes NE, Lane HA. ERBB receptors and cancer: the complexity of targeted inhibitors. Nat Rev Cancer 2005; 5(5):341–54.

144. Cohen MH, Williams GA, Sridhara R, Chen G, McGuinn WD, Morse D et al. United States Food and Drug Administration Drug Approval summary: Gefitinib (ZD1839; Iressa) tablets. Clin Cancer Res 2004; 10(4):1212–8.

145. Cohen MH, Johnson JR, Chen Y-F, Sridhara R, Pazdur R. FDA drug approval summary: erlotinib (Tarceva) tablets. Oncologist 2005; 10(7):461–6.

146. Solca F, Dahl G, Zoephel A, Bader G, Sanderson M, Klein C et al. Target binding properties and cellular activity of afatinib (BIBW 2992), an irreversible ErbB family blocker. J Pharmacol Exp Ther 2012; 343(2):342–50.

147. Moore MJ, Goldstein D, Hamm J, Figer A, Hecht JR, Gallinger S et al. Erlotinib plus gemcitabine compared with gemcitabine alone in patients with advanced pancreatic cancer: a phase III trial of the National Cancer Institute of Canada Clinical Trials Group. J Clin Oncol 2007; 25(15):1960–6.

148. Pao W, Miller VA, Politi KA, Riely GJ, Somwar R, Zakowski MF et al. Acquired resistance of lung adenocarcinomas to gefitinib or erlotinib is associated with a second mutation in the EGFR kinase domain. PLoS Med 2005; 2(3):e73.

149. Slamon DJ, Leyland-Jones B, Shak S, Fuchs H, Paton V, Bajamonde A et al. Use of chemotherapy plus a monoclonal antibody against HER2 for metastatic breast cancer that overexpresses HER2. N Engl J Med 2001; 344(11):783–92.

150. Smith I, Procter M, Gelber RD, Guillaume S, Feyereislova A, Dowsett M et al. 2-year follow-up of trastuzumab after adjuvant chemotherapy in HER2-positive breast cancer: a randomised controlled trial. Lancet 2007; 369(9555):29–36.

151. Brandl K, Sun L, Neppl C, Siggs OM, Le Gall SM, Tomisato W et al. MyD88 signaling in nonhematopoietic cells protects mice against induced colitis by regulating specific EGF receptor ligands. Proceedings of the National Academy of Sciences 2010; 107(46):19967–72.

152. Lahoti TS, Hughes JM, Kusnadi A, John K, Zhu B, Murray IA et al. Aryl hydrocarbon receptor antagonism attenuates growth factor expression, proliferation, and migration in fibroblast-like synoviocytes from patients with rheumatoid arthritis. J Pharmacol Exp Ther 2014; 348(2):236–45.

153. Shirasawa S, Sugiyama S, Baba I, Inokuchi J, Sekine S, Ogino K et al. Dermatitis due to epiregulin deficiency and a critical role of epiregulin in immune-related responses of keratinocyte and macrophage. Proceedings of the National Academy of Sciences 2004; 101(38):13921–6.

154. Means AL, Ray KC, Singh AB, Washington MK, Whitehead RH, Harris RC et al. Overexpression of heparin-binding EGF-like growth factor in mouse pancreas results in fibrosis and epithelial metaplasia. Gastroenterology 2003; 124(4):1020–36.

155. Perugorria MJ, Latasa MU, Nicou A, Cartagena-Lirola H, Castillo J, Goñi S et al. The epidermal growth factor receptor ligand amphiregulin participates in the development of mouse liver fibrosis. Hepatology 2008; 48(4):1251–61.

156. Takemura T, Yoshida Y, Kiso S, Kizu T, Furuta K, Ezaki H et al. Conditional loss of heparin-binding EGF-like growth factor results in enhanced liver fibrosis after bile duct ligation in mice. Biochem Biophys Res Commun 2013; 437(2):185–91.

157. Polosa R, Prosperini G, Leir SH, Holgate ST, Lackie PM, Davies DE. Expression of c-erbB receptors and ligands in human bronchial mucosa. Am J Respir Cell Mol Biol 1999; 20(5):914–23.

158. Aida. Distribution of epidermal growth factor and epidermal growth factor receptor in human lung: Immunohistochemical and immunoelectron-microscopic studies. Respir. Int. Rev. Thorac. Dis. 1994; 61:161.

159. Vermeer PD, Panko L, Karp P, Lee JH, Zabner J. Differentiation of human airway epithelia is dependent on erbB2. Am J Physiol Lung Cell Mol Physiol 2006; 291(2):L175-80.

160. Schramm F, Schaefer L, Wygrecka M. EGFR Signaling in Lung Fibrosis. Cells 2022; 11(6).

161. Epstein Shochet G, Brook E, Eyal O, Edelstein E, Shitrit D. Epidermal growth factor receptor paracrine upregulation in idiopathic pulmonary fibrosis fibroblasts is blocked by nintedanib. American Journal of Physiology-Lung Cellular and Molecular Physiology 2019; 316(6):L1025-L1034.

162. Stancil IT, Michalski JE, Davis-Hall D, Chu HW, Park J-A, Magin CM et al. Pulmonary fibrosis distal airway epithelia are dynamically and structurally dysfunctional. Nat Commun 2021; 12(1):4566.

163. Zhou Y, Lee J-Y, Lee C-M, Cho W-K, Kang M-J, Koff JL et al. Amphiregulin, an epidermal growth factor receptor ligand, plays an essential role in the pathogenesis of transforming growth factor-β-induced pulmonary fibrosis. J Biol Chem 2012; 287(50):41991–2000.

164. Andrianifahanana M, Wilkes MC, Repellin CE, Edens M, Kottom TJ, Rahimi RA et al. ERBB receptor activation is required for profibrotic responses to transforming growth factor beta. Cancer Res 2010; 70(19):7421–30.

165. Andrianifahanana M, Wilkes MC, Gupta SK, Rahimi RA, Repellin CE, Edens M et al. Profibrotic TGFβ responses require the cooperative action of PDGF and ErbB receptor tyrosine kinases. FASEB J 2013; 27(11):4444–54.

166. Madtes DK, Rubenfeld G, Klima LD, Milberg JA, Steinberg KP, Martin TR et al. Elevated transforming growth factor-alpha levels in bronchoalveolar lavage fluid of patients with acute respiratory distress syndrome. Am J Respir Crit Care Med 1998; 158(2):424–30.

167. Baughman RP, Lower EE, Miller MA, Bejarano PA, Heffelfinger SC. Overexpression of transforming growth factor-alpha and epidermal growth factor-receptor in idiopathic pulmonary fibrosis. Sarcoidosis Vasc Diffuse Lung Dis 1999; 16(1):57–61.

168. Madtes DK, Busby HK, Strandjord TP, Clark JG. Expression of transforming growth factor-alpha and epidermal growth factor receptor is increased following bleomycin-induced lung injury in rats. American Journal of Respiratory Cell and Molecular Biology 1994; 11(5):540–51.

169. Madtes DK, Elston AL, Hackman RC, Dunn AR, Clark JG. Transforming growth factor-alpha deficiency reduces pulmonary fibrosis in transgenic mice. Am J Respir Cell Mol Biol 1999; 20(5):924–34.

170. Hardie WD, Le Cras TD, Jiang K, Tichelaar JW, Azhar M, Korfhagen TR. Conditional expression of transforming growth factor-alpha in adult mouse lung causes pulmonary fibrosis. American Journal of Physiology-Lung Cellular and Molecular Physiology 2004; 286(4):L741-9.

171. Hardie WD, Korfhagen TR, Sartor MA, Prestridge A, Medvedovic M, Le Cras TD et al. Genomic profile of matrix and vasculature remodeling in TGF-alpha induced pulmonary fibrosis. Am J Respir Cell Mol Biol 2007; 37(3):309–21.

172. Hardie WD, Davidson C, Ikegami M, Leikauf GD, Le Cras TD, Prestridge A et al. EGF receptor tyrosine kinase inhibitors diminish transforming growth factor-α-induced pulmonary fibrosis. American Journal of Physiology-Lung Cellular and Molecular Physiology 2008; 294(6):L1217-L1225.

173. Hardie WD, Prows DR, Leikauf GD, Korfhagen TR. Attenuation of acute lung injury in transgenic mice expressing human transforming growth factor-alpha. Am J Physiol 1999; 277(5):L1045-50.

174. Lange AW, Sridharan A, Xu Y, Stripp BR, Perl A-K, Whitsett JA. Hippo/Yap signaling controls epithelial progenitor cell proliferation and differentiation in the embryonic and adult lung. J Mol Cell Biol 2015; 7(1):35–47.

175. Choi J-Y, Lee H, Kwon E-J, Kong H-J, Kwon O-S, Cha H-J. TGFβ promotes YAP-dependent AXL induction in mesenchymal-type lung cancer cells. Mol Oncol 2021; 15(2):679–96.

176. Nethery DE, Moore BB, Minowada G, Carroll J, Faress JA, Kern JA. Expression of mutant human epidermal receptor 3 attenuates lung fibrosis and improves survival in mice. J Appl Physiol (1985) 2005; 99(1):298–307.

177. Kettle R, Simmons J, Schindler F, Jones P, Dicker T, Dubois G et al. Regulation of neuregulin 1beta1-induced MUC5AC and MUC5B expression in human airway epithelium. Am J Respir Cell Mol Biol 2010; 42(4):472–81.

178. Rice AB, Moomaw CR, Morgan DL, Bonner JC. Specific Inhibitors of Platelet-Derived Growth Factor or Epidermal Growth Factor Receptor Tyrosine Kinase Reduce Pulmonary Fibrosis in Rats. The American Journal of Pathology 1999; 155(1):213–21.

179. Paez JG, Jänne PA, Lee JC, Tracy S, Greulich H, Gabriel S et al. EGFR mutations in lung cancer: correlation with clinical response to gefitinib therapy. Science 2004; 304(5676):1497–500.

180. Wang P, Tian Q, Liang Z, Yang Z, Xu S, Sun J et al. Gefitinib attenuates murine pulmonary fibrosis induced by bleomycin. Chin Med J (Engl) 2010; 123(16):2259–64.

181. Ishii Y, Fujimoto S, Fukuda T. Gefitinib prevents bleomycin-induced lung fibrosis in mice. Am J Respir Crit Care Med 2006; 174(5):550–6.

182. Suzuki H, Aoshiba K, Yokohori N, Nagai A. Epidermal growth factor receptor tyrosine kinase inhibition augments a murine model of pulmonary fibrosis. Cancer Res 2003; 63(16):5054–9.

183. Faress JA, Nethery DE, Kern EFO, Eisenberg R, Jacono FJ, Allen CL et al. Bleomycin-induced pulmonary fibrosis is attenuated by a monoclonal antibody targeting HER2. Journal of Applied Physiology 2007; 103(6):2077–83.

184. Le Cras TD, Korfhagen TR, Davidson C, Schmidt S, Fenchel M, Ikegami M et al. Inhibition of PI3K by PX-866 Prevents Transforming Growth Factor-α–Induced Pulmonary Fibrosis. The American Journal of Pathology 2010; 176(2):679–86.

185. Madala SK, Schmidt S, Davidson C, Ikegami M, Wert S, Hardie WD. MEK-ERK pathway modulation ameliorates pulmonary fibrosis associated with epidermal growth factor receptor activation. Am J Respir Cell Mol Biol 2012; 46(3):380–8.

186. Ando M, Okamoto I, Yamamoto N, Takeda K, Tamura K, Seto T et al. Predictive factors for interstitial lung disease, antitumor response, and survival in non-small-cell lung cancer patients treated with gefitinib. J Clin Oncol 2006; 24(16):2549–56.

187. Toyoda. Epiregulin. A novel epidermal growth factor with mitogenic activity for rat primary hepatocytes. J. Biol. Chem. 1995; 270:7495.

188. Riese DJ, Cullum RL. Epiregulin: Roles in normal physiology and cancer. Semin Cell Dev Biol 2014; 28:49–56.

189. Yusta B, Holland D, Koehler JA, Maziarz M, Estall JL, Higgins R et al. ErbB signaling is required for the proliferative actions of GLP-2 in the murine gut. Gastroenterology 2009; 137(3):986–96.

190. Shirakata Y, Komurasaki T, Toyoda H, Hanakawa Y, Yamasaki K, Tokumaru S et al. Epiregulin, a novel member of the epidermal growth factor family, is an autocrine growth factor in normal human keratinocytes. Journal of Biological Chemistry 2000; 275(8):5748–53.

191. Roy S, Khanna S, Rink C, Biswas S, Sen CK. Characterization of the acute temporal changes in excisional murine cutaneous wound inflammation by screening of the wound-edge transcriptome. Physiol Genomics 2008; 34(2):162–84.

192. Morita S, Shirakata Y, Shiraishi A, Kadota Y, Hashimoto K, Higashiyama S et al. Human corneal epithelial cell proliferation by epiregulin and its cross-induction by other EGF family members. Mol Vis 2007; 13:2119–28.

193. Zhang Y, Kobayashi T, Hayashi Y, Yoshioka R, Shiraishi A, Shirasawa S et al. Important role of epiregulin in inflammatory responses during corneal epithelial wound healing. Invest Ophthalmol Vis Sci 2012; 53(4):2414–23.

194. Taylor DS, Cheng X, Pawlowski JE, Wallace AR, Ferrer P, Molloy CJ. Epiregulin is a potent vascular smooth muscle cell-derived mitogen induced by angiotensin II, endothelin-1, and thrombin. Proc Natl Acad Sci U S A 1999; 96(4):1633–8.

195. Koo B-H, Kim D-S. Factor Xa induces mitogenesis of vascular smooth muscle cells via autocrine production of epiregulin. Journal of Biological Chemistry 2003; 278(52):52578–86.

196. Sugiyama S, Nakabayashi K, Baba I, Sasazuki T, Shirasawa S. Role of epiregulin in peptidoglycan-induced proinflammatory cytokine production by antigen presenting cells. Biochem Biophys Res Commun 2005; 337(1):271–4.

197. Inatomi O, Andoh A, Yagi Y, Bamba S, Tsujikawa T, Fujiyama Y. Regulation of amphiregulin and epiregulin expression in human colonic subepithelial myofibroblasts. Int J Mol Med 2006; 18(3):497–503.

198. Hsu D, Fukata M, Hernandez YG, Sotolongo JP, Goo T, Maki J et al. Toll-like receptor 4 differentially regulates epidermal growth factor-related growth factors in response to intestinal mucosal injury. Lab Invest 2010; 90(9):1295–305.

199. Malhotra J, Malvezzi M, Negri E, La Vecchia C, Boffetta P. Risk factors for lung cancer worldwide. European Respiratory Journal 2016; 48(3):889–902.

200. Kometani T, Yoshino I, Miura N, Okazaki H, Ohba T, Takenaka T et al. Benzo[a]pyrene promotes proliferation of human lung cancer cells by accelerating the epidermal growth factor receptor signaling pathway. Cancer Letters 2009; 278(1):27–33.

201. Alyaqoub FS, Liu Y, Tao L, Steele VE, Lubet RA, Pereira MA. Modulation by bexarotene of mRNA expression of genes in mouse lung tumors. Molecular Carcinogenesis 2007; 47(3):165–71.

202. Tsuji S, Kuwahara Y, Takagi H, Sugiura M, Nakanishi Y, Wakamatsu M et al. Gene expression analysis in the lung of the rasH2 transgenic mouse at week 4 prior to induction of malignant tumor formation by urethane and N-methylolacrylamide. The Journal of Toxicological Sciences 2015; 40(6):685–700.

203. Chen K-Y, Tseng C-H, Feng P-H, Sun W-L, Ho S-C, Lin C-W et al. 3-Nitrobenzanthrone promotes malignant transformation in human lung epithelial cells through the epiregulin-signaling pathway. Cell Biology and Toxicology 2021; 38(5):865–87.

204. Miura Y, Sunaga N. Role of Immunotherapy for Oncogene-Driven Non-Small Cell Lung Cancer. Cancers (Basel) 2018; 10(8):245.

205. Farooqui M, Bohrer LR, Brady NJ, Chuntova P, Kemp SE, Wardwell CT et al. Epiregulin contributes to breast tumorigenesis through regulating matrix metalloproteinase 1 and promoting cell survival. Molecular Cancer 2015; 14(1).

206. Li T, Feng R, Chen B, Zhou J. EREG is a risk factor for the prognosis of patients with cervical cancer. Frontiers in Medicine 2023; 10.

207. Zhang J, Iwanaga K, Choi KC, Wislez M, Raso MG, Wei W et al. Intratumoral Epiregulin Is a Marker of Advanced Disease in Non–Small Cell Lung Cancer Patients and Confers Invasive Properties on*EGFR*-Mutant Cells. Cancer Prevention Research 2008; 1(3):201–7.

208. Zhang Y, Qiu F, Ye T, Lee SH, Xu J, Jia L et al. Epiregulin increases stemness-associated genes expression and promotes chemoresistance of non-small cell lung cancer via ERK signaling. Stem Cell Research & Therapy 2022; 13(1).

209. Shigeishi. Expression of epiregulin, a novel epidermal growth factor ligand associated with prognosis in human oral squamous cell carcinomas. Oncol. Rep. 2008; 19:1557.

210. Sunaga N, Miura Y, Masuda T, Sakurai R. Role of Epiregulin in Lung Tumorigenesis and Therapeutic Resistance. Cancers (Basel) 2024; 16(4):710.

211. Kohsaka S, Hinohara K, Wang L, Nishimura T, Urushido M, Yachi K et al. Epiregulin enhances tumorigenicity by activating the ERK/MAPK pathway in glioblastoma. Neuro-Oncology 2014; 16(7):960–70.

212. Sunaga. Clinicopathological and biological significance of epiregulin expression in non-small cell lung cancer. J. Thorac. Oncol. 2013; 8:S426.

213. Herrera-Juárez M, Serrano-Gómez C, Bote-de-Cabo H, Paz-Ares L. Targeted therapy for lung cancer: Beyond EGFR and ALK. Cancer 2023; 129(12):1803–20.

214. Yatabe Y. Molecular pathology of non-small cell carcinoma. Histopathology 2023; 84(1):50–66.

215. Leonetti A, Facchinetti F, Rossi G, Minari R, Conti A, Friboulet L et al. BRAF in non-small cell lung cancer (NSCLC): Pickaxing another brick in the wall. Cancer Treatment Reviews 2018; 66:82–94.

216. Sunaga N, Kaira K, Imai H, Shimizu K, Nakano T, Shames DS et al. Oncogenic KRAS-induced epiregulin overexpression contributes to aggressive phenotype and is a promising therapeutic target in non-small-cell lung cancer. Oncogene 2012; 32(34):4034–42.

217. Shin DH, Kim SH, Choi M, Bae Y-K, Han C, Choi BK et al. Oncogenic KRAS promotes growth of lung cancer cells expressing SLC3A2-NRG1 fusion via ADAM17-mediated shedding of NRG1. Oncogene 2021; 41(2):280–92.

218. Saad MI, Alhayyani S, McLeod L, Yu L, Alanazi M, Deswaerte V et al. ADAM 17 selectively activates the IL -6 trans-signaling/ ERK MAPK axis in KRAS -addicted lung cancer. EMBO Molecular Medicine 2019; 11(4).

219. Yang Z, Chan KI, Kwok HF, Tam KY. Novel Therapeutic Anti-ADAM17 Antibody A9(B8) Enhances EGFR-TKI–Mediated Anticancer Activity in NSCLC. Translational Oncology 2019; 12(11):1516–24.

220. Wang Y, Jing Y, Ding L, Zhang X, Song Y, Chen S et al. Epiregulin reprograms cancer-associated fibroblasts and facilitates oral squamous cell carcinoma invasion via JAK2-STAT3 pathway. J Exp Clin Cancer Res 2019; 38(1):274.

221. Li H, Zhang J, Chen S-W, Liu L-L, Li L, Gao F et al. Cancer-associated fibroblasts provide a suitable microenvironment for tumor development and progression in oral tongue squamous cancer. J Transl Med 2015; 13:198.

222. Celià-Terrassa T, Jolly MK. Cancer Stem Cells and Epithelial-to-Mesenchymal Transition in Cancer Metastasis. Cold Spring Harbor Perspectives in Medicine 2019; 10(7):a036905.

223. Tokizaki S, Podyma-Inoue KA, Matsumoto T, Takahashi K, Kobayashi M, Ibi H et al. Inhibition of transforming growth factor-β signals suppresses tumor formation by regulation of tumor microenvironment networks. Cancer Sci 2023; 115(1):211–26.

224. Fang L, Cheng J-C, Chang H-M, Sun Y-P, Leung PCK. EGF-like growth factors induce COX-2-derived PGE2 production through ERK1/2 in human granulosa cells. J Clin Endocrinol Metab 2013; 98(12):4932–41.

225. Minghetti L. Cyclooxygenase-2 (COX-2) in inflammatory and degenerative brain diseases. J Neuropathol Exp Neurol 2004; 63(9):901–10.

226. Nah S-S, Won H-J, Ha E, Kang I, Cho HY, Hur S-J et al. Epidermal growth factor increases prostaglandin E2 production via ERK1/2 MAPK and NF-kappaB pathway in fibroblast like synoviocytes from patients with rheumatoid arthritis. Rheumatol Int 2010; 30(4):443–9.

227. Odell ID, Steach H, Gauld SB, Reinke-Breen L, Karman J, Carr TL et al. Epiregulin is a dendritic cell-derived EGFR ligand that maintains skin and lung fibrosis. Sci Immunol 2022; 7(78):eabq6691.

228. Arae K, Hirata M, Kurata S, Kamiya S, Taguchi H. *Mycoplasma pneumoniae* induces interleukin-8 production via the epidermal growth factor receptor pathway. Microbiology and Immunology 2011; 55(10):748–50.

229. Liu K, Gualano RC, Hibbs ML, Anderson GP, Bozinovski S. Epidermal Growth Factor Receptor Signaling to Erk1/2 and STATs Control the Intensity of the Epithelial Inflammatory Responses to Rhinovirus Infection. Journal of Biological Chemistry 2008; 283(15):9977–85.

230. Nardella C, Clohessy JG, Alimonti A, Pandolfi PP. Pro-senescence therapy for cancer treatment. Nature Reviews Cancer 2011; 11(7):503–11.

231. Zglinicki T von. Oxidative stress shortens telomeres. Trends Biochem Sci 2002; 27(7):339–44.

232. Sedelnikova OA, Horikawa I, Zimonjic DB, Popescu NC, Bonner WM, Barrett JC. Senescing human cells and ageing mice accumulate DNA lesions with unrepairable double-strand breaks. Nat Cell Biol 2004; 6(2):168–70.

233. Delavaine L, La Thangue NB. Control of E2F activity by p21Waf1/Cip1. Oncogene 1999; 18(39):5381–92.

234. Kaplon J, Zheng L, Meissl K, Chaneton B, Selivanov VA, Mackay G et al. A key role for mitochondrial gatekeeper pyruvate dehydrogenase in oncogene-induced senescence. Nature 2013; 498(7452):109–12.

235. Purvis JE, Karhohs KW, Mock C, Batchelor E, Loewer A, Lahav G. p53 dynamics control cell fate. Science 2012; 336(6087):1440–4.

236. Zhang R, Chen W, Adams PD. Molecular dissection of formation of senescence-associated heterochromatin foci. Mol Cell Biol 2007; 27(6):2343–58.

237. Shah PP, Donahue G, Otte GL, Capell BC, Nelson DM, Cao K et al. Lamin B1 depletion in senescent cells triggers large-scale changes in gene expression and the chromatin landscape. Genes Dev 2013; 27(16):1787–99.

238. Rai M, Curley M, Coleman Z, Demontis F. Contribution of proteases to the hallmarks of aging and to age-related neurodegeneration. Aging Cell 2022; 21(5):e13603.

239. Rodier F, Coppé J-P, Patil CK, Hoeijmakers WAM, Muñoz DP, Raza SR et al. Persistent DNA damage signalling triggers senescence-associated inflammatory cytokine secretion. Nat Cell Biol 2009; 11(8):973–9.

240. Coppé J-P, Kauser K, Campisi J, Beauséjour CM. Secretion of vascular endothelial growth factor by primary human fibroblasts at senescence. Journal of Biological Chemistry 2006; 281(40):29568–74.

241. Laberge R-M, Awad P, Campisi J, Desprez P-Y. Epithelial-mesenchymal transition induced by senescent fibroblasts. Cancer Microenviron 2012; 5(1):39–44.

242. Jun J-I, Lau LF. The Matricellular Protein CCN1/CYR61 Induces Fibroblast Senescence and Restricts Fibrosis in Cutaneous Wound Healing. Nat Cell Biol 2010; 12(7):676–85.

243. Aoshiba K, Tsuji T, Kameyama S, Itoh M, Semba S, Yamaguchi K et al. Senescence-associated secretory phenotype in a mouse model of bleomycin-induced lung injury. Exp Toxicol Pathol 2013; 65(7-8):1053–62.

244. Aoshiba K, Tsuji T, Nagai A. Bleomycin induces cellular senescence in alveolar epithelial cells. Eur Respir J 2003; 22(3):436–43.

245. Baker DJ, Wijshake T, Tchkonia T, LeBrasseur NK, Childs BG, van de Sluis B et al. Clearance of p16Ink4a-positive senescent cells delays ageing-associated disorders. Nature 2011; 479(7372):232–6.

246. Hashimoto M, Asai A, Kawagishi H, Mikawa R, Iwashita Y, Kanayama K et al. Elimination of p19ARF-expressing cells enhances pulmonary function in mice. JCI Insight 2016; 1(12):e87732.

247. Liu Q, Xu X, Zhao M, Wei Z, Li X, Zhang X et al. Berberine induces senescence of human glioblastoma cells by downregulating the EGFR-MEK-ERK signaling pathway. Molecular Cancer Therapeutics 2015; 14(2):355–63.

248. Wang M, Morsbach F, Sander D, Gheorghiu L, Nanda A, Benes C et al. EGF receptor inhibition radiosensitizes NSCLC cells by inducing senescence in cells sustaining DNA double-strand breaks. Cancer Res 2011; 71(19):6261–9.

249. Shang D, Sun D, Shi C, Xu J, Shen M, Hu X et al. Activation of epidermal growth factor receptor signaling mediates cellular senescence induced by certain pro-inflammatory cytokines. Aging Cell 2020; 19(5):e13145.

250. Zacarias-Fluck MF, Morancho B, Vicario R, Luque Garcia A, Escorihuela M, Villanueva J et al. Effect of cellular senescence on the growth of HER2-positive breast cancers. J Natl Cancer Inst 2015; 107(5).

251. Tzouvelekis A, Ntolios P, Karameris A, Vilaras G, Boglou P, Koulelidis A et al. Increased expression of epidermal growth factor receptor (EGF-R) in patients with different forms of lung fibrosis. Biomed Res Int 2013; 2013:654354.

252. Akamatsu H, Inoue A, Mitsudomi T, Kobayashi K, Nakagawa K, Mori K et al. Interstitial Lung Disease Associated with Gefitinib in Japanese Patients with EGFR-mutated Non-small-cell

Lung Cancer: Combined Analysis of Two Phase III Trials (NEJ 002 and WJTOG 3405). Japanese Journal of Clinical Oncology 2013; 43(6):664–8.

253. Lieber M, Smith B, Szakal A, Nelson-Rees W, Todaro G. A continuous tumor-cell line from a human lung carcinoma with properties of type II alveolar epithelial cells. Int J Cancer 1976; 17(1):62–70.

254. Reddel RR, Ke Y, Gerwin BI, McMenamin MG, Lechner JF, Su RT et al. Transformation of human bronchial epithelial cells by infection with SV40 or adenovirus-12 SV40 hybrid virus, or transfection via strontium phosphate coprecipitation with a plasmid containing SV40 early region genes. Cancer Res 1988; 48(7):1904–9.

255. Walters DM, Kleeberger SR. Mouse models of bleomycin-induced pulmonary fibrosis. Curr Protoc Pharmacol 2008; Chapter 5:Unit 5.46.

256. Liu T, Los Santos FG de, Phan SH. The Bleomycin Model of Pulmonary Fibrosis. Methods Mol Biol 2017; 1627:27–42.

257. Schindelin J, Arganda-Carreras I, Frise E, Kaynig V, Longair M, Pietzsch T et al. Fiji: an open-source platform for biological-image analysis. Nat Methods 2012; 9(7):676–82.

258. Arason AJ, Jonsdottir HR, Halldorsson S, Benediktsdottir BE, Bergthorsson JT, Ingthorsson S et al. deltaNp63 has a role in maintaining epithelial integrity in airway epithelium. PLoS One 2014; 9(2):e88683.

259. Hasegawa K, Sato A, Tanimura K, Uemasu K, Hamakawa Y, Fuseya Y et al. Fraction of MHCII and EpCAM expression characterizes distal lung epithelial cells for alveolar type 2 cell isolation. Respir Res 2017; 18(1):150.

260. Kim J, Chu J, Shen X, Wang J, Orkin SH. An extended transcriptional network for pluripotency of embryonic stem cells. Cell 2008; 132(6):1049–61.

261. Chakraborty A, Mastalerz M, Ansari M, Schiller HB, Staab-Weijnitz CA. Emerging Roles of Airway Epithelial Cells in Idiopathic Pulmonary Fibrosis. Cells 2022; 11(6).

262. Crystal RG, Randell SH, Engelhardt JF, Voynow J, Sunday ME. Airway epithelial cells: current concepts and challenges. Proceedings of the American Thoracic Society 2008; 5(7):772–7.

263. Rock JR, Onaitis MW, Rawlins EL, Lu Y, Clark CP, Xue Y et al. Basal cells as stem cells of the mouse trachea and human airway epithelium. Proceedings of the National Academy of Sciences 2009; 106(31):12771–5.

264. Barkauskas CE, Cronce MJ, Rackley CR, Bowie EJ, Keene DR, Stripp BR et al. Type 2 alveolar cells are stem cells in adult lung. J Clin Invest 2013; 123(7):3025–36.

265. Jonsdottir HR, Arason AJ, Palsson R, Franzdottir SR, Gudbjartsson T, Isaksson HJ et al. Basal cells of the human airways acquire mesenchymal traits in idiopathic pulmonary fibrosis and in culture. Lab Invest 2015; 95(12):1418–28.

266. Chilosi M, Poletti V, Murer B, Lestani M, Cancellieri A, Montagna L et al. Abnormal re-epithelialization and lung remodeling in idiopathic pulmonary fibrosis: the role of deltaN-p63. Lab Invest 2002; 82(10):1335–45.

267. Ray S, Chiba N, Yao C, Guan X, McConnell AM, Brockway B et al. Rare SOX2+ Airway Progenitor Cells Generate KRT5+ Cells that Repopulate Damaged Alveolar Parenchyma following Influenza Virus Infection. Stem Cell Reports 2016; 7(5):817–25.

268. Kathiriya JJ, Wang C, Zhou M, Brumwell A, Cassandras M, Le Saux CJ et al. Human alveolar type 2 epithelium transdifferentiates into metaplastic KRT5+ basal cells. Nat Cell Biol 2022; 24(1):10–23.

269. Liu Q, Liu K, Cui G, Huang X, Yao S, Guo W et al. Author Correction: Lung regeneration by multipotent stem cells residing at the bronchioalveolar-duct junction. Nat Genet 2019; 51(4):766.

270. Strunz M, Simon LM, Ansari M, Kathiriya JJ, Angelidis I, Mayr CH et al. Alveolar regeneration through a Krt8+ transitional stem cell state that persists in human lung fibrosis. Nat Commun 2020; 11(1):3559.

271. Habermann AC, Gutierrez AJ, Bui LT, Yahn SL, Winters NI, Calvi CL et al. Single-cell RNA sequencing reveals profibrotic roles of distinct epithelial and mesenchymal lineages in pulmonary fibrosis. Sci Adv 2020; 6(28):eaba1972.

272. Zuo W-L, Yang J, Gomi K, Chao I, Crystal RG, Shaykhiev R. EGF-Amphiregulin Interplay in Airway Stem/Progenitor Cells Links the Pathogenesis of Smoking-Induced Lesions in the Human Airway Epithelium. Stem Cells 2017; 35(3):824–37.

273. Kurie JM, Shin HJ, Lee JS, Morice RC, Ro JY, Lippman SM et al. Increased epidermal growth factor receptor expression in metaplastic bronchial epithelium. Clin Cancer Res 1996; 2(10):1787–93.

274. Shaykhiev R, Zuo W-L, Chao I, Fukui T, Witover B, Brekman A et al. EGF shifts human airway basal cell fate toward a smoking-associated airway epithelial phenotype. Proc Natl Acad Sci U S A 2013; 110(29):12102–7.

275. Jaeger B, Schupp JC, Plappert L, Terwolbeck O, Artysh N, Kayser G et al. Airway basal cells show a dedifferentiated KRT17highPhenotype and promote fibrosis in idiopathic pulmonary fibrosis. Nat Commun 2022; 13(1):5637.

276. Moreno-Valladares M, Moncho-Amor V, Silva TM, Garcés JP, Álvarez-Satta M, Matheu A. KRT5(+)/p63(+) Stem Cells Undergo Senescence in the Human Lung with Pathological Aging. Aging Dis 2023; 14(3):1013–27.

277. Essers J, Theil AF, Baldeyron C, van Cappellen WA, Houtsmuller AB, Kanaar R et al. Nuclear dynamics of PCNA in DNA replication and repair. Mol Cell Biol 2005; 25(21):9350–9.

278. Smith RE, Strieter RM, Phan SH, Lukacs N, Kunkel SL. TNF and IL-6 mediate MIP-1alpha expression in bleomycin-induced lung injury. J Leukoc Biol 1998; 64(4):528–36.

279. Tompkins DH, Besnard V, Lange AW, Keiser AR, Wert SE, Bruno MD et al. Sox2 activates cell proliferation and differentiation in the respiratory epithelium. Am J Respir Cell Mol Biol 2010; 45(1):101–10.

280. Ochieng JK, Schilders K, Kool H, Boerema-De Munck A, Buscop-Van Kempen M, Gontan C et al. Sox2 regulates the emergence of lung basal cells by directly activating the transcription of Trp63. Am J Respir Cell Mol Biol 2014; 51(2):311–22.

281. Miller I, Min M, Yang C, Tian C, Gookin S, Carter D et al. Ki67 is a Graded Rather than a Binary Marker of Proliferation versus Quiescence. Cell Reports 2018; 24(5):1105-1112.e5.

282. Ben-Porath I, Weinberg RA. The signals and pathways activating cellular senescence. The International Journal of Biochemistry & Cell Biology 2005; 37(5):961–76.

283. B Moore B, Lawson WE, Oury TD, Sisson TH, Raghavendran K, Hogaboam CM. Animal models of fibrotic lung disease. Am J Respir Cell Mol Biol 2013; 49(2):167–79.

10 Publication List

Parts of this work were published in the following papers:

1) ***EGFR Signaling in Lung Fibrosis.***

   Schramm F, Schaefer L, Wygrecka M

   - Cells. 2022 March; 11(6):986. doi: 10.3390/cells11060986

2) ***Cellular activities of factor XII in lung fibrosis.***

   Schramm F, Hadzic S, Jablonska E, Birnhuber A, Rubio K, Schulte L, Kreuter M, Bonella F, Barreto G, Weissmann N, Kwapiszewska G, Renne T, Markart P, Preissner KT, Prasse A, Wygrecka M

   - Pneumologie. 2022 May; 76(S 01):42. doi: 10.1055/s-0042-1747785
   - Presented at 62th DGP Congress (Kongress der Deutschen Gesellschaft für Pneumologie und Beatmungsmedizin e.V.).
   - **Winner of DGP Poster Price 2022.**

Additional papers that were co-authored during the work on the doctoral thesis:

1) ***Sex-specific differences in plasma levels of FXII, HK, and FXIIa-C1-esterase inhibitor complexes in community-acquired pneumonia.***

   Ehrlich K, Wilhelm J, Markart P, Weisser H, Wolff JC, Bein G, Pak O, Barreto G, Weissmann N, **Schramm F**, Seeger W, Schaefer L, Kuebler WM, Wygrecka M; CAPNETZ Study Group.

   - American Journal of Physiology: Lung Cellular and Molecular Physiology. 2021 October 1;321(4):L764-L774. doi: 10.1152/ajplung.00162.2021

2) ***Altered fibrin clot structure and dysregulated fibrinolysis contribute to thrombosis risk in severe COVID-19.***

   Wygrecka M, Birnhuber A, Seeliger B, Michalick L, Pak O, Schultz AS, **Schramm F**, Zacharias M, Gorkiewicz G, David S, Welte T, Schmidt JJ, Weissmann N, Schermuly RT, Barreto G, Schaefer L, Markart P, Brack MC, Hippenstiel S, Kurth F, Sander LE, Witzenrath M, Kuebler WM, Kwapiszewska G, Preissner KT.

   - Blood Advances. 2022 February 8;6(3):1074-1087. doi: 10.1182/bloodadvances.2021004816

3) ***Dimethyl fumarate and 4-octyl itaconate are anticoagulants that suppress Tissue Factor in macrophages via inhibition of Type I Interferon.***

   Ryan TAJ, Hooftman A, Rehill AM, Johansen MD, Brien ECO, Toller-Kawahisa JE, Wilk MM, Day EA, Weiss HJ, Sarvari P, Vozza EG, **Schramm F**, Peace CG, Zotta A, Miemczyk S, Nalkurthi C, Hansbro NG, McManus G, O'Doherty L, Gargan S, Long A, Dunne J, Cheallaigh CN, Conlon N, Carty M, Fallon PG, Mills KHG, Creagh EM, Donnell JSO, Hertzog PJ, Hansbro PM, McLoughlin RM, Wygrecka M, Preston RJS, Zasłona Z, O'Neill LAJ.

   - Nature Communications. 2023 June 14;14(1):3513. doi: 10.1038/s41467-023-39174-1

11 Declaration

Hiermit erkläre ich, dass ich die vorliegende Arbeit selbstständig und ohne unzulässige Hilfe oder Benutzung anderer als der angegebenen Hilfsmittel angefertigt habe. Alle Textstellen, die wörtlich oder sinngemäß aus veröffentlichten oder nichtveröffentlichten Schriften entnommen sind und alle Angaben, die auf mündlichen Auskünften beruhen, sind als solche kenntlich gemacht. Bei den von mir durchgeführten und in der Dissertation erwähnten Untersuchungen habe ich die Grundsätze guter wissenschaftlicher Praxis, wie sie in der „Satzung der Justus-Liebig-Universität Gießen zur Sicherung guter wissenschaftlicher Praxis“ niedergelegt sind, eingehalten sowie ethische, datenschutzrechtliche und tierschutzrechtliche Grundsätze befolgt. Ich versichere, dass Dritte von mir weder unmittelbar noch mittelbar geldwerte Leistungen für Arbeiten erhalten haben, die im Zusammenhang mit dem Inhalt der vorgelegten Dissertation stehen, und dass die vorgelegte Arbeit weder im Inland noch im Ausland in gleicher oder ähnlicher Form einer anderen Prüfungsbehörde zum Zweck einer Promotion oder eines anderen Prüfungsverfahrens vorgelegt wurde. Alles aus anderen Quellen und von anderen Personen übernommene Material, das in der Arbeit verwendet wurde oder auf das direkt Bezug genommen wird, wurde als solches kenntlich gemacht. Insbesondere wurden alle Personen genannt, die direkt und indirekt an der Entstehung der vorliegenden Arbeit beteiligt waren. Mit der Überprüfung meiner Arbeit durch eine Plagiatserkennungssoftware bzw. ein internetbasiertes Softwareprogramm erkläre ich mich einverstanden.

_____ _____

Gießen, Datum Unterschrift

12 Acknowledgements

I would like to express my appreciation to everyone who assisted me during my time in the lab and at the office:

My deepest gratitude goes to my supervisor, Prof. Dr. Malgorzata Wygrecka, who gave me the opportunity to work in her group and entrusted me with the project. I am sincerely thankful for her guidance and enthusiasm throughout my research, which made this thesis possible. Her constant motivation pushed me to complete the thesis.

Special thanks go to Mirjam and Benjamin Weiß. Without them, I would never have been introduced to Prof. Malgorzata Wygrecka and her group, nor would I have begun studying medicine as a second degree in the first place.

I would like to thank Dr. Ioannis Alexopoulos and Dr. Oleg Pak for assisting me in acquiring immunofluorescence images and Ewa Bieniek for her assistance with IHC stainings. I also extend my gratitude to PD Dr. Ulrich Gärtner, Prof. Wolfgang Kummer and Annika Seipp for their support with EM analysis. My thanks go to Dr. Nelli Baal and Olga Dakischew for helping establish FACS stainings as well as Dr. Leigh Marsh for helping with the final FACS analysis.

I would also like to thank all the people who have worked with me at AG Wygrecka over the years, especially Mirka, Simone, Kristin, Anne, Astrid, Kim and Agnes, who provided me with the most assistance during my time in the lab and made the time at the lab more enjoyable. Thank you, Stefan, for assisting me with the animal work and for all the conversations during hours of performing intubation and instillations. Thank you, Aysan, for taking over the project from me, advancing it to the next level and for your help at the very end of the thesis.

I am grateful to Nadine for her love and patience with me during difficult times of working on the thesis and for allowing me to work through the night, since I am unable to write during the day.

Finally, I would like to thank my parents and my grandmother for their invaluable support and faith in me, without you - none of this would have been possible.